Freshwater ecosystem monitoring using satellite remote sensing and field surveys

Catherine Diane Kuhn

A dissertation

submitted in partial fulfillment of the

requirements for the degree of

Doctor of Philosophy

University of Washington

2021

Reading Committee:

David Butman, Chair

Jessica Lundquist

Josh Lawler

Program Authorized to Offer Degree:

Environmental and Forest Sciences

University of Washington

Abstract

Freshwater ecosystem monitoring using satellite remote sensing and field surveys

Catherine Diane Kuhn

Chair of the Supervisory Committee:

Dr. David E. Butman

School of Environmental and Forest Sciences

Freshwater ecosystems transfer and transform energy, nutrients and carbon. The color of lakes and rivers, as observed from space, can provide clues to their ecological function and response to anthropogenic activities. Despite this, remote sensing science has been slower to mature for freshwaters relative to terrestrial and marine ecosystems. This research pairs physical and biogeochemical measurements collected during field campaigns with airborne and satellite remote sensing to improve our understanding of the links between color and chemistry in lakes and rivers. Using remote sensing, we mapped over 3,000 river miles in order to better understand uncertainties introduced to remote sensing retrievals during atmospheric correction of satellite imagery. Building from this work, we then conducted remote sensing analysis of ~500,000 lakes combined with a subset of intensive field surveys to (1) establish the relationship between color and gross primary productivity in shallow arctic-boreal lakes, (2) quantify multi-decadal trends

in lake color across arctic-boreal North America, and (3) evaluate the effect of climate variability on arctic-boreal lake color trends.

We found that atmospheric correction can bias model results by 3 – 59% for estimates of chlorophyll-*a* and turbidity derived from Landsat-8 and Sentinel-2 for three large river systems: the Columbia, Amazon and Mississippi. We also discovered the green band (reflectance ~ 560 nm) was the least impacted by uncertainties from processor or sensor choice, implying that the green band is most suitable for historical or cross-sensor analysis. This chapter has been published in *Remote Sensing of the Environment*. Applying this framework in the high northern latitudes, moderate resolution (30m) satellite and high resolution (5 m) hyperspectral airborne remote sensing imagery were used to infer gross primary productivity rates from arctic-boreal lakes within the NASA Arctic-Boreal Experiment (ABoVE) domain. This study was published in *Environmental Research Letters*. We then use the Landsat archive to map annual growing season greenness from 1985 – 2019 for lakes throughout the entire ABoVE domain. Over a quarter of lakes showed significant color change. Declining greenness was the dominant trend and was most common in areas also undergoing warming and precipitation increases. This finding, which has been submitted to *Proceedings of the National Academy of the Sciences*, provides evidence in support of the hypothesis that warming is restructuring arctic-boreal lake ecological dynamics because of changes, in part due to changing hydrologic connectivity. Collectively, these studies have advanced our understanding of the ecological significance of lake and river color, including opportunities to uncover new relationships between lake color and chemistry by combining novel geochemistry data with remote sensing.

TABLE OF CONTENTS

LIST OF FIGURES

LIST OF TABLES

LIST OF ABBREVIATIONS

ABoVE……...Arctic-Boreal Vulnerability Experiment

ACOLITE……... Atmospheric Correction for OLI lite

AVIRIS-NG……...…Airborne Visible-Infrared Imaging Spectrometer - Next Generation

CDOM……Chromophoric Dissolved Organic Carbon

CH_4…….……Methane

CO_2……..…… Carbon Dioxide

Chl-*a*……Chlorophyll-*a*

DOC……Dissolved Organic Carbon

DSF……Dark Spectrum Fitting

GEE……..Google Earth Engine

GPP……Gross Primary Productivity

FNU……..Formazin Nephelometric Unit

L8……...……Landsat-8

LaSRC…….Land Surface Reflectance Code

QGIS……Quantum Geospatial Information System

MAPD……Mean Absolute Percent Difference

NASA ……...……National Aeronautics and Space Administration

NIR ……..……Near Infrared

RMSD……..…Root Mean Squared Difference

R_{rs}……..……..…Remote sensing reflectance

R_s…….……Surface reflectance

S2……...……Sentinel-2

SeaDAS……..…….SEAWIFS Data Analysis System

SWEEP.. ……..Serverless Workflow Enablement and Execution Platform

USGS……United States Geologic Survey

VNIR…….……Visible and Near Infrared

ACKNOWLEDGEMENTS

This research was made possible with support from the United States Geological Survey (U.S.G.S) and a 2017 NASA Earth and Space Science Fellowship entitled “When atmospheric correction matters: Improving retrievals of inland water properties from remote sensing and field data” and by an Integral Environmental Big Data Award. This work has also benefited tremendously from partnership with the NASA Arctic and Boreal Vulnerability Experiment (ABoVE) campaign and my early graduate studies were made possible by the Seattle Chapter of the ARCS Foundation.

Pursuing a PhD at the University of Washington has been a privilege and a joyous adventure. I am deeply grateful to my family, friends, and colleagues for their support. In particular, my advisor Dr. David Butman has been an outstanding mentor. Whether teaching me how to run a vacuum pump or helping me navigate publishing, David’s integrity, humor, and follow-through have taught me many invaluable lessons. I also want to acknowledge my committee members for their support. Thanks to Dr. David Beck for introducing me to data science and for sparking my first forays in Python; to Dr. Jessica Lundquist for kindly yet firmly illuminating my statistical pitfalls and for giving me a solid foundation in critical data analysis; to Dr. Josh Lawler for his supportive advice on navigating graduate school; and to Dr. Michael Goodchild for wonderful conversations about maps and for teaching me that spatial is special.

Thanks to countless other folks who have laughed, listened, advised and re-energized me along the way. Tom DeLuca, Dan Brown and Lisa Graumlich have provided thoughtful leadership at SEFS and COE. Thank you to our current and past SEFS staff for helping me navigate complex budget, shipping and dissertation logistics. Thanks also to my SEFS peers for camaraderie, cold dips off the dock and constructive feedback, in particular Anna Simpson,

Caitlin Littlefield, Russell Kramer, Matthew Aghai, Laura Nelson, Lila Westreich, Zach Johnson, Courtney Bobsin and Meghan Halabisky among many others. I am also so grateful for the intellectual and emotional support from the brilliant minds in the Landscape Biogeochemistry group, especially Matthew Bogard, Fenix Tigreros-Garcia and Benjamin Miller.

Thanks to my 2017 NASA's Ocean Optics classmates, as well as Emmanuel Boss and Curt Mobley, for teaching me all about optics. I want to thank Brian Bergamaschi and Bryan Downing for the opportunity to travel to the USGS California Water Science Center and for teaching me how to collect calibration/validation measurements. Thanks to the eclectic and wonderful eScience folks for helping me build to scale and for providing a, in particular Amanda Tan, Rob Fatland, Don Seitung and Anthony Arendt. Without the computing resources made available to me through the eScience Institute and Google Earth Engine, I would still be downloading Landsat tiles to my computer. Thank you to Monika Moskal and the RSGAL's group for use of the ASD Field Spectrometer and to Aline de Matos Valerio at Brazil's National Institute for Space Research for teaching me how to use it carefully over water. Thanks to Jeff Richey for providing Amazon River data, and to Eric Vermote and Nima Pahlevan at NASA for Landsat and Sentinel-2 data processing. Thanks also to Jon Wang, Uma Bhatt and Jill Deines for generously sharing your time and expertise in Landsat trend and climate analysis.

I greatly appreciate Rob Striegl, Kim Wickland and Mark Dornblaser at the U.S.G.S for sharing their combined decades of field expertise. This research received complementary supported from numerous other grants, NASA-ABoVE Project 14-14TE-0012 (awards NNH16AC03I and NNX15AU14A), the U.S. Geological Survey (USGS) Land Carbon Program and FAPESP Grants 12/51187-0 and 2014/21564-2. Thanks to our expert guides, Robert Grandjambe and Jim Webster (rest in peace), for navigating me to incredible places up north.

Thanks to the excellent mentors who have inspired me and nurtured my curiosity about the world, including Tracy Ostrom, Peter Raymond and Barb Morgan. I am grateful to the Earth Science Women's Network for connecting me to role models and providing sustaining emotional, professional and moral support.

Thanks to my big, loving, wild and fun family and friends, especially my siblings for moral support and my parents for letting me play in the creek so much when I was a kid. Finally, thanks to my incredible partner, Andrew Tuller, and our hound associate, Ruby, for believing in me especially when I found it hard to believe in myself.

Published Materials

A portion of the materials presented in this dissertation have been published through the peer-review process. These articles are reproduced in full here with journal permission and may be cited as follows:

Kuhn, Catherine, Aline de Matos Valerio, Nick Ward, Luke Loken, Henrique Oliveira Sawakuchi, Milton Kampel, Jeffrey Richey et al. "Performance of Landsat-8 and Sentinel-2 surface reflectance products for river remote sensing retrievals of chlorophyll-*a* and turbidity." Remote Sensing of Environment 224 (2019): 104-118. https://doi.org/10.1016/j.rse.2019.01.023

Kuhn, Catherine, Matthew Bogard, Sarah Ellen Johnston, Aji John, Eric Vermote, Rob Spencer, Mark Dornblaser, Kim Wickland, Rob Striegl, and David Butman. "Satellite and airborne remote sensing of gross primary productivity in boreal Alaskan lakes." *Environmental Research Letters* 15, no. 10 (2020): 105001. https://doi.org/10.1088/1748-9326/aba46f

Kuhn, Catherine and David Butman, "Declining greenness in arctic-boreal lakes". *Proceedings of the National Academy of the Sciences*. (Accepted February 2021)

DEDICATION

This dissertation is dedicated to my family.

Chapter 1. INTRODUCTION

The color of lakes and rivers provides insight into their ecological condition and function (Kirk, 1994). Despite this, the remote sensing of inland waters has received less attention in the past relative to terrestrial and marine remote sensing (Topp *et al.*, 2020). This has been due in large part to historic limitations in spatial, spectral and temporal resolution of satellite sensors (Hestir *et al.*, 2015; Mouw *et al.*, 2015). In the past decades, the advent of *in situ* continuous sensors for rapid ecosystem characterization has developed in parallel with the explosion in space-based earth observation data (Gorelick *et al.*, 2017; Kraemer, 2020). These twin lines of innovation have created massive opportunity for advancing our understanding of environmental processes at unprecedented scales. The central goal of this research is to leverage "big data" technologies to characterize freshwater ecosystem properties and processes in areas impacted by human activities and climate variability.

One of the greatest challenges to accurate characterization of water spectral properties is the removal of atmospheric signals during the process of atmospheric correction (Ruddick, Ovidio and Rijkeboer, 2000). Earlier research efforts leveraged atmospheric correction techniques developed for marine ecosystems (Gordon and Wang, 1994; Gordon, 1997), but these fail to take into account signals in the near-infrared and shortwave infrared that result from sediment, bright adjacent land pixels, or shallow bottoms, all of which are common in inland waters (Shi and Wang, 2009). In Chapter 1, I test the influence of different atmospheric corrections on retrievals of surface reflectance over the Mississippi, Amazon and Columbia rivers using Landsat-8 and Sentinel-2 imagery. I compare two Landsat-8 and Sentinel-2 aquatic remote sensing reflectance products to the standard USGS land surface reflectance product over

the Amazon, Columbia and Mississippi rivers. Reflectance products are then evaluated for their comparative performance in retrieving chlorophyll-*a* and turbidity in reference to ship-borne, underway *in situ* validation measurements. Models were independently evaluated using over 31,000 field observations of over 3,000 kilometers of main channels across all three rivers. The land surface product shows the best agreement (4% Mean Absolute Percent Difference (MAPD)) with field measurements of reflectance collected on the Amazon River. Models were able to achieve between 3 – 30% MAPD from field measurements, an uncertainty comparable to current global ocean primary productivity models derived from remote sensing (Siegel *et al.*, 2001). Results show choice of atmospheric correction routine can bias Landsat-8 retrievals of chlorophyll-*a* and turbidity by as much as 59% and 35%, respectively. Using a more restrictive time window for matching *in situ* and satellite imagery can reduce differences by 5 – 31% depending on correction technique. This work highlights the challenges of satellite retrievals over rivers and underscores the need for future optical and biogeochemical research aimed at improving our understanding of the absorbing and scattering properties of river water and their relationships to remote sensing reflectance.

Chapter 2 provides evidence that the Land Surface Reflectance Code (LaSRC) provides sufficient accuracy for retrieving reflectance and in-water constituents in turbid waters. Subsequent chapters build off this research by adapting the workflows in the context of the Arctic-Boreal Vulnerability Experiment (ABoVE) domain. In Chapter 3, this approach is leveraged to develop an empirical model for estimating integrated gross primary production (GPP) for shallow arctic and boreal lakes from airborne (AVIRIS-NG) and satellite (Sentinel-2, Landsat-8 and CubeSats) imagery. In terrestrial and marine ecosystems, remote sensing has been used to estimate gross primary production (GPP) for decades, but few applications exist for

shallow freshwater ecosystems. We found that *in situ* GPP derived from stable oxygen isotopes ($\delta^{18}O$) can be inferred from lake greenness (Rrs_{560}; $r^2 = 0.78$, $p<0.001$, PlanetScope) as observed from satellite and airborne remote sensing platforms as well as from lake reflectance in the red-edge region (Rrs_{703}; $r^2 = 0.8$, $p<0.001$, ASD FieldScope) across a range of optically and limnologically-diverse lakes in interior Alaska. Confounding influences were ruled out by field measurements of optical conditions, which showed lakes overall were shallow (< 2 m) and relatively clear as inferred from low turbidities (< 1 FNU) and low absorption from chromophoric dissolved organic matter (CDOM) (< 2 a_{254}). In shallow waters where sunlight reaches lake bottoms, both submerged vegetation (macrophytes and algae) and phytoplankton likely contribute to gross primary productivity. The stable isotopes and remotely-sensed lake color used here integrate both components. This work provides evidence of the feasibility of using color indices for mapping not just ecologic properties, but also processes, in shallow lakes.

In Chapter 4, we then scale this approach by extracting annual time series of lake color from 1984 to 2018, with a focus on lake greenness, from ~500,000 arctic and boreal lakes. The highest concentration of the world's lakes are found in arctic-boreal regions (Verpoorter *et al.*, 2014), and consequently are undergoing the most rapid warming (Overland *et al.*, 2018). However, the ecological response of arctic-boreal lakes to warming remains highly uncertain. Historical trends in lake color from remote sensing observations can provide insights into changing lake ecology, yet have not been examined at the continental scale. Here, we analyze time series of 30m Landsat growing season composites to quantify trends in lake color for $>4x10^5$ waterbodies in boreal and Arctic western North America. We find lake greenness declined 15% from the first to the last decade of analysis within the 6.3 X 10^6 km^2 study region but with significant spatial variability. Greening declines were more likely to be found in areas

also undergoing increases in air temperature and precipitation. These findings support the hypothesis that warming has increased connectivity between lakes and the land surface (Bring *et al.*, 2016), with implications for lake carbon cycling and energy budgets. This study provides spatially-explicit information linking climate to pan-arctic lake color changes, a finding that will help target future ecological monitoring in remote yet rapidly changing regions. Overall, this dissertation advances our understanding of the challenges and opportunities inherent in satellite monitoring of freshwater ecosystems. These findings collectively put forth a new set of methods for generating insights into ecological processes and properties in lakes and rivers using satellite remote sensing.

References

Bring, A. *et al.* (2016) 'Arctic terrestrial hydrology: A synthesis of processes, regional effects, and research challenges', *Journal of Geophysical Research G: Biogeosciences*, 121(3), pp. 621–649.

Gordon, H. R. (1997) 'Atmospheric correction of ocean color imagery in the Earth Observing System era', *Journal of Geophysical Research: Atmospheres*. Wiley Online Library, 102(D14), pp. 17081–17106.

Gordon, H. R. and Wang, M. (1994) 'Retrieval of water-leaving radiance and aerosol optical thickness over the oceans with SeaWiFS: a preliminary algorithm', *Applied optics*. Optical Society of America, 33(3), pp. 443–452.

Gorelick, N. *et al.* (2017) 'Google Earth Engine: Planetary-scale geospatial analysis for everyone', *Remote Sensing of Environment*, 202, pp. 18–27. doi: 10.1016/j.rse.2017.06.031.

Hestir, E. L. *et al.* (2015) 'Measuring freshwater aquatic ecosystems: The need for a hyperspectral global mapping satellite mission', *Remote Sensing of Environment*, 167, pp. 181–195. doi: https://doi.org/10.1016/j.rse.2015.05.023.

Kirk, J. T. O. (1994) *Light and photosynthesis in aquatic ecosystems*. Cambridge university press.

Kraemer, B. M. (2020) 'Rethinking discretization to advance limnology amid the ongoing information explosion', *Water Research*. Elsevier, p. 115801.

Mouw, C. B. *et al.* (2015) 'Aquatic color radiometry remote sensing of coastal and inland waters: Challenges and recommendations for future satellite missions', *Remote Sensing of Environment*. Elsevier, 160, pp. 15–30.

Overland, J. E. *et al.* (2018) 'Surface air temperature', *Arctic report card*. NOAA.

Ruddick, K. G., Ovidio, F. and Rijkeboer, M. (2000) 'Atmospheric correction of SeaWiFS imagery for turbid coastal and inland waters', *Applied optics*. Optical Society of America, 39(6), pp. 897–912.

Shi, W. and Wang, M. (2009) 'An assessment of the black ocean pixel assumption for MODIS SWIR bands', *Remote Sensing of Environment*. Elsevier, 113(8), pp. 1587–1597.

Siegel, D. A. *et al.* (2001) 'Bio-optical modeling of primary production on regional scales: the Bermuda BioOptics project', *Deep Sea Research Part II: Topical Studies in Oceanography*. Elsevier, 48(8–9), pp. 1865–1896.

Topp, S. N. *et al.* (2020) 'Research Trends in the Use of Remote Sensing for Inland Water Quality Science: Moving Towards Multidisciplinary Applications', *Water*. Multidisciplinary Digital Publishing Institute, 12(1), p. 169.

Verpoorter, C. *et al.* (2014) 'A global inventory of lakes based on high-resolution satellite

imagery', *Geophysical Research Letters*. Wiley Online Library, 41(18), pp. 6396–6402.

Chapter 2. PERFORMANCE OF LANDSAT-8 AND SENTINEL-2 SURFACE REFLECTANCE PRODUCTS FOR RIVER REMOTE SENSING RETRIEVALS OF CHLOROPHYLL-A AND TURBIDITY

Kuhn et al., 2019. Remote Sensing of the Environment. 224, 104 – 118.

2.1 INTRODUCTION

Rivers sustain terrestrial ecosystems and human communities (UN 2009) yet are being transformed worldwide by anthropogenic pressures and environmental change (Vörösmarty et al. 2010). Threats include harmful algal blooms, sediment loading, warming and eutrophication (Whitehead et al. 2009; Malmqvist et al. 2008). In terrestrial, ocean, coastal and lake ecosystems, satellites have been increasingly marshalled for ecological monitoring (Smith 2003; Valerio et al. 2017), yet rivers have received relatively little attention in the field of aquatic remote sensing, in part due to their small spatial scale (< 100 km) and because of their large dynamic range of optically significant constituents, such as phytoplankton, chromophoric dissolved organic matter (CDOM), and non-algal particles, that do not co-vary. This optical complexity, when combined with rapid changes in river flow and chemistry, results in a challenging observational environment (Hestir et al. 2015).

The dynamic nature of rivers necessitates the ability to evaluate ecosystem characteristics

beyond point samplings to understand spatiotemporal variation and monitor long-term changes. For example, products retrieved from satellites such as chlorophyll-*a (*Chl-*a)*, CDOM, and turbidity have been used for evaluating important processes/factors such as sediment and DOM transport (Saraceno et al. 2009), total suspended matter (Shi et al. 2015) ecosystem productivity (Carr et al. 2006; Saba et al. 2011), and even greenhouse gas fluxes (Fay and McKinley 2017) in the case of marine and lake settings, but these approaches are seldom applied to rivers.

Both atmospheric correction and bio-optical models are key processing steps to water color remote sensing (Ruddick, et al., 2000a). During atmospheric correction, remote sensing reflectance (R_{rs} (λ); sr^{-1}), defined as the ratio of water-leaving radiance below the water surface to downwelling irradiance above the water surface (Mobley 1999), is recovered from at-sensor measurements by correcting for surface effects and atmospheric influences. This process is paramount for the robust retrieval of chlorophyll-*a*, CDOM and sediment at regional and global scales (McCain et al. 2006) yet remains one of the largest sources of error and foremost challenges in aquatic remote sensing (Mobley et al. 2016; Mouw et al. 2015).

While sensor-specific atmospheric correction routines for land and ocean applications have existed for decades (Gordon and Wang 1994, Gordon 1997), inland water techniques are still emerging. Atmospheric correction over water requires greater precision than over land because 70 to 90% of the top of the atmosphere signal over water is known to be from atmospheric effects and sun and sky glint from the water surface (Wang 2010). In light of this challenge, the joint National Aeronautics and Space Administration (NASA) and United States Geologic Survey (USGS) Landsat-8 Surface Reflectance Code (LaSRC), while primarily designed for terrestrial applications, has been modified to include a routine over surface waters (Vermote et al. 2016). At coarser resolutions, significant progress has been made in developing

specialized corrections for coastal ocean applications. For example, NASA's Ocean Color Biology Processing Group (OBPG) regularly generates atmospherically-corrected Level-2 products from ocean color sensors including the Moderate Resolution Imaging Spectroradiometer (MODIS) and Visible Infrared Imaging Radiometer Suite (VIIRS) (Barnes and Hu 2016; O'Reilly et al. 1998; M. Wang and Shi 2007a) using the SeaWiFS Data Analysis System (SeaDAS).

The large pixel size (>250 m) of standard ocean color products limits their use at smaller spatial scales relevant to inland waters (Mouw et al. 2015).While not designed for ocean color applications, moderate-resolution missions (10 – 100 m) such as the Operational Land Imager (OLI) on board NASA's Landsat-8 (L8) and the Multispectral Instrument (MSI) on board the European Space (ESA) Agency's Sentinel-2 (S2), abbreviated hereafter as L8 and S2, provide an improvement over prior generations of moderate-resolution sensors used for monitoring near-surface water constituents.

For example, Franz et al. (2015) demonstrated the atmospheric correction of L8 in SeaDAS over the Chesapeake Bay for the retrieval of Chl-*a*. Pahlevan (2017a) used atmospherically-corrected S2 images to map total suspended sediment in moderately turbid coastal waters. Lymburner et al. (2016) used a land-based atmospheric correction of L8 over Australian lakes and produced reasonable estimates of surface reflectance, which were then successfully used to retrieve total suspended matter (TSM). L8-retrieved TSM values showed a strong correlation with *in situ* data, but the land-based atmospheric correction was thought to introduce a positive bias.

Surface reflectance over complex waters has also been estimated using a software platform called ACOLITE for both L8 (Vanhellemont and Ruddick 2014) and S2 (Vanhellemont

and Ruddick 2016) for turbid coastal waters. Thus, the number of specialized atmospheric correction routines has increased substantially (Dörnhöfer and Oppelt 2016) since the first ocean color correction was developed (Gordon 1978) and performance comparisons over land are underway (Doxani et al. 2018). Despite this, few papers compare their merits (Hadjimitsis et al. 2004; Doxani et al. 2018; Martins et al. 2017) and standardized surface reflectance products are not yet available for inland water applications.

A second major barrier impeding our ability to evaluate water color retrievals is the limited number of concurrent, *in situ*, validation measurements (O'Reilly et al. 1998). Multi-parameter ship-borne sensing platforms are increasingly used in coastal and ocean settings to retrieve bio-optical properties (Werdell et al. 2013; Aiken and Hooker 1997; Brewin et al. 2016; Matsuoka et al. 2016; Dall'Olmo et al. 2009; Slade et al. 2010; Fichot et al. 2015). These underway measurement systems allow for large-scale validation of satellite-based products. Underway measurements have also allowed us to expand our observations over larger areas of the river's surface, resulting in changes in our understanding of riverine carbon dynamics at the global scale (Sawakuchi et al. 2017). Conversely, in inland waters, especially rivers, the use of underway flow-through systems for calibration and validation of satellite products is still incipient.

In light of these advances, here we evaluate the potential of three atmospheric corrections to L8 and S2, validated with high-resolution underway measurements of river constituents, to develop space-based retrievals of Chl-*a* and turbidity in large rivers. Our primary objective is to examine the influence of three atmospheric correction routines (LaSRC, SeaDAS, ACOLITE) on estimating these parameters.

To achieve this goal, we begin by analyzing surface reflectance estimates, abbreviated hereafter as R_{rs} for readability, from three atmospheric correction routines and evaluating the differences in remote sensing reflectance spectra. We compare the reflectance spectra generated by this analysis to in-river field measurements as well as to satellite-derived spectra from the literature. We then examine the influence of these spectral differences on the performance of standard bio-optical algorithms for Chl-*a* and turbidity. Our goal is to examine how current remote sensing approaches may or may not suffice for estimating water constituents across a range of river conditions.

2.2 Site Descriptions

Continuous, underway data coincident to satellite overpasses were collected from the main stem of the Amazon, Columbia and Mississippi rivers (Table 2.1, Figure 2.1). The rivers represent a natural gradient in water color from very clear to very turbid. The cruises are part of an ongoing effort (Stadler et al. 2018, Ward et al. 2018; Crawford et al. 2016, 2017) to characterize carbon cycling in major rivers using large-scale underway sampling transects.

Table 2.1 Campaign details for underway data used in this study. LCR and UMR cruises were sampled at 1 Hz resolutions. Amazon cruises were sampled at 0.02 Hz resolution. Counts (N) are given for datasets after binning to 1-minute intervals but prior to filtering for quality control.

Dataset	River and Region	Period	Distance	Variable	N
A-LW	Amazon Low Water Lower Amazon, Brazil, South America	2016-11-04 - 2016-11-09	~526 km	Chl-*a**, Turb**, $R_{rs}(\lambda)$	3838
A-HW	Amazon High Water Lower Amazon, Brazil, South America	2017-04-26 - 2017-05-02	~526 km	Chl-*a*, Turb, $R_{rs}(\lambda)$	4299
LCR	Lower Columbia, USA, North America	2016-07-12 - 2016-07-18	~568 km	Chl-*a*, Turb	1436
UMR	Upper Mississippi, USA, North America	2015-08-01 - 2015-08-13	1385 km	Chl-*a*, Turb	4170

* Chlorophyll-*a* concentration (mg/m^3) ** Turbidity (FNU)

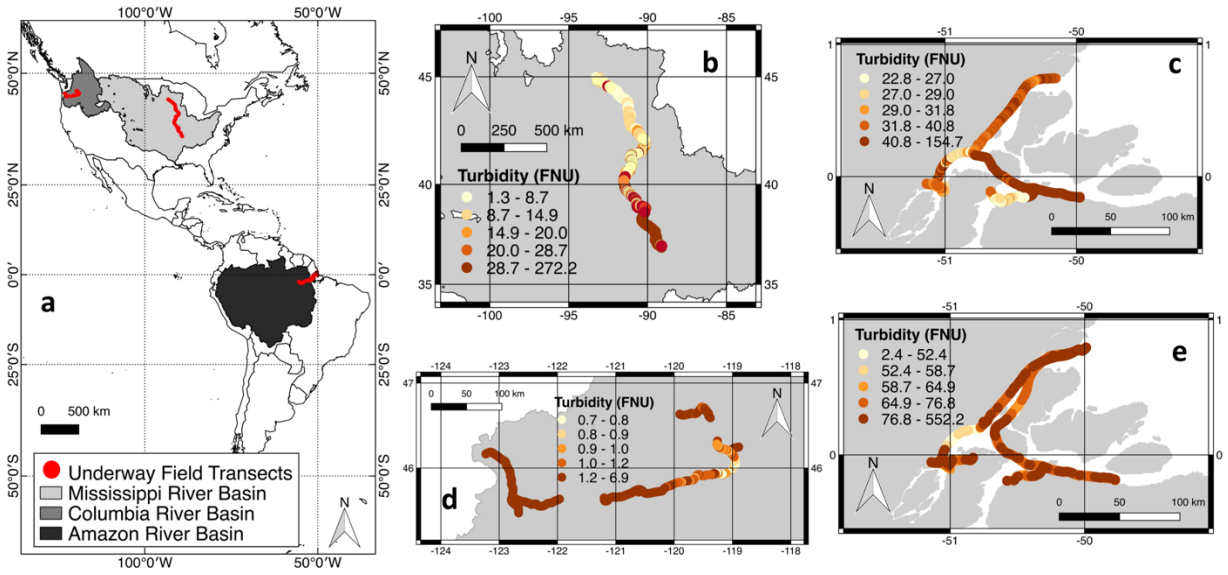

Figure 2.1 Field site locations and turbidity gradients. Map showing location of three large river basins: Amazon, Columbia and Mississippi (grey) and the field transects (red) (a). Overall 13,000 measurements of turbidity (FNU) were recorded during the four cruises, revealing spatial gradients in water clarity. (b) Upper Mississippi River transect August 2015 (c) Lower Amazon River cruise on November 2016 (d) Lower Columbia River Cruise in July 2016 and the (e) Lower Amazon River cruise on April 2017.

2.3 METHODS

The overarching methodological framework (Figure 2.2d) for this study was to match satellite and *in situ* measurements for three optically diverse river systems ranging from the shallow and productive waters of the Mississippi (Figure 2.2a) to the relatively clearer, deeper waters (Figure 2.2b) of the Columbia river with the two cruises during Amazon High Water (HW) and Low Water (LW) acting as a very turbid endpoint (Figure 2.2c).

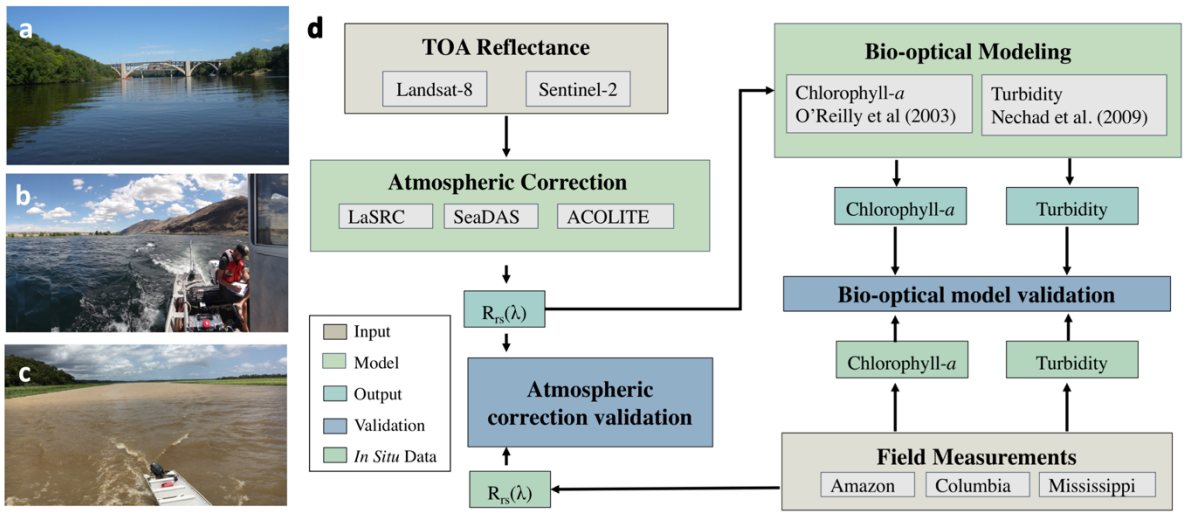

Figure 2.2. Study sites photos and major steps of analysis. Photos for the Mississippi (a), Columbia (b) and Amazon (c) rivers and overarching methodological framework (d) showing major modeling steps, inputs and outputs.

2.3.1 Underway river datasets for algorithm evaluation

Custom, flow-through systems delivered river water on board from an average depth of 0.2 m where it passed through a series of optical sensors configured to log simultaneously with a GPS unit as described in Crawford et al. (2017, 2016); Turner et al. (2016); Ward et al. (2016). Optical parameters measured included turbidity (FNU) (ISO-7027 method, 860 +/- 15 nm excitation, 90° scattering) and Chl-*a* fluorescence (mg m^{-3}, excitation 470 nm +/- 15 nm and emissions +/- 685 20 nm), as measured by a Yellow Springs Instrument (YSI) EXO2 sonde.

Fluorometers are well-suited for inline, large-scale mapping because of small sensor size and lower power requirements. Chlorophyll-*a* fluorescence (Chl-*a*) is commonly held to be a proxy for chlorophyll-*a* concentration. Known biases associated with fluorometric Chl-*a* include interference from other bio-optical components like non-algal particles as well as variability in phytoplankton physiology and species composition which can cause changes in the fluorescence

to Chl-*a* ratio (Roesler et al. 2017; Mouw et al. 2013; Dierssen 2010). Unfortunately, HPLC pigment data is not available so natural variations between Chl-*a* concentrations and fluorescence for these large rivers remain to be studied.

Turbidity, in its formal optical definition, refers to the amount of attenuation and back scattering of light due to suspended solids and dissolved load. Data were logged per second at boat speeds ranging from 15 to 40 km h^{-1} representing roughly a point every 4 to 11 meters, or two to seven measurements per pixel depending on sensor. The Amazon cruise data were collected at one minute intervals; the Mississippi and Columbia datasets were converted from 1 second intervals to 1 minute median bins (Dall'Olmo et al. 2009) to match the GPS unit logging interval.

2.3.2 *In situ* hyperspectral radiometry

While biogeochemical data exists for rivers worldwide, parallel radiometric measurements over rivers are very rare. As such, *in situ* reflectance measurements were only possible during the Amazon field campaigns. *In situ* radiometric data were collected at stationary sampling sites during the Amazon cruises (Valerio et al. 2017) to provide a more quantitative assessment of atmospheric correction techniques.

Above-water hyperspectral radiometry data were collected using a portable hyperspectral radiometer FieldSpec® (ASD Inc.) which collects radiance (L, $\mu W\ m^{-2} sr^{-1}$) in the range of 350 to 1100 nm (bandwidth 1nm) and a field-of-view of 25°. The acquisition geometry followed (Mobley 1999) recommendations to avoid shadows and sun and sky glint contamination. Total water- leaving radiance (L_w), sky radiance (L_{sky}) and the radiance from a white Spectralon reference panel (L_g) were consecutively measured 6 to 10 times in the same sequence using a fixed geometry, averaged and resampled to match satellite sensor bandwidths. During days with

sparse clouds, the radiometer integration time was adjusted every time the sunlight condition changed and new measurements were made. The L_g was used to estimate the downwelling irradiance (E_d) (Eq. 2.1):

$$E_d(\lambda) = L_g(\lambda) f_c \pi \quad \text{(Eq. 2.1)}$$

where f_c is a correction factor estimated in laboratory by the ratio of a standard Spectralon reference that remains in the laboratory by the Spectralon panel used at the fieldwork. The remote sensing reflectance (R_{rs}) can be computed according to (Eq. 2.2):

$$R_{rs} = \frac{L_w}{E_d} = \frac{L_u - \rho_{air-river} * L_{sky}}{E_d} \quad \text{(Eq. 2.2)}$$

where L_u is the upwelling radiance that reaches the sensor and $\rho_{air-river}$ is a sun and sky glint correction coefficient at the air-sea interface. There are several methods in the literature to correct the optical signal from sky glint interference. The sun glint interference at this point should be minimum after redundant measurements made following viewing geometry proposed by Mobley (1999). The residual sun glint plus sky glint suggested by Ruddick et al (2005) were corrected in the present study using the approach of Ruddick et al. (2006) for turbid to highly turbid waters. The $\rho_{air-river}$ is a function of wind and cloud cover (Eq. 2.3).

$$\frac{L_{sky}(\lambda=750)}{E_D(\lambda=750)} \geq 0.05 \rightarrow \rho_{air-river} = 0.0256 \quad \text{(Eq. 2.3)}$$

or

$$\frac{L_{sky}(\lambda=750)}{E_D(\lambda=750)} < 0.05 \rightarrow \rho_{air-river} = 0.0256 + 0.00039W + 0.000034W^2 \quad \text{(Eq. 2.4)}$$

where W is the wind (m s^{-1}) measured concomitantly with the radiometric measurements. The residual glint and white offset correction were not performed for the spectra dataset. This correction usually is based on NIR spectrum (e.g. $R_{rs}(780)$ and $Rr_s(780)$, Ruddick et al., 2005) and assumes that its shape is largely determined by pure water absorption. In very turbid waters with high NIR reflectance like the Amazon River (Figure 2.1), the NIR variability is not linear (Wang et al. 2012; Goyens et al 2013) After R_{rs} was calculated, the coefficient of variation (cv = (standard deviation/mean)·100) of the R_{rs} spectra replicates was computed for each station. Only the spectrum (considering the interval of 400-840 nm) with cv close or lower than 10% between the replicates was kept and averaged to get the final spectrum utilized in this study as a representative of R_{rs} at each station.

2.3.3 Satellite data

L8, launched as a collaboration between the United States Geologic Survey (USGS) and National Aeronautics and Space Administration (NASA) on February 11, 2013, carries onboard the OLI pushbroom multispectral radiometer. While the 16-day revisit period is similar to previous Landsat missions, L8's OLI sensor possesses several major enhancements including an additional band for coastal and aerosol applications (443 nm) and cirrus clouds (1374 nm). Designed to provide continuity with Landsat (Irons et al. 2012), the MultiSpectral Instrument (MSI) onboard ESA's S2 has a 5-day revisit time and 13 spectral bands in the visible to near infrared (443 nm–2190 nm) (Drusch et al. 2012) and is also available through a variety of web providers including the USGS Earth Explorer site and Google Earth Engine (Gorelick et al.

2017a).

Compared to L8, the S2 sensor features a higher spatial resolution (10, 20 and 60 m), shorter revisit period (5 days) and three additional bands in the near-infrared (703, 740, and 783 nm) region. Both instruments (Appendix A, Table 2.5) are quantized at 12-bits, and have much higher signal to noise ratios compared to previous Landsat missions and less frequent saturation over highly reflective targets (Pahlevan et al. 2014; Roy et al. 2014). While existing ocean color missions like the MOderate Resolution Imaging Spectroradiometer (MODIS) also have high radiometric resolution (16 bits) and more frequent revisit times (1-2 days), the finer spatial (10 to 60 m) resolution of L8 and S2 is their major advantage over coarser ocean color sensors like Ocean and Land Color Instrument on board Sentinel-3 (300 m) and MODIS (250-1000 m).

Collection 1 Level 1 L8 and Level 1C Top of the Atmosphere (TOA) S2 data acquired during each cruise were identified by filtering to each region (Figure 2.1) and cruise duration (Table 2.1) in Google Earth Engine (Gorelick et al. 2017a). Over 140 total images were acquired over the rivers during the cruises. Of these, 121 were found unsuitable because of significant cloud cover (>90%) or lack of overlap with the cruise transects in space or time (within ≤ 24 hours). The final 19 TOA images (Table 2.2) were downloaded from the USGS Earth Explorer (https://earthexplorer.usgs.gov/) in January 2018 and defined in their native World Geodetic System 84 (WGS84) datum and Universal Transverse Mercator (UTM) projection for use as inputs to the atmospheric correction routines. Note that the fusion of these two sensors into continuous time series is possible but outside the scope of this study.

Table 2.2. Satellite overpasses from L8 and S2 coincident (+/- 24 hours or fewer) of cruise activities using a more restrictive time window where possible. S2 images that share a time stamp have been repackaged by the USGS Earth Resources Observation and Science Center (EROS) into 100 km X 100 km granules, or tiles, excerpted from the same datatake.

Sensor	River	Overpass Date	Overpass Time (UTC)	Time Window (+/- hours)*	Path/Row or Tile
Landsat-8	Mississippi	8/7/15	16:47:13, 16:46:50	3	025/032, 025/031
	Columbia*	7/13/16	18:42:58, 18:43:22	24	044/027, 044/028
	Amazon LW	11/6/16	13:34:59, 13:35:23	3	225/060, 225/059
	Amazon HW	5/1/16	13:33:56, 13:34:20	3	225/060, 225/059
Sentinel-2	Mississippi*	8/7/15	16:42:10	12	T15SYD, T16SBJ
	Columbia*	7/14/16	19:04:59, 19:01:37	12	T10TGR, T10TGS, T11TLM, T10TFR, T11TLL
	Amazon LW	11/5/16	13:51:10	3	T22MDE, T22MEE, T22NEF, T22MFE
			Total	Images =	19

* Window of time in hours between closest coincident image acquisition and field measurements.

2.3.4 Atmospheric correction techniques

In this study we test three atmospheric corrections using Level 1 TOA data as an input: the Landsat Surface Reflectance Code (LaSRC); the l2gen processor in SeaDAS; and a third method called ACOLITE (Vanhellemont and Ruddick 2015). The first two are used by the USGS and NASA's

OBPG to create land and ocean products. The last method is an open-source software processor developed at the Royal Belgian Institute of Natural Sciences (Vanhellemont and Ruddick 2014; 2015; 2016). The overall differences between processors is described here and in Appendix A, Table 2.6.

The Landsat Surface Reflectance Code (LaSRC), was originally developed at NASA Goddard Flight Center for terrestrial applications. LaSRC uses the Second Simulation of the Satellite Signal in the Solar Spectrum (6SV) model and auxiliary data from MODIS climate grids to estimate aerosols, air temperature, water vapor (MOD09CMG), and ozone (MOD09CMA) (Vermote et al. 2016). LaSRC uses the coastal blue band (443 – 450 nm), where aerosols typically have a strong signal, in combination with the red band for retrieving aerosols (Roy et al. 2014). The resulting USGS Collection 1 L8 reflectance product is widely available, including from the USGS Earth Explorer (Woodcock et al. 2008) and cloud providers such as Google Earth Engine, Amazon Web Services and Planet Labs. For this application, L8 and S2 images were processed in their native resolution (Appendix A, Table 2.5) using LaSRC (v 3.5.5) at NASA Goddard Space Flight Center's Terrestrial Information Systems Laboratory.

NASA's OBPG has, in parallel, developed an approach specifically tuned for water and distributed in SeaDAS (version 7.0). SeaDAS's level 2 (l2gen, v9.1.0) processor was used to produce remote sensing reflectance products for L8 (Franz et al. 2015) and S2 (Pahlevan et al. 2017a). To accommodate complex coastal waters, ocean color processing now incorporates an iterative, NIR-based correction (Bailey et al. 2010), which has been shown to reduce negative SeaWiFS retrievals in the blue (412 - 490 nm) by 40 – 100% for low to moderately turbid waters. For highly turbid waters (TSM > 35 mg L^{-1}), however, NIR bands can saturate at

calibrated TOA reflectance values > 2.0 (unitless) (USGS 2018a). To address this, we used NIR in combination with SWIR bands (1 μm < λ < 3 μm), the latter of which appears dark even over very turbid water (Shi and Wang 2009). Combining the NIR and SWIR bands has been shown to produce radiometrically stable R_{rs} estimates over turbid waters (Pahlevan et al. 2017c) more successfully than when either band is used in isolation (see Appendix A, 2.7.2). The ratio of NIR to SWIR Rayleigh-corrected radiance reflectance was used, in combination with the relative humidity, to assign an aerosol type from a suite of models (Ahmad et al. 2010; Gordon and Wang 1994). Results were then extracted using a spatially smoothed filter as described by Pahlevan et al. (2017a, b) for L8 (30m) and S2 (20m) to minimize noise.

We also processed images using a third open-source software platform called ACOLITE (version 20170718.0). Designed specifically for atmospheric correction over marine and inland waters, ACOLITE supports both S2 and L8, and is publicly available for download (http://odnature.naturalsciences.be/remsem/acolite-forum/) (Vanhellemont and Ruddick 2014; Vanhellemont and Ruddick 2016, Vanhellemont 2015). In ACOLITE (version 20170718.0), TOA data were converted to water-leaving radiance reflectance ($\rho w = \pi \times R_{rs}$, dimensionless) in their native resolution by the removal of aerosols after radiometric calibration using sensor-specific gains (Pahlevan et al. 2014). Aerosol type, specified as an epsilon value (ε), was derived from user-designated, scene-specific aerosol correction bands (NIR-SWIR in this case). Aerosol reflectance derived thus was then extrapolated to the visible bands and removed from the total signal. Here we chose a combined NIR-SWIR method with an ε fixed per-scene to reduce pixel-level noise (Dogliotti et al. 2011). Clouds, land, glint and human infrastructure were masked using a SWIR (~1609 nm) threshold suggested by Vanhellemont and Ruddick (2015) and Wang and Shi (2006) in which Rayleigh-corrected reflectances above > 0.0215 (dimensionless) are

considered to be non-water. Note that since the preparation of this manuscript, a new version of ACOLITE (Python 20180925.0) has been released that selects the atmospheric correction band from any part of the spectrum based on the resulting path radiance (Vanhellemont and Ruddick 2018). This dark spectrum fitting method selects the "black pixel" in any wavelength, including the visible, and from whichever target, including building and tree shadows, that is the darkest. These changes are expected to alleviate some of the issues associated with using the SWIR band for atmospheric correction over water in the presence of adjacency effects.

2.3.5 Water color algorithms

In this study, standard satellite water color algorithms for inland waters were applied to atmospherically corrected data. Testing new approaches to bio-optical models in freshwater is an area of active research (for additional discussion see Appendix A, 2.7.1) outside the scope of this study. Here we selected standard, cross-platform approaches. Turbidity was estimated using a semi-empirical red band algorithm with L8's 655 nm band and S2's 665 nm band (Dogliotti et al. 2015; Nechad, Ruddick, and Neukermans 2009). Chl-*a* was estimated using the widely-tested OC3 algorithm. A complete description is given in Appendix A, 2.7.3. Intended for concentrations > 0.2 mg m^{-3}, OC3 relates ratios of the maximum of the two blue bands (443 or 490 nm) and green bands (560 nm) to Chl-*a* with a fourth-order polynomial relationship (O'Reilly et al. 1998). While the red and NIR bands are more commonly used for estimating Chl-*a* in special cases of very turbid waters (Sun et al. 2014; Le et al. 2011; Dall'Olmo et al. 2009) to avoid overestimating chlorophyll-*a* erroneously, we wanted to evaluate the performance of the models that underpin standard suites of existing data products over the dynamic range of our river sites as pre-existing products are likely to be of interest to the water management and

limnology communities. Atmospherically corrected satellite data from the three approaches were used to produce spatially continuous estimates of Chl-*a* and turbidity over three river systems.

2.3.6 Satellite data to *in situ* matchup considerations

Outputs of the 19 images selected in this study (Table 2.2) from each of the three correction routines were then cloud-optimized, or tiled, for import into Google Cloud Storage (GCS). Satellite to *in situ* matchups were generated by importing all cloud-optimized imagery from GCS and field data points into Google Earth Engine (GEE) (Gorelick et al. 2017a) for masking and sampling. To avoid the influence of clouds, all images were masked to clear, cloud-free pixels. L8 LaSRC Level 2 products allow users to specify both cloud and cloud shadow-free and water-only pixels using the pixel_qa band (60 m, where pixel_qa = 324), thus masking any pixels flagged with medium or high confidence as land, cloud, or ice (Foga et al. 2017). S2's quality bands were used to mask clouds QA60 band (60 m, where QA60 = 0). However, this band only indicates the presence or absence of clouds without the additional flags for water presence/absence available from the L8 L2 product so the dilated shoreline mask described below was used to isolate water pixels.

Shoreline effects from mixed pixels and breaking surf at the water's edge can contaminate dark targets and are a special concern for inland waters (Franz et al. 2015). To reduce this effect and minimize sub-pixel variability, field measurements collected within 3 pixels of the shoreline were discarded using a dilated shoreline mask. Shorelines were estimated using a land mask derived from the Surface Water Occurrence dataset (Pekel et al. 2016) where water occurrence > 90% is classified as water (0) and <90% is classified as land (1). Each sampling point's distance to the nearest non-zero land pixel (i.e. the shoreline) was then calculated using a fast distance transform function and points close to shore (< 3 L8 pixels) were

excluded, resulting in a dataset representative of open water at a distance greater than 90m from the shore. Data from both sensors was masked at 90m for a conservative shoreline estimate.

Bailey and Werdell (2006) suggest match-ups between satellite and *in situ* data should ideally be restricted to field measurements collected within a 3-hour window of satellite overpass. However, other authors have demonstrated successful matchups using less restrictive windows of up to 3 days in lakes (Olmanson et al. 2008; Kloiber et al. 2002; Sriwongsitanon et al. 2011; Tebbs et al. 2013) under stable hydrologic and atmospheric conditions. For S2 and L8, local overpass times were around 11 a.m. ± 0.5 h, which allowed for a time difference of <3 hours in most cases unless otherwise noted. The difference in acquisition versus *in situ* time is noted for each cruise and sensor (Table 2.2).

To generate matchups, we sampled a 3 X 3 pixel box centered on each validation point. We required a majority of pixels (n => 5 pixels) inside each 3 X 3 box to be retrieved to ensure sample size homogeneity within each box. Medians, arithmetic means, standard deviations and counts were calculated for 3 X 3 pixel box for R_{rs}, Chl-*a* and turbidity. A final filter included only points for which a valid reflectance was retrieved by all correction routines. This step ensured uncertainties were calculated using the same set of values.

To further constrain absolute accuracy, another set of filters as recommended by Werdell and Bailey (2006) was imposed for turbidity and Chl-*a* (Appendix A, Figure 2.11). As such, negative values and pixels outside of one standard deviation were excluded to reduce the influence of extreme outliers and mixed pixels. As a result of these quality control steps, only high-quality chlorophyll-*a* and turbidity validation points were used, which restricted the final validation analysis to Columbia and Amazon High Water Landsat-8 acquisitions. The resulting data arrays were exported from GEE for statistical analysis and visualization using Python

(version 2.7, Python Software Foundation, https://www.python.org/) and R (version 3.4.3, R Core Team 2017, https://www.r-project.org/) in Jupyter Notebooks (Kluyver et al. 2016).

2.3.7 Evaluation Functions

We evaluated algorithm performance following Bailey and Werdell (2006) to facilitate comparison to other studies. Statistics relating any satellite to *in situ* values included the median satellite to *in situ* ratio (R_t), the semi-interquartile range (SIQR) and the root mean square difference (RMSD). These metric, though widely used, should be deployed cautiously and in combination with more robust metrics that allow for non-Gaussian distributions and large dynamic ranges (Seegers et al. 2018). Therefore, we also calculated the median absolute percent difference (MAPD). These metrics are defined as:

$$R_t = \text{median}\left(\frac{X^{mod}}{X^{obs}}\right) \quad \text{(Eq. 2.5)}$$

$$SIQR = \frac{Q_3 - Q_1}{2} \quad \text{(Eq. 2.6)}$$

$$RMSD\ (\Psi) = \sqrt{\frac{\sum_{i=1}^{n}(X^{mod} - X^{obs})^2}{n}} \quad \text{(Eq. 2.7)}$$

$$MAPD = \text{median}\left(100 * \frac{|X^{mod} - X^{obs}|}{X^{obs}}\right) \quad \text{(Eq. 2.8)}$$

Where X^{obs} and X^{mod} are the *in situ* and satellite values for each sample point, n is the number of samples, and the Q_1 and Q_3 are the 25th and 75th quartiles respectively. The SIQR demonstrates the spread or uncertainty associated with the satellite-retrieved values and the median ratio captures the overall bias. The Slope (S) and Intercept (I) were estimated by applying a reduced major axis (RMA) type II regression model (R package lmodel2 (Legendre, 2014)) to

accommodate errors in both the field and satellite measurements (Ricker 1973).

$$\text{Slope (S)} = \frac{X^{mod} - 1}{X^{obs}} \quad \text{(Eq. 2.9)}$$

$$\text{Intercept (I)} = X^{mod} - S * X^{obs} \quad \text{(Eq. 2.10)}$$

2.4 Results and Discussion

2.4.1 Underway data quality control

The compiled dataset resulted in > 13,000 measurements over 31 days and 3,000 river kilometers. Measurements were collected over two different hydrologic conditions, Amazon low water (LW) and high water (HW) conditions in a tidally-influenced system and spanned a productivity gradient from the mesotrophic ($0.1 < \text{Chl-}a \leq 1$ mg m^{-3}) Columbia to the eutrophic (Chl-*a* >75 mg m^{-3}) Mississippi (Franz et al. 2005). To our knowledge, this is the first use of high resolution, underway data for evaluating estimates of river turbidity and Chl-*a* from L8. *In situ* values across these rivers revealed large gradients of turbidity (Figure 2.1b-e, Figure 2.2b) at both small (e.g. mainstem versus tributary) and large (e.g. tropical versus temperate coniferous forest biomes) scales.

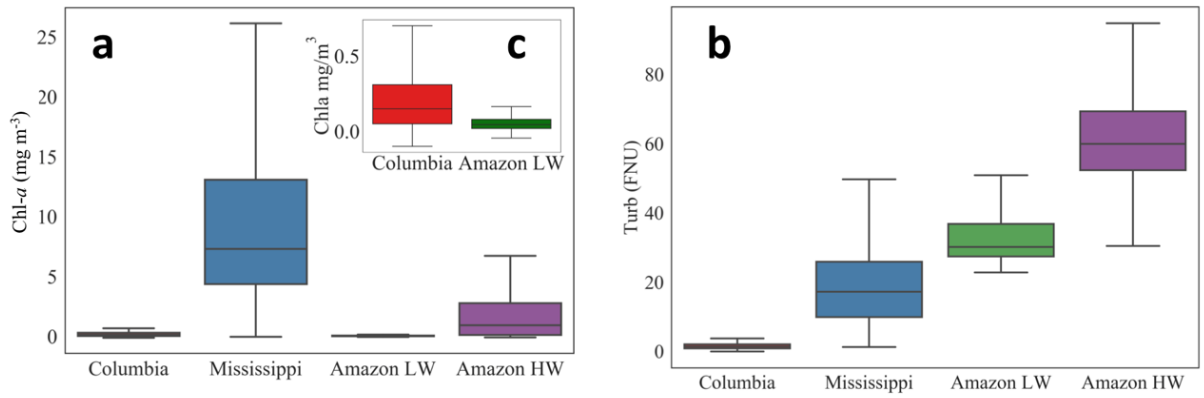

Figure 2.3. Chlorophyll-*a* (a) and turbidity (b) from each cruise. Low Chl-*a* systems (c) included the Columbia River and the Lower Amazon low water cruise.

The dynamic range observed here (Figure 2.3) falls within the range measured at 3,400 marine stations (0.012 – 72.12 mg m^{-3}) as reported in NASA's bio-Optical Marine Algorithm Data set (NOMAD) (Werdell and Bailey 2005) as well as the range from the current largest Chl-*a* ocean color validation set (0 – 100 mg m^{-3}) described by Seeger et al (2018). Therefore, our *in situ* dataset for three major inland rivers falls within the range used to develop satellite-based ocean color products, providing evidence that rivers should fall within the dynamic range used to develop current ocean and coastal water techniques. For the rivers (Mississippi and Columbia) where higher-frequency measurements were binned, the median and standard deviation of the 1-minute bins was 44.7 (4.7 ug/L) and 2.19 (0.37 ug/L) for Chl-*a* and was 26.3 FNU (2.09) FNU and 1.8 (0.12) FNU for the Mississippi and Columbia River respectively. The relatively low standard deviation suggests spatial stability throughout the main stem.

Of the 13,744 field validation points acquired across all cruises, 6,405 spatially coincided with a satellite overpass. Restricting to a 24-hour window reduced the dataset size by 90% (Figure 2.4a). In order to ensure the same sample size for each technique, we included only

pixels that passed all three corrections without masking (Figure 2.4b). Pixels flagged under certain criteria are not processed and this varied by routine.

For example, after masking with the QA band, LaSRC yielded 708 validation points, but ACOLITE and SeaDAS returned valid retrievals for 62% and 37% of those points respectively. This discrepancy is due to the fact that each routine uses a different set of flags, with SeaDAS (32 flags; Hooker et al. 2003) being more detailed in this case than ACOLITE (4 flags).

Less than 1% of samples were excluded due to low coverage (< 5 pixels) inside the sampled 3 X 3 pixel window (Figure 2.4c). The shoreline mask only excluded 8% of pixels (Figure 2.4d), likely because boat surveys generally maintained a steady course in deeper navigation channels and because of the previous coverage filter which reduced sampling window variability.

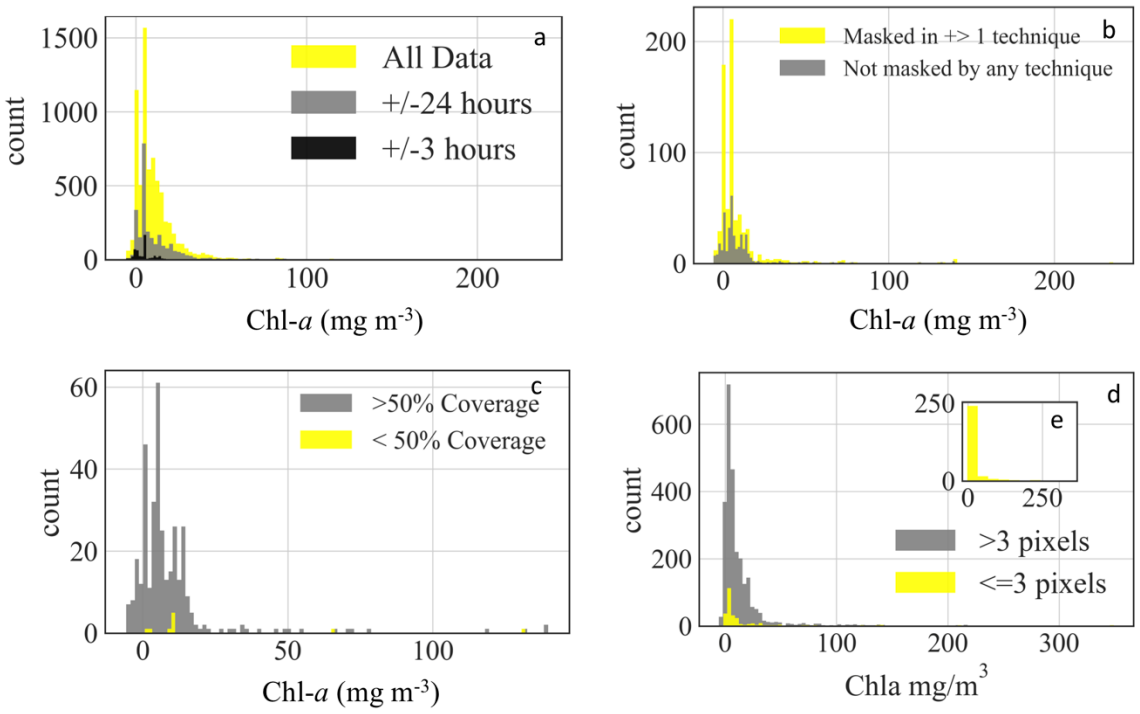

Figure 2.4. Results from quality control procedure. The method used (similar to Brewin et al. 2016; Werdell et al. 2013) resulting in the following: (a) Histogram showing the number of points that spatially coincided with the overpass (yellow) overlaid by those that spatiotemporally coincided within 24 (grey) and 3 (black) hours. (b) Histogram showing the points that escaped flagging across all routines (grey). (c) Histogram showing the distribution of all points remaining after Step 2 (grey) overlaid by the samples excluded because of <50% coverage (i.e. < 5 pixels) inside the 3 X 3 sampling window surrounding each validation point. (d) Step 4: Histogram showing the distribution of points excluded (in yellow) because of their proximity (<=3 pixels) to shore with an inset (e) showing just the distribution of the masked pixels.

2.4.2 Atmospheric correction

Here we will first evaluate the number of failed retrievals, as indicated by negative R_{rs} values, for each correction technique. We then discuss the differences between the land-based and aquatic correction techniques and quantitatively compare those results to field R_{rs} measurements. Finally, we evaluate bias, based on differences from field observations, in the resulting chlorophyll-*a* and turbidity retrievals introduced by each correction.

2.4.2.1 Negative Rrs retrievals

Analysis of L8 and S2 R_{rs} observations over rivers are still relatively rare. Figure 2.5 shows the range of possible R_{rs} values in the green band across the entire river surface captured for the mosaicked images (Table 2.2) before the quality control described in Section 2.3.6. This characterization shows the general performance of the atmospheric corrections before any uncertainties introduced by sampling the data at specific points. Negative retrievals can be an important diagnostic in determining the validity of R_{rs}. Across the dataset, 1% of L8 and 2% of S2 pixels showed $R_{rs} \leq 0$ sr^{-1} in the green bands (Figure 2.5); more negative retrievals were observed in the blue bands (2% L8 and 10% S2), which are known to be sensitive to aerosol selection errors.

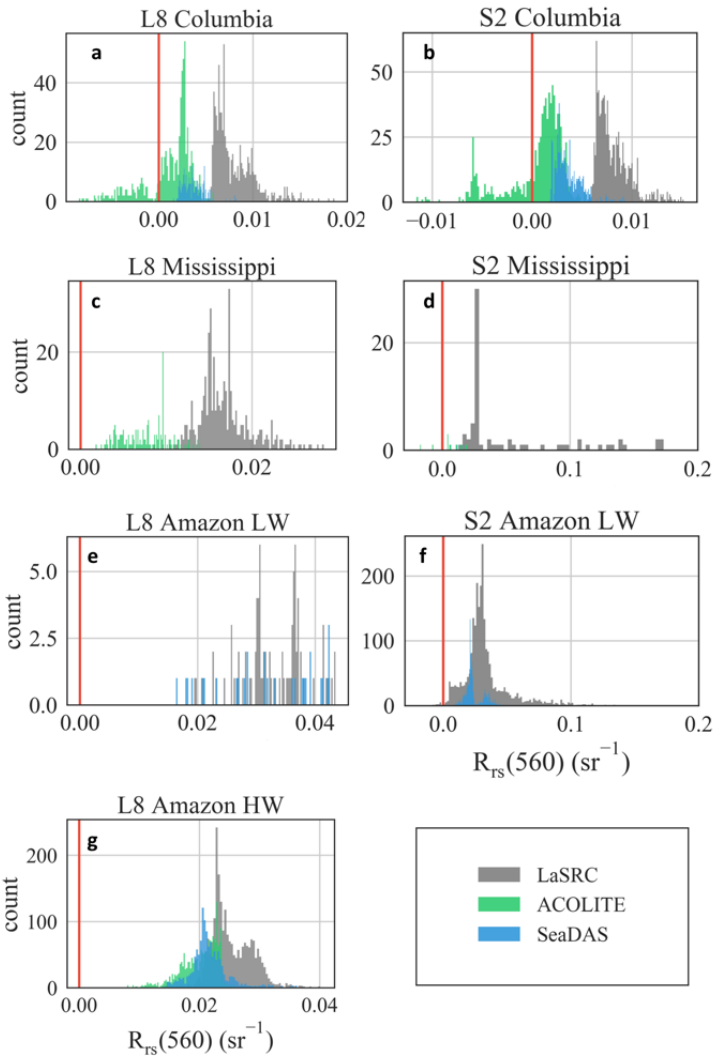

Figure 2.5. Distributions of S2 and L8-derived R_{rs} (sr^{-1}). Here shown for the green channel (560 nm) as estimated by the three atmospheric correction techniques for L8 (a,c,e,g) and S2 (b,d,f). Distributions were derived from images listed in Table 2.2 before any quality control. As noted, L8 and S2 acquisitions are not comparable because they did not occur on the same day and there were no S2 matchups during Amazon HW. The red line indicates zero; points falling below are negative retrievals. Note the change in x-axis between cruises reflective of the large gradient of water types surveyed here.

Negative retrievals can indicate a problem with atmospheric correction. Aquatic correction routines assume any SWIR reflectance to be from aerosols and subtract it as such from the rest of the spectra during the aerosol removal step. This assumption is based on the fact that even very shallow water absorbs longer wavelength light and thus should be dark ($R_{rs} \sim 0$ sr^{-1}) in the SWIR bands (Wang and Shi 2007; Shi and Wang 2009). However, SWIR signals from strong adjacency effects over inland water pixels have been widely documented in most (although not all, see Pahlevan 2018) cases. While SWIR signals over water could be caused by emergent macrophytes (Dogliotti et al. 2018) nearby land pixels contributing SWIR signals are more likely the cause (Richter et al. 2006; Bulgarelli and Zibordi 2018). For example, 96% of negative retrievals were from the Columbia (Figure 2.5a,b), whose shorelines feature steep and bright cliffs. The Amazon LW and Mississippi images had fewer failed returns (< 1%) (Figure 2.5c-f) although adjacency effects are present in the TOA spectra of all rivers in this study.

The negative retrieval rate was twice as high for S2 (5%) than for L8 (2%) in the visible to near-infrared bands (~ 400 – 865 nm). In addition to adjacency effects, another contributing factor could be S2's higher spatial resolution. Smaller pixels resolve smaller wave features (Kay et al. 2009), amplifying the confounding effects of sun glitter. ACOLITE produced the most negative blue band retrievals (14%) relative to SeaDAS (8%) and LaSRC (6%).

After removal of failed retrievals, the resulting spectral plots derived from the scenes listed in Table 2.2 and processed as described in Section 2.3.6 show the top of the atmosphere (TOA) reflectance (unitless) and R_{rs} (sr^{-1}) for the land (LaSRC) and aquatic (SeaDAS and ACOLITE) corrections for L8 (Figure 2.6) and S2 (Figure 2.7). The terrestrial technique produced higher R_{rs} values than aquatic techniques by 36% MAPD, or 0.008 sr^{-1} (Figure 2.6, Figure 2.7), across the L8 and S2 visible and near-infrared bands.

2.4.2.2 Land-based versus aquatic corrections

After removal of failed retrievals, the resulting spectral plots derived from the scenes listed in Table 2.2 and processed as described in 2.3.6 show the top of the atmosphere (TOA) reflectance (unitless) and R_{rs} (sr^{-1}) for the land (LaSRC) and aquatic (SeaDAS and ACOLITE) corrections for L8 (Figure 2.6) and S2 (Figure 2.7). The terrestrial technique produced higher R_{rs} values than aquatic techniques by 36% MAPD, or 0.008 sr−1 (Figure 2.6, Figure 2.7), across the L8 and S2 visible and near-infrared bands.

Clearer waters (Figure 2.6e) showed larger departures between aquatic and terrestrial L8 techniques (0.004 sr^{-1}) in contrast to the turbid Amazon where differences narrowed to 0.001 sr^{-1} (Figure 2.6h) across bands. During the Amazon LW (Figure 2.6g) aquatic and terrestrial methods overlapped, with notably high SeaDAS variability (IQR = 0.01 sr^{-1}) in the 430 – 512 nm range likely resulting from poor image quality. During the more turbid, Amazon HW cruise, techniques converged in the NIR where differences between LaSRC and aquatic techniques closed to 0.0002 sr^{-1}.

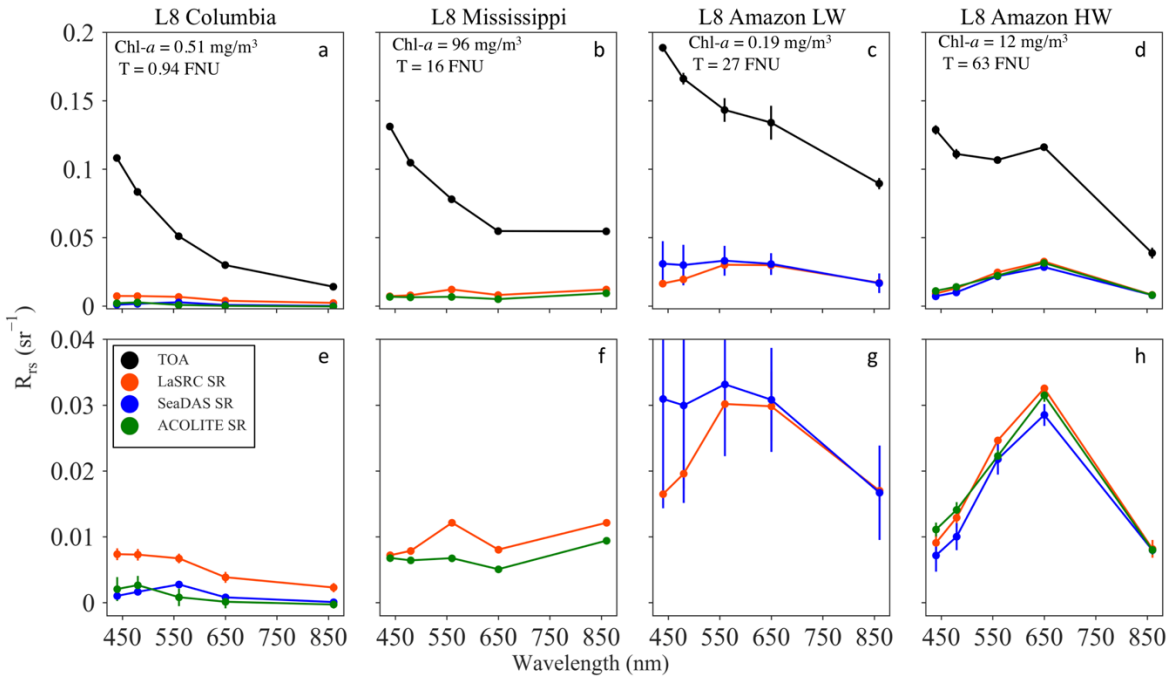

Figure 2.6. L8 TOA and R_{rs}. L8 R_{rs} median spectra and interquartile range (25%, 75%) by river contextualized against TOA values (unitless, top row) and subset to only R_{rs} (bottom row). Median spectra for each river are derived from mosaicked campaign images (Table 2.2) after atmospheric correction and the quality control process described in Section 2.3.6 with a ± 24 h filter to capture adequate samples, (n = 180, 3, 9 and 240) for the Columbia (a, d), the Mississippi (b, f, e), Amazon LW (c, g) and Amazon HW (d, h) respectively. *In situ* values collected on the same day and time as the overpass for mean chlorophyll-*a* (Chl-*a*) and turbidity (T) are shown in the top row for context.

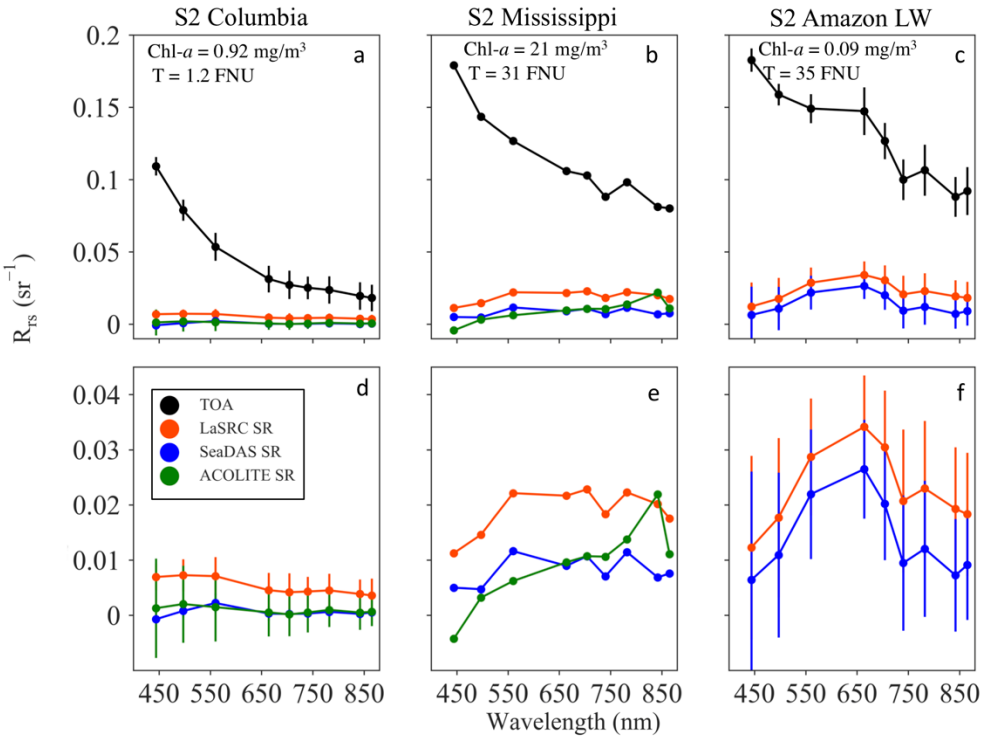

Figure 2.7. S2 river TOA and remote sensing reflectance spectra. Median S2 Rrs spectra and interquartile ranges (25%, 75%) extracted by river contextualized against TOA values (top row) and subset to only remote sensing reflectance (bottom row). Median spectra for each river are derived from mosaicked campaign images after atmospheric correction (Section 2.3.4) and the quality control process described in Section 2.3.6. Resulting median spectra from the quality controlled points (n = 416, 4, and 1305) for the Columbia (a, d), the Mississippi (b, e), and Amazon LW (c, f) respectively. *In situ* values collected on the same day and time as the overpass for Chl-*a* and turbidity are shown in the top rows.

Larger differences were observed in S2. Terrestrial and aquatic techniques diverged by 62%, yielding differences in R_{rs} an order of magnitude higher for S2 (0.01 sr^{-1}) than for L8 (0.003 sr^{-1}). By processor, LaSRC L8 R_{rs} was on average 0.0027 and 0.0031 sr^{-1} greater than ACOLITE and

SeaDAS respectively. For S2 the difference from LaSRC was larger for ACOLITE (0.02 sr^{-1}) but not SeaDAS (0.002 sr^{-1}).

Differences in R_{rs} result from differences in processor assumptions and correction bands. LaSRC estimates aerosols over land using the blue and red bands and extrapolates over water. This assumption would not be appropriate over open ocean waters distant from shore but could be reasonable across the shorter spatial scales relevant to inland waters. In contrast, aquatic techniques assume water absorbs NIR-SWIR strongly and therefore any SWIR reflectance is assigned to aerosols. However, as noted in Section 2.4.2.1., NIR remote sensing reflectance values > 0 sr^{-1} at the water surface were observed in all rivers (Figure 2.6 a-d, Figure 2.7 a-c), likely stemming from adjacency effects or sun and sky glint (Bulgarelli and Zibordi 2018). Thus, while the SWIR-based black pixel assumption might be reasonable even over turbid waters, it becomes problematic for systems with strong adjacency effects such as inland waters. For waterbodies with nearby and/or bright shorelines, strong NIR/SWIR adjacency effects may be too strong for the NIR/SWIR atmospheric correction and consequently terrestrial or alternative methods may perform best.

However, considering the significant methodological differences in approaches, this convergence between aquatic and terrestrial techniques is encouraging and suggests choice of atmospheric correction may be less important when using L8 in highly reflective systems. The range of spectral shapes shown here also fall within that observed within an analysis conducted by Spyrakos et al. (2018) of over 250 inland and coastal water R_{rs} spectra. The differences in spectra across optical gradients observed here are similar to those reported by Jackson et al. (2017) in a recent analysis of a large scale *in situ* R_{rs} and Chl-*a* dataset (OC-CCI v2.0, Valente et al. 2016).

Users must be warned, however, that small differences in spectra can lead to large differences in the absolute accuracy of satellite-retrieved Chl-*a* and turbidity values, especially if the biases are spectrally-dependent. For example, band ratio models could be more impacted by differences in spectral shapes than magnitudes because of their dependence on relative contributions from each band. Here, processors resolved similar spectral shapes despite differences in magnitudes.

2.4.2.3 Aquatic corrections

While the terrestrial and aquatic methods produced spectra of differing magnitudes, the two aquatic corrections agree within 0.0006 sr^{-1} across rivers and sensors. Differences were the smallest (0.001 sr^{-1}) between in the blue and coastal blue bands for the Columbia (Figure 2.6e), for the green (0.0005 sr^{-1}) and NIR bands (0.00004 sr^{-1}) on the Amazon HW (Figure 2.6h).

The difference between sensors was again pronounced, with a much larger gap between aquatic methods spectra for S2 (0.002 sr^{-1}) than for L8 (0.0009 sr^{-1}). Zhang et al. (2018) reported S2 produced higher R_{rs} values than L8 over land. These differences are likely related to environmental conditions or ground sampling resolution and not sensor specifications (Pahlevan et al. 2017a,b). Despite difference between sensors, aquatic method disagreements are small relative to the differences between terrestrial and aquatic techniques. The similarity of these estimates likely stems from their shared use of the NIR-SWIR bands for atmospheric correction, in contrast to land-based methods which uses different targets (dark dense vegetation), bands (blue and red) and assumptions.

Differences between aquatic methods showed spectral dependence. The S2 Mississippi spectra show a green peak (0.02 sr^{-1}) in the LaSRC spectra but not in ACOLITE (Figure 2.7b). The aquatic corrections also vary in L8's green band (560 nm) over the Columbia (Figure 2.6e),

where SeaDAS shows a peak (0.003 sr^{-1}) not observed in the ACOLITE spectra. A similar peak is observed in the S2 SeaDAS data (0.002 sr^{-1}) for the Columbia, despite only moderate *in situ* Chl-*a* (0.5-1 mg/m^{-3}). A major processing difference that could influence these differences is that SeaDAS uses a modeled NIR value from iterative NIR processing while ACOLITE uses the NIR bands as given. While these spectral differences, as stated before, are likely to impact bio-optical models, the remote sensing reflectance estimated by these two aquatic techniques remain on the same order of magnitude.

2.4.2.4 Validation of remote sensing reflectance

Radiometric measurements for R_{rs} validation were collected during Amazon high and low water coincident to L8 acquisitions (Table 2.2, Figure 2.8). Unfortunately, no coincident S2 overpasses occurred. *In situ* measurements show peaks (0.03 – 0.04 sr^{-1}) in the red and near-infrared characteristic of highly scattering waters (Figure 2.8) and strong absorption in the shorter wavelengths due to organic matter. These spectra show agreement with the shape and range (0 – 0.02 sr^{-1}) measured over turbid Amazon floodplain lakes (Martins et al. 2017) and coastal waters (0 – 0.035 sr^{-1}) influenced by the Amazon (Froidefond et al. 2002).

In comparisons to *in situ* radiometry (Figure 2.8), LaSRC had the best agreement with an average MAPD across the spectrum of 17% (low water) and 4% (high water) with a RMSD as low as 0.001 sr^{-1} during high water. This is approaching the +/- 5% uncertainty benchmark often cited as a target for clear water radiances and bottom-of-the-atmosphere reflectance (Drusch et al. 2012; Bailey and Werdell 2006; Hooker et al. 1992). LaSRC also showed less uncertainty than the aquatic techniques evidenced by a narrower SIQR (Table 2.3).

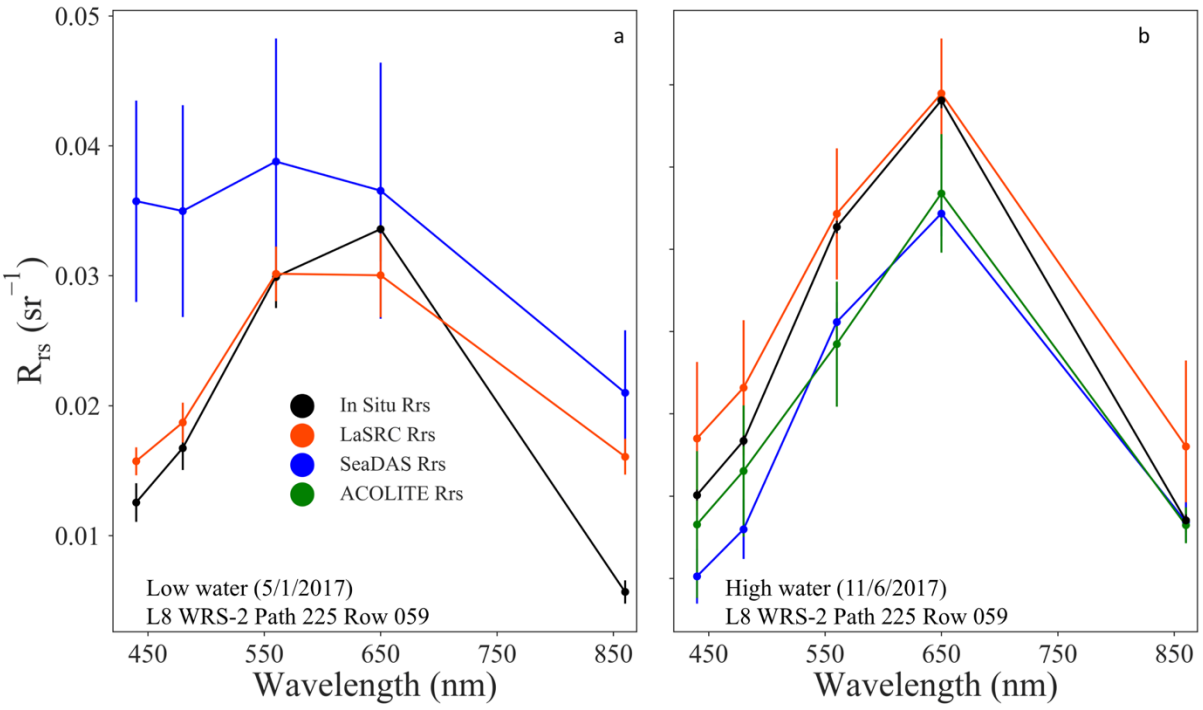

Figure 2.8. Satellite R_{rs} shown with *in situ* R_{rs}. Median spectra and interquartile range (25%, 75%) for resampled *in situ* radiometry in comparison to coincident L8 R_{rs} over the Amazon River during low water (a) and high water (b). Each overpass date and WRS-2 path/row are listed below the spectra. Hyperspectral *in situ* radiometry was collected at stationary stations on L8 overpass dates as listed on the plot and in Table 2.2.

Aquatic techniques for the scenes analyzed here showed reasonable spectra with the exception of SeaDAS LW (Figure 2.8a,b). Median ratios were $0.82 < R_t < 1.17$ with the SIQR indicating uncertainties of < 0.30 except for SeaDAS (Table 2.3). No valid pixels coincident with field measurements were retrieved by ACOLITE during low water due to SWIR masking. During Amazon (HW) where all three corrections were available, ACOLITE MAPD (~8%) fell between LaSRC and SeaDAS. SeaDAS showed the least agreement with *in situ* measurements (MAPD of ~ 17 - 79%). These results fall within the range reported by Wei et al. (2018) for L8

as corrected by both SeaDAS and ACOLITE using the NIR/SWIR method over optically shallow and turbid waters, although ACOLITE shows higher performance here, possibly because this study used a fixed epsilon and a SWIR mask whereas Wei et al. (2018) used a per-pixel epsilon and did not specify use of a SWIR mask. Differences in these processing options could lead to higher MAPDs, especially because of the relatively low signal-to-noise ratios of the SWIR bands. RMSD ranged an order of magnitude (0.001- 0.01 sr^{-1}) but across both cruises LaSRC had a lower RMSD than either aquatic technique. For example, LaSRC showed an order of magnitude lower RMSD than SeaDAS during LW and 50% and 75% lower RMSD than ACOLITE and SeaDAS during HW.

Table 2.3. Validation statistics for L8 atmospheric correction techniques over the Amazon river for the low (LW) and high water (HW) seasons for the OLI across the VNIR bands.

Cruise	Correction	R_t (SIQR)	MAPD (%)	RMSD (sr^{-1})	Slope	r^2
LW	SeaDAS	1.79 (1.35)	79.39	0.01	0.46	0.52
LW	LaSRC	1.17 (0.30)	16.76	0.005	0.58	0.92
HW	ACOLITE	0.95 (0.13)	8.15	0.002	0.84	0.98
HW	SeaDAS	0.82 (0.09)	17.36	0.004	0.85	0.99
HW	LaSRC	0.96 (0.05)	3.87	0.001	0.95	1.00

During high water, *in situ* R_{rs} was underestimated by the aquatic technique and the terrestrial technique overestimates. During low water the bias varied spectrally. For example, satellite-retrieved reflectance was higher than *in situ* data in the blue and NIR during Amazon LW (Figure 2.8a). Adjacency effects could explain why the NIR signal observed from space is

higher than *in situ* values (Bulgarelli and Zibordi 2018). The presence of strong glint could also contribute additional NIR signal as observed by both field and satellite measurements.

Glint, a common issue for L8 and S2, could contribute additional scattered light to the satellite-observed signal and is currently not corrected for over turbid waters by most standard approaches. Glint-removal methods are predominantly developed for clear-water marine systems yet can profoundly influence R_{rs} estimates (Gilerson et al. 2018). For water retrievals, glint corrections can cause up to 43% MAPD in R_{rs}, significantly impacting the resulting Chl-*a* retrievals (Garaba et al. 2015). Little research exists on this topic for inland waters, although Overstreet and Legleiter (2017) evaluated glint corrections over shallow rivers and Brando et al. (2016) evaluated glint effects in underway river samples. Harmel et al. (2018) developed a glint correction that reduced bias between *in situ* and satellite R_{rs} by 60%. However, neither *in situ* nor satellite observations over turbid waters are currently glint corrected in standard approaches, representing a major limitation.

In the opposite case, negative bias in the aquatic techniques was observed in comparison to field measurements during the Amazon high water cruise. The underestimation could be due to overcorrection resulting from adjacency effects or other factors such as cloud shadows observed in some areas of the scene and absorbing aerosols. Absorbing aerosols are not accounted for in current aerosol models (Gordon and Wang 1994) but are common in coastal zones. Absorbing aerosols are known to vary seasonally over the Amazon river mouth due to agricultural burning (Herman et al. 1997). These factors could all contribute to underestimation in the shorter wavelengths (440 and 480 nm) as observed in the high water cruise (Figure 2.8b). It is also important to note the bidirectional reflectance effects, which are not considered or corrected for in these routines, could also add to discrepancies between field and satellite

observations.

While the terrestrial approach, LaSRC, showed the closest match with field spectra, radiometry was not available from the Columbia and Mississippi so the relative difference between satellite and *in situ* R_{rs} over less turbid waters remains unknown. The larger gap between techniques over the Columbia suggest that comparisons to field radiometry over clearer inland waters should be a research priority.

2.4.3 Chlorophyll-a and turbidity

We examined the sensitivity and absolute accuracy of satellite-retrieved concentrations to atmospheric correction by comparing satellite and *in situ* measurements of Chl-*a* and turbidity for cruises in which both aquatic techniques were available (see Figure 2.8 for WRS Path/Row), which includes the L8 images acquired during the Columbia and Amazon HW cruises.

2.4.3.1 Chlorophyll-a sensitivity to atmospheric correction

Overall, SeaDAS-derived Chl-*a* estimates were on average 2.7 times higher than ACOLITE and twice as high as field measurements Figure 2.9. For example, the 0.002 sr^{-1} and 0.001 sr^{-1} difference between SeaDAS and ACOLITE in the green and blue bands resulted in a difference of 6 mg m^{-3} Chl-*a*. Satellite-derived Chl-*a* estimates from SeaDAS and LaSRC overestimated Chl-*a* by ~4.7 mg m^{-3} and 0.6 mg m^{-3}, with median ratios exceeding 1 (Figure 2.9, Table 2.4).

The absolute percent difference for SeaDAS (MAPD =59%) was higher than ACOLITE (MAPD = 30%) and LaSRC (MAPD = 32%), with SeaDAS-derived Chl-*a* in some cases being overestimated by an order of magnitude in the mesotrophic waters of the Columbia River. ACOLITE products underestimated Chl-*a* by ~ 1.29 mg m^{-3} across both rivers but approximated

field values more closely than SeaDAS; for the Columbia river ACOLITE and *in situ* Chl-*a* distributions were not significantly different (p-value = 0.1).

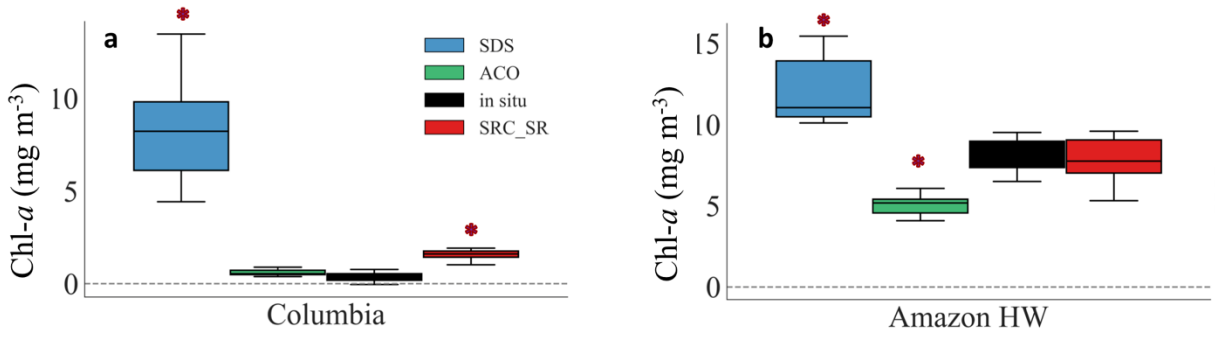

Figure 2.9. Landsat-derived Chl-a in comparison to *in situ* measurements. Given by river for the Columbia (a) and Amazon High Water (b) based on median of images for each river as listed in Table 2.2. Note the y-axis change. Red dots indicate significant difference from field measurements (p-value > 0.01) While TOA images are available for all the rivers, cloud masking and invalid pixel flagging result in low pixel counts and thus no paired, valid pixels for the Mississippi and Amazon LW.

As all three estimates were made using the same bio-optical algorithm (OC3), the major factor controlling these differences is the reflectance product used as an input and the underlying atmospheric correction processors used to generate those reflectance products. The consistent overestimation by SeaDAS directly results from the differences in blue and green bands (Section 2.4.2.2 – 2.4.2.3) observed in the reflectance spectra. In this case, higher remote sensing reflectance accuracies over the Amazon resulted in satellite-retrieved Chl-*a* values close to field measurements.

Table 2.4. Combined difference metrics (n = 320) compared *in situ* to satellite-retrieved chlorophyll-*a* (Chl-*a*) and turbidity (T) from both correction routines for data acquired within 24 hours.

Correction	MAPD (%)	R_t	RMSD	Parameter	Time Difference
ACO	30	0.70	0.13	Chl-*a*	+/- 3
SDS	59	1.59	0.30	Chl-*a*	+/- 3
LaSRC	32	1.32	0.08	Chl-*a*	+/- 3
ACO	3	1.03	0.22	T	+/- 3
SDS	13	0.86	0.15	T	+/- 3
LaSRC	35	1.35	0.48	T	+/- 3

The differences we observe here in these river systems are equivalent to those observed in other systems. For example, Dörnhöfer et al. (2018) also used a multisensory approach to estimate Chl-*a* over German Lakes resulting in RMSD's of between 3.6 to 19.7 mg m^{-3} with errors varying between L8 and S2 sensors. Regardless of correction, differences from *in situ* measurements are lower than the factor of five commonly reported as seen in global ocean empirically-based Chl-*a* satellite retrievals (Dierssen and Karl 2010a) and fall below, with the exception of SeaDAS, the 40% error reported for the widely-used OC4v4 standard Chl-*a* product (Laliberté et al. 2018), where errors were also largest in waters with <0.5 mg m^{-3} Chl-*a*. It is important to note that the established OC3 coefficients were calibrated in reference to high performance liquid chromatography pigments (HPLC) whereas our underway validation data is derived from instantaneous fluorometers.

Where matchups were available at the exact moment of the satellite overpass, we

conducted an sensitivity analysis to quantify changes in accuracies resulting from using more or less restrictive time windows. Boucher et al. (2016) showed using a time window of 2 instead of 5 days improved agreement between L8-retrieved and *in situ* Chl-*a* values in northeastern lakes. In this study, using a time window of +/- 3 instead of 24 hours reduced differences by 5% (ACOLITE) and 31% (SeaDAS) for Chl-*a*.

The blue green Chl-*a* algorithms tested here are designed for systems in which Chl-*a* is the dominant absorber. Consequently, in optically complex waters combinations of other components can result in a false Chl-*a* signal. For example, in terrestrially-influenced waters, non-algal particles and CDOM can also absorb in shorter wavelengths, changing the blue-green ratio and therefore overestimating Chl-*a*. Non-algal particles and CDOM can also contribute fluorescence, resulting in an overestimation of fluorometric Chl-*a* (Roesler et al. 2017). For turbid systems like the Amazon, CDOM and suspended matter absorbs strongly in shorter wavelengths, creating a green peak even in the absence of Chl-*a*. Valerio et al. (2018) reported CDOM absorption coefficients at 412 nm between 1.0-7.0 m^{-1} in non-turbid tributaries and the mainstem. The sensitivity of results to correction techniques, sensors and bio-optical model choice shown here indicates that satellite-retrieved Chl-*a* values should be interpreted with great caution in optically complex waters, especially because the relatively wide L8 bands are less than optimal for detecting aquatic signals in optically complex environments.

2.4.3.2 Turbidity sensitivity to atmospheric correction

In contrast to Chl-*a*, for turbidity SeaDAS and ACOLITE show greater agreement with *in situ* measurements (Figure 2.10). Differences between satellite-retrieved and measured values range from underestimates of 13 FNU (SeaDAS) to overestimates of 12 FNU (LaSRC). Over the Columbia ACOLITE and SeaDAS-derived turbidity were statistically similar to *in situ*

measurements (p-value = 0.02) (Figure 2.10a). LaSRC had a larger mean absolute difference to *in situ* measurements (35%) than ACOLITE (3%) or SeaDAS (13%) (Table 2.4) with larger differences observed at higher turbidities (Figure 2.10b).

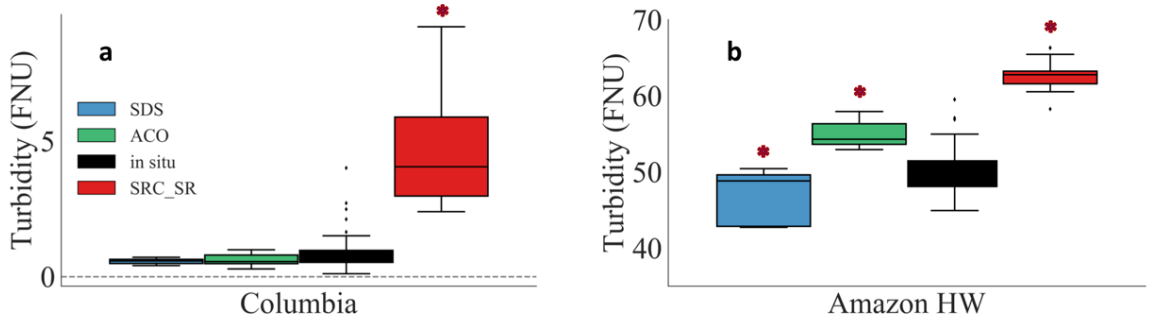

Figure 2.10. Average Landsat-derived estimates of turbidity in comparison to *in situ* measurements. Scene ID's can be found in Table 2.2. The red dot indicates distributions that are statistically different from field measurements (p-value < 0.01).

Over the Amazon, the range of satellite-retrieved turbidity (mean = 47 – 62 FNU) bracketed *in situ* values (mean = 50 FNU). Surprisingly, however, the R_{rs} spectra with the lowest MAPD across the spectral for Amazon HW did not result in the most accurate turbidity estimate. LaSRC over-predicted turbidity across both rivers which follows from high red band peaks (Figure 2.5). Turbidity derived from *in situ* radiometry (636 - 673 nm) was also overestimated (70 FNU) in reference to direct measurements (50 FNU). Thus both satellite and *in situ* reflectance values overestimate turbidity. This could result from additional contributions in the red from surface glint that could be addressed in future studies through the use of in-water radiometry or could also potentially be remedied by revisiting the turbidity algorithm calibration coefficients or using longer wavelengths (Dogliotti et al. 2015; Novoa et al. 2017).

The turbidity algorithm used here is directly comparable across platforms and thus

differences can be mainly attributable to the atmospheric correction and performance of the bio-optical algorithm across a wide dynamic range. Inconsistencies in radiometric calibration between the two sensors are expected to contribute no more than 6% of total uncertainty (Pahlevan et al. 2019). The wide range of turbidities observed in this study suggests a blended approach that utilizes different algorithms at different reflectance ranges such as used for Chl-*a* (Hu et al. 2012) may be necessary to map turbidity across the entire dynamic range.

While turbidity is not a direct measure of a biogeochemical quantity (Boss et al. 2009), its relative ease of measurement, including through crowd-sourced smartphone apps (Leeuw and Boss 2018) and usefulness for water quality monitoring (Nechad et al. 2009; Dogliotti et al. 2015) makes it a practical candidate for satellite remote sensing of aquatic optical conditions. These results show that while absolute accuracies of retrievals still require improvement, bio-optical algorithms are broadly able to discriminate between rivers with significantly different optical types.

2.5 Summary and Further Work

This study highlights innovative underway field techniques used in combination with L8 and S2 satellite imagery to identify uncertainties in river remote sensing. We show that while all three corrections result in spectra on the same order of magnitude in most cases, the terrestrial atmospheric correction method produces a 36% greater R_{rs} than aquatic techniques. The two aquatic approaches agree within 0.0006 sr^{-1} but that varied by band, which in turn influences satellite-derived Chl-*a* and turbidity estimates. Where radiometric data were available, the atmospheric corrections performed sufficiently well at retrieving riverine R_{rs}, achieving mean absolute differences as low as 4% relative to field measurements in turbid waters. When

combined with bio-optical models, these R_{rs} estimates can be useful for examining broad gradients in spatial patterns of Chl-*a* and turbidity.

However, we strongly advise the cautious interpretation of these results because of uncertainties inherent to water color remote sensing that have yet to be resolved. Specifically, we advise future work on river remote sensing should occur in four major areas, especially as the application of remote sensing for water resource management applications is an increasing priority (McClain and Meister 2012).

First, our findings show terrestrial correction techniques were able to resolve R_{rs} over the Amazon River comparably to aquatic methods, likely because adjacency effects undermine SWIR-based aquatic correction approaches and despite the fact that terrestrial techniques do not correct for glint. To test this interaction, radiometric measurements over a range of river conditions is needed in addition to research examining adjacency effects. For example, (De Keukelaere et al. (2018) show improved reflectance results using an L8/S2 atmospheric correction framework (iCOR) designed to work over inland waters with an explicit adjacency correction (Sterckx et al. 2015). More radiometric validation data, especially over oligotrophic systems, is a major research need. Such measurements are required to constrain estimates of R_{rs} and to develop retrieval algorithms with sufficient absolute accuracy (Werdell et al. 2018).

Next, the assumptions and limitations of standard bio-optical retrieval methods need to be systematically re-evaluated in the context of rivers. While algorithms can resolve large differences in signals between systems, uncertainties in their quantitative, absolute accuracy must not be ignored (Pahlevan et al 2016) especially because the wide bandwidths of the L8 and S2 sensors make them less than optimal for detecting aquatic signals in optically complex environments. A need exists to compare algorithm performance, especially across missions, to

achieve product continuity (Mouw et al. 2015) and advance the field of inland water remote sensing. A first step is the development of sensor-agnostic, open source bio-optical models that can take outputs from a range of correction processors. This will accelerate testing over a wider range of sensors and water types.

Global measurements of river inherent optical properties are needed to inform a process-based understanding of the relationship between river biogeochemistry, optical conditions and remote sensing reflectance. More geographically diverse radiometric and inherent optical property (e.g. particle backscattering coefficients, absorptions coefficients, diffuse attenuation) measurements are required. Fully understanding river productivity requires field measurements of parallel optical and biogeochemical properties. For example, although Chl-*a* is generally low in the Amazon River main stem, evidence from dissolved oxygen stable isotopes suggest that primary production may still be occurring at up to 50% the rate of respiration (Gagne-Maynard et al. 2017). Establishing turbidity, CDOM and non-algal particle concentration thresholds for the use of blue/green chlorophyll-*a* algorithms could prevent the masking of chlorophyll-*a* by sediments and the overestimation of chlorophyll-*a* caused by the presence of non-algal particles and CDOM. Spyrakos et al. (2018) has made progress in classifying inland waters by their reflectance, which could be one approach to developing flexible bio-optical retrieval algorithms such as available for the open oceans. Future research is required to determine the dynamic range of river optical properties, their relationship to biogeochemistry, and their influence on remote sensing reflectance.

Finally, in addition to uncertainty from retrieval algorithms, a fourth major difficulty is establishing time benchmarks between field and satellite measurements in rivers, especially those influenced by short duration processes such as tides. We show constraining matchups to within 3

hours can improve satellite-retrieved and *in situ* Chl-*a* agreement by more than 30%, yet many large-scale sampling campaigns are still designed without consideration for overpass schedules. The mismatch in time scales between river processes (hours to days) and sensor return (5 to 16 days) times is a major limitation of current moderate to high resolution satellite missions. We have attempted to address that here by collecting underway data and using a strict data quality control process, but it is worth noting such efforts significantly reduce sample size (by 90%) and consequent statistical power. National, regional and local water quality programs should coordinate sampling with satellite overpasses. Future sensors should combine moderate spatial resolutions (<100 m) with more frequent revisit periods (hours to days) (Muller-Karger et al. 2018). Standardization of underway optical measurements for remote sensing through community protocols is in progress for the ocean (Werdell et al. 2013; Boss et al. 2018). Developing similar protocols for inland water surveys would improve comparability across studies and provide datasets of sufficient volume for inland water remote sensing calibration and validation.

2.6 REFERENCES

Ahmad, Ziauddin, Bryan A Franz, Charles R McClain, Ewa J Kwiatkowska, Jeremy Werdell, Eric P Shettle, and Brent N Holben. 2010. "New Aerosol Models for the Retrieval of Aerosol Optical Thickness and Normalized Water-Leaving Radiances from the SeaWiFS and MODIS Sensors over Coastal Regions and Open Oceans." *Applied Optics* 49 (29): 5545–60.

Aiken, James, and Stanford Hooker. 1997. "The Atlantic Meridional Transect: Spatially Extensive Calibration and Validation of Optical Properties and Remotely Sensed Measurements of Ocean Colour." Alliance of Marine Remote Sensing.

Bailey, Sean W., and P. Jeremy Werdell. 2006. “A Multi-Sensor Approach for the on-Orbit Validation of Ocean Color Satellite Data Products.” *Remote Sensing of Environment* 102 (1–2): 12–23.

Barnes, Brian B, and Chuanmin Hu. 2016. “Dependence of Satellite Ocean Color Data Products on Viewing Angles: A Comparison between SeaWiFS, MODIS, and VIIRS.” *Remote Sensing of Environment* 175 (March): 120–29.

Boss, E., S. Ackleson, B. Balch, A. Chase, G. Dall’Olmo, S. Freeman, J. N. Haëntjens, et al. 2018. “Inherent Optical Property Measurements and Protocols: Best Practices for the Collection and Processing of Ship-Based Underway Flow-through Optical Data.” http://ioccg.org/wp-content/uploads/2017/11/inline_report_15nov2017.pdf.

Boss, Emmanuel, Lisa Taylor, Sherryl Gilbert, Kjell Gundersen, Nathan Hawley, Carol Janzen, Tom Johengen, Heidi Purcell, Charles Robertson, and Daniel W H Schar. 2009. “Comparison of Inherent Optical Properties as a Surrogate for Particulate Matter Concentration in Coastal Waters.” *Limnology and Oceanography: Methods* 7 (11): 803–10.

Boucher, J M, K C Weathers, H Norouzi, S Prakash, and S J Saberi. 2016. “Assessing the Effectiveness of Landsat 8 Chlorophyll-*a* Retrieval Algorithms for Regional Freshwater Management.” Ecological applications 28.4 (2018): 1044-1054.

Brando, Vittorio E, Jenny L Lovell, Edward A King, David Boadle, Roger Scott, and Thomas Schroeder. 2016. “The Potential of Autonomous Ship-Borne Hyperspectral Radiometers for the Validation of Ocean Color Radiometry Data.” *Remote Sensing* 8 (2): 150.

Brewin, Robert J W, Giorgio Dall’Olmo, Silvia Pardo, Virginie van Dongen-Vogels, and Emmanuel S Boss. 2016. “Underway Spectrophotometry along the Atlantic Meridional Transect Reveals High Performance in Satellite Chlorophyll Retrievals.” *Remote Sensing of*

Environment 183: 82–97.

Bulgarelli, Barbara, and Giuseppe Zibordi. 2018. "On the Detectability of Adjacency Effects in Ocean Color Remote Sensing of Mid-Latitude Coastal Environments by SeaWiFS, MODIS-A, MERIS, OLCI, OLI and MSI." *Remote Sensing of Environment* 209: 423–38.

Carr, Mary-Elena, Marjorie A M Friedrichs, Marjorie Schmeltz, Maki Noguchi Aita, David Antoine, Kevin R Arrigo, Ichio Asanuma, Olivier Aumont, Richard Barber, and Michael Behrenfeld. 2006. "A Comparison of Global Estimates of Marine Primary Production from Ocean Color." *Deep Sea Research Part II: Topical Studies in Oceanography* 53 (5): 741–70.

Crawford, John T., Luke C. Loken, Emily H. Stanley, Edward G. Stets, Mark M. Dornblaser, and Robert G. Striegl. 2016. "Basin Scale Controls on CO 2 and CH 4 Emissions from the Upper Mississippi River." *Geophysical Research Letters*, 43(5), 1973-1979.

Crawford, John T, David E Butman, Luke C Loken, Philipp Stadler, Catherine Kuhn, and Robert G Striegl. 2017. "Spatial Variability of CO2 Concentrations and Biogeochemistry in the Lower Columbia River." *Inland Waters* 7 (4): 417–27.

Dall'Olmo, G, T K Westberry, M J Behrenfeld, Emmanuel Boss, and W H Slade. 2009. "Significant Contribution of Large Particles to Optical Backscattering in the Open Ocean." *Biogeosciences* 6 (6): 947–67.

Dierssen, Heidi M. 2010. "Perspectives on Empirical Approaches for Ocean Color Remote Sensing of Chlorophyll in a Changing Climate." *Proceedings of the National Academy of Sciences* 107 (40): 17073–78.

Dierssen, Heidi M, and David M Karl. 2010. "Perspectives on Empirical Approaches for Ocean Color Remote Sensing of Chlorophyll in a Changing Climate." *Proceedings of the National*

Academy of Sciences 107 (40): 17073–78..

Dogliotti, A I, K Ruddick, B Nechad, and C Lasta. 2011. "Improving Water Reflectance Retrieval from MODIS Imagery in the Highly Turbid Waters of La Plata River." In *Proceedings of the VI International Conference Current Problems in Optics of Natural Waters (ONW'2011), St. Petersburg, Russia*, 6–9.

Dogliotti, Ana, Juan Gossn, Quinten Vanhellemont, and Kevin Ruddick. 2018. "Detecting and Quantifying a Massive Invasion of Floating Aquatic Plants in the Río de La Plata Turbid Waters Using High Spatial Resolution Ocean Color Imagery." *Remote Sensing* 10 (7): 1140.

Dogliotti, Ana Inés, K G Ruddick, B Nechad, D Doxaran, and E Knaeps. 2015. "A Single Algorithm to Retrieve Turbidity from Remotely-Sensed Data in All Coastal and Estuarine Waters." *Remote Sensing of Environment* 156: 157–68.

Dörnhöfer, Katja, Philip Klinger, Thomas Heege, and Natascha Oppelt. 2018. "Multi-Sensor Satellite and *in situ* Monitoring of Phytoplankton Development in a Eutrophic-Mesotrophic Lake." *Science of The Total Environment* 612: 1200–1214.

Dörnhöfer, Katja, and Natascha Oppelt. 2016. "Remote Sensing for Lake Research and Monitoring–Recent Advances." *Ecological Indicators* 64: 105–22.

Doxani, Georgia, Eric Vermote, Jean-Claude Roger, Ferran Gascon, Stefan Adriaensen, David Frantz, Olivier Hagolle, André Hollstein, Grit Kirches, and Fuqin Li. 2018. "Atmospheric Correction Inter-Comparison Exercise." *Remote Sensing* 10 (2): 352.

Drusch, M., U. Del Bello, S. Carlier, O. Colin, V. Fernandez, F. Gascon, B. Hoersch, et al. 2012. "Sentinel-2: ESA's Optical High-Resolution Mission for GMES Operational Services." *Remote Sensing of Environment* 120 (May): 25–36.

Fay, Amanda R., and Galen A. McKinley. 2017. "Correlations of Surface Ocean PCO_2 to

Satellite Chlorophyll on Monthly to Interannual Timescales." *Global Biogeochemical Cycles* 31 (3): 436–55.

Fichot, Cédric G, Bryan D Downing, Brian A Bergamaschi, Lisamarie Windham-Myers, Mark Marvin-DiPasquale, David R Thompson, and Michelle M Gierach. 2015. "High-Resolution Remote Sensing of Water Quality in the San Francisco Bay–Delta Estuary." *Environmental Science & Technology* 50 (2): 573–83.

Foga, Steve, Pat L Scaramuzza, Song Guo, Zhe Zhu, Ronald D Dilley, Tim Beckmann, Gail L Schmidt, John L Dwyer, M Joseph Hughes, and Brady Laue. 2017. "Cloud Detection Algorithm Comparison and Validation for Operational Landsat Data Products." *Remote Sensing of Environment* 194: 379–90.

Franz, Bryan A, Sean W Bailey, Norman Kuring, and P Jeremy Werdell. 2015. "Ocean Color Measurements with the Operational Land Imager on Landsat-8: Implementation and Evaluation in SeaDAS."

Franz, Bryan A, P Jeremy Werdell, Gerhard Meister, Sean W Bailey, Robert E Eplee, Gene C Feldman, Ewa J Kwiatkowska, Charles R McClain, Frederick S Patt, and Donna Thomas. 2005. "The Continuity of Ocean Color Measurements from SeaWiFS to MODIS." In *Earth Observing Systems X*, 5882:58820W. International Society for Optics and Photonics.

Froidefond, Jean-Marie, Laure Gardel, Daniel Guiral, Mario Parra, and Jean-François Ternon. 2002. "Spectral Remote Sensing Reflectances of Coastal Waters in French Guiana under the Amazon Influence." *Remote Sensing of Environment* 80 (2): 225–32.

Gagne-Maynard, William C, Nicholas D Ward, Richard G Keil, Henrique O Sawakuchi, Alan C Da Cunha, Vania Neu, Daimio C Brito, Diani F Da Silva Less, Joel E M Diniz, and Aline De Matos Valerio. 2017. "Evaluation of Primary Production in the Lower Amazon River

Based on a Dissolved Oxygen Stable Isotopic Mass Balance." *Frontiers in Marine Science* 4: 26.

Garaba, Shungudzemwoyo P, Daniela Voß, Jochen Wollschläger, and Oliver Zielinski. 2015. "Modern Approaches to Shipborne Ocean Color Remote Sensing." *Applied Optics* 54 (12): 3602–12.

Gilerson, Alexander, Carlos Carrizo, Robert Foster, and Tristan Harmel. 2018. "Variability of the Reflectance Coefficient of Skylight from the Ocean Surface and Its Implications to Ocean Color." *Optics Express* 26 (8): 9615–33.

Gordon, Howard R. 1978. "Removal of Atmospheric Effects from Satellite Imagery of the Oceans." *Applied Optics* 17 (10): 1631–36.

Gordon, Howard R, and Menghua Wang. 1994. "Retrieval of Water-Leaving Radiance and Aerosol Optical Thickness over the Oceans with SeaWiFS: A Preliminary Algorithm." *Applied Optics* 33 (3): 443–52.

Gorelick, Noel, Matt Hancher, Mike Dixon, Simon Ilyushchenko, David Thau, and Rebecca Moore. 2017. "Google Earth Engine: Planetary-Scale Geospatial Analysis for Everyone." Remote Sensing of Environment 202: 18-27.

Goyens, Clémence, Cédric Jamet, and T Schroeder. 2013. "Evaluation of Four Atmospheric Correction Algorithms for MODIS-Aqua Images over Contrasted Coastal Waters." *Remote Sensing of Environment* 131: 63–75.

Hadjimitsis, Diofantos G, C R I Clayton, and V S Hope. 2004. "An Assessment of the Effectiveness of Atmospheric Correction Algorithms through the Remote Sensing of Some Reservoirs." *International Journal of Remote Sensing* 25 (18): 3651–74.

Harmel, Tristan, Malik Chami, Thierry Tormos, Nathalie Reynaud, and Pierre-Alain Danis.

2018. “Sunglint Correction of the Multi-Spectral Instrument (MSI)-SENTINEL-2 Imagery over Inland and Sea Waters from SWIR Bands.” *Remote Sensing of Environment* 204: 308–21.

Herman, J R, P K Bhartia, Or Torres, C Hsu, C Seftor, and E Celarier. 1997. “Global Distribution of UV-absorbing Aerosols from Nimbus 7/TOMS Data.” *Journal of Geophysical Research: Atmospheres* 102 (D14): 16911–22.

Hestir, Erin Lee, Vittorio E Brando, Mariano Bresciani, Claudia Giardino, Erica Matta, Paolo Villa, and Arnold G Dekker. 2015. “Measuring Freshwater Aquatic Ecosystems: The Need for a Hyperspectral Global Mapping Satellite Mission.” *Remote Sensing of Environment* 167: 181–95.

Hooker, Stanford B, Elaine R Firestone, Wayne E Esaias, Gene C Feldman, Watson W Gregg, and Charles R Mcclain. 1992. “SeaWiFS Technical Report Series. Volume 1: An Overview of SeaWiFS and Ocean Color.” 1: 34.

Hooker, Stanford, Elaine R Firestone, Frederick S Patt, Robert A Barnes, Robert E Eplee Jr, Bryan A Franz, Wayne D Robinson, Gene Carl Feldman, and Sean W Bailey. 2003. “Algorithm Updates for the Fourth SeaWiFS Data Reprocessing.” NASA Center for AeroSpace Information.

Hu, Chuanmin, Zhongping Lee, and Bryan Franz. 2012. “Chlorophyll Algorithms for Oligotrophic Oceans: A Novel Approach Based on Three-band Reflectance Difference.” *Journal of Geophysical Research: Oceans* 117 (C1).

Irons, James R, John L Dwyer, and Julia A Barsi. 2012. “The next Landsat Satellite: The Landsat Data Continuity Mission.” *Remote Sensing of Environment* 122: 11–21.

Jackson, Thomas, Shubha Sathyendranath, and Frédéric Mélin. 2017. “An Improved Optical

Classification Scheme for the Ocean Colour Essential Climate Variable and Its Applications." *Remote Sensing of Environment* 203: 152–61.

Kay, Susan, John D Hedley, and Samantha Lavender. 2009. "Sun Glint Correction of High and Low Spatial Resolution Images of Aquatic Scenes: A Review of Methods for Visible and near-Infrared Wavelengths." *Remote Sensing* 1 (4): 697–730.

Keukelaere, L. De, S. Sterckx, S. Adriaensen, E. Knaeps, I. Reusen, C. Giardino, M. Bresciani, et al. 2018. "Atmospheric Correction of Landsat-8/OLI and Sentinel-2/MSI Data Using ICOR Algorithm: Validation for Coastal and Inland Waters." *European Journal of Remote Sensing* 51 (1): 525–42.

Kloiber, Steven M, Patrick L Brezonik, Leif G Olmanson, and Marvin E Bauer. 2002. "A Procedure for Regional Lake Water Clarity Assessment Using Landsat Multispectral Data." *Remote Sensing of Environment* 82 (1): 38–47.

Kluyver, Thomas, Benjamin Ragan-Kelley, Fernando Pérez, Brian E Granger, Matthias Bussonnier, Jonathan Frederic, Kyle Kelley, Jessica B Hamrick, Jason Grout, and Sylvain Corlay. 2016. "Jupyter Notebooks-a Publishing Format for Reproducible Computational Workflows." In *ELPUB*, 87–90.

Laliberté, Julien, Pierre Larouche, Emmanuel Devred, and Susanne Craig. 2018. "Chlorophyll-*a* Concentration Retrieval in the Optically Complex Waters of the St. Lawrence Estuary and Gulf Using Principal Component Analysis." *Remote Sensing* 10 (2): 265.

Le, Chengfeng, Yunmei Li, Yong Zha, Deyong Sun, Changchun Huang, and Hong Zhang. 2011. "Remote Estimation of Chlorophyll-*a* in Optically Complex Waters Based on Optical Classification." *Remote Sensing of Environment* 115 (2): 725–37.

Leeuw, Thomas, and Emmanuel Boss. 2018. "The HydroColor App: Above Water

Measurements of Remote Sensing Reflectance and Turbidity Using a Smartphone Camera." *Sensors* 18 (1): 256.

Legendre, Pierre. 1998. "Model II Regression User's Guide, R Edition." *R Vignette* 14.

———. 2014. "Lmodel2: Model II Regression. R Package Version 1.7-2." Available at: ht tp://CRAN. R-project. org/package= lmodel2 (accessed 2 March 2015).

Malmqvist, Björn, Simon D Rundle, Alan P Covich, Alan G Hildrew, Christopher T Robinson, and Colin R Townsend. 2008. "Prospects for Streams and Rivers: An Ecological Perspective." *Aquatic Ecosystems: Trends and Global Prospects*, 19–29.

Martins, Vitor, Claudio Barbosa, Lino de Carvalho, Daniel Jorge, Felipe Lobo, and Evlyn Novo. 2017. "Assessment of Atmospheric Correction Methods for Sentinel-2 MSI Images Applied to Amazon Floodplain Lakes." *Remote Sensing* 9 (4): 322.

Matsuoka, A, M Babin, and EC Devred. 2016. "A New Algorithm for Discriminating Water Sources from Space: A Case Study for the Southern Beaufort Sea Using MODIS Ocean Color and SMOS Salinity Data." *Remote Sensing of Environment*.

McCain, Charles, Stanford Hooker, Gene Feldman, and Paul Bontempi. 2006. "Satellite Data for Ocean Biology, Biogeochemistry, and Climate Research." *Eos, Transactions American Geophysical Union* 87 (34): 337–43.

McClain, Charles, and Gerhard Meister. 2012. "Mission Requirements for Future Ocean-Colour Sensors."

Mobley. 1999. "Estimation of the Remote-Sensing Reflectance from above-Surface Measurements." *Applied Optics* 38 (36): 7442–55.

Mobley, Jeremy Werdell, Bryan Franz, Ziauddin Ahmad, and Sean Bailey. 2016. "Atmospheric Correction for Satellite Ocean Color Radiometry."

Mouw, Colleen B, Haidi Chen, Galen A McKinley, Steven Effler, David O'Donnell, Mary Gail Perkins, and Chris Strait. 2013. "Evaluation and Optimization of Bio-optical Inversion Algorithms for Remote Sensing of Lake Superior's Optical Properties." *Journal of Geophysical Research: Oceans* 118 (4): 1696–1714.

Mouw, Colleen B, Steven Greb, Dirk Aurin, Paul M DiGiacomo, Zhongping Lee, Michael Twardowski, Caren Binding, Chuanmin Hu, Ronghua Ma, and Timothy Moore. 2015. "Aquatic Color Radiometry Remote Sensing of Coastal and Inland Waters: Challenges and Recommendations for Future Satellite Missions." *Remote Sensing of Environment* 160: 15–30.

Muller-Karger, Frank E, Erin Hestir, Christiana Ade, Kevin Turpie, Dar A Roberts, David Siegel, Robert J Miller, David Humm, Noam Izenberg, and Mary Keller. 2018. "Satellite Sensor Requirements for Monitoring Essential Biodiversity Variables of Coastal Ecosystems." *Ecological Applications* 28 (3): 749–60.

Nechad, B, K G Ruddick, and G Neukermans. 2009. "Calibration and Validation of a Generic Multisensor Algorithm for Mapping of Turbidity in Coastal Waters." In *Proc. of SPIE Vol*, 7473:74730H – 1.

Novoa, Stéfani, David Doxaran, Anouck Ody, Quinten Vanhellemont, Virginie Lafon, Bertrand Lubac, and Pierre Gernez. 2017. "Atmospheric Corrections and Multi-Conditional Algorithm for Multi-Sensor Remote Sensing of Suspended Particulate Matter in Low-to-High Turbidity Levels Coastal Waters." *Remote Sensing* 9 (1): 61.

O'Reilly, John E, Stephane Maritorena, B Greg Mitchell, David A Siegel, Kendall L Carder, Sara A Garver, Mati Kahru, and Charles McClain. 1998. "Ocean Color Chlorophyll Algorithms for SeaWiFS." *Journal of Geophysical Research: Oceans* 103 (C11): 24937–53.

Olmanson, Leif G, Marvin E Bauer, and Patrick L Brezonik. 2008. “A 20-Year Landsat Water Clarity Census of Minnesota’s 10,000 Lakes.” *Remote Sensing of Environment* 112 (11): 4086–97.

Overstreet, Brandon T., and Carl J. Legleiter. 2017. “Removing Sun Glint from Optical Remote Sensing Images of Shallow Rivers.” *Earth Surface Processes and Landforms* 42 (2): 318–33.

Pahlevan, N, B Smith, C Binding, and D M O’Donnell. 2017. “Spectral Band Adjustments for Remote Sensing Reflectance Spectra in Coastal/Inland Waters.” *Optics Express* 25 (23): 28650–67.

Pahlevan, Nima, Sandeep K Chittimalli, Sundarabalan V Balasubramanian, and Vincenzo Vellucci. 2019. “Sentinel-2/Landsat-8 Product Consistency and Implications for Monitoring Aquatic Systems.” *Remote Sensing of Environment* 220: 19–29.

Pahlevan, Nima, Zhongping Lee, Jianwei Wei, Crystal B Schaaf, John R Schott, and Alexander Berk. 2014. “On-Orbit Radiometric Characterization of OLI (Landsat-8) for Applications in Aquatic Remote Sensing.” *Remote Sensing of Environment* 154: 272–84.

Pahlevan, Nima, S Sarkar, B.A Franz, S.V. Balasubramanian, and J. He. 2017. “Sentinel-2 MultiSpectral Instrument (MSI) Data Processing for Aquatic Science Applications: Demonstrations and Validations.” *Remote Sensing of Environment* 201 (November): 47–56.

Pahlevan, Nima, Sudipta Sarkar, and Bryan A. Franz. 2016. “Uncertainties in Coastal Ocean Color Products: Impacts of Spatial Sampling.” *Remote Sensing of Environment* 181 (August): 14–26.

Pahlevan, Nima, John R. Schott, Bryan A. Franz, Giuseppe Zibordi, Brian Markham, Sean Bailey, Crystal B. Schaaf, Michael Ondrusek, Steven Greb, and Christopher M. Strait. 2017.

"Landsat 8 Remote Sensing Reflectance (Rrs) Products: Evaluations, Intercomparisons, and Enhancements." *Remote Sensing of Environment* 190: 289–301.

Pekel, Jean-François, Andrew Cottam, Noel Gorelick, and Alan S Belward. 2016. "High-Resolution Mapping of Global Surface Water and Its Long-Term Changes." *Nature*.

Richter, Rudolf, Martin Bachmann, Wouter Dorigo, and A Muller. 2006. "Influence of the Adjacency Effect on Ground Reflectance Measurements." *IEEE Geoscience and Remote Sensing Letters* 3 (4): 565–69.

Ricker, W E. 1973. "Linear Regressions in Fishery Research." *Journal of the Fisheries Research Board of Canada* 30 (3): 409–34.

Roesler, Collin, Julia Uitz, Hervé Claustre, Emmanuel Boss, Xiaogang Xing, Emanuele Organelli, Nathan Briggs, et al. 2017. "Recommendations for Obtaining Unbiased Chlorophyll Estimates from *in situ* Chlorophyll Fluorometers: A Global Analysis of WET Labs ECO Sensors." *Limnology and Oceanography: Methods* 15 (6): 572–85.

Roy, D P, M A Wulder, T R Loveland, Woodcock C.E., R G Allen, M C Anderson, D Helder, et al. 2014. "Landsat-8: Science and Product Vision for Terrestrial Global Change Research." *Remote Sensing of Environment* 145 (April): 154–72.

Ruddick, Kevin, Vera De Cauwer, and Barbara Van Mol. 2005. "Use of the near Infrared Similarity Reflectance Spectrum for the Quality Control of Remote Sensing Data." In *Remote Sensing of the Coastal Oceanic Environment*, 5885:588501. International Society for Optics and Photonics.

Ruddick, Kevin, Vera De Cauwer, Young-Je Park, and Gerald Moore. 2006. "Seaborne Measurements of near Infrared Water-leaving Reflectance: The Similarity Spectrum for Turbid Waters." *Limnology and Oceanography* 51 (2): 1167–79.

Ruddick, Kevin George, Fabrice Ovidio, and Machteld Rijkeboer. 2000. “Atmospheric Correction of SeaWiFS Imagery for Turbid Coastal and Inland Waters.” *Applied Optics* 39 (6): 897–912.

Saba, V S, M A M Friedrichs, David Antoine, R A Armstrong, I Asanuma, M J Behrenfeld, A M Ciotti, M Dowell, N Hoepffner, and K J W Hyde. 2011. “An Evaluation of Ocean Color Model Estimates of Marine Primary Productivity in Coastal and Pelagic Regions across the Globe.”

Saraceno, John Franco, Brian A Pellerin, Bryan D Downing, Emmanuel Boss, Philip A M Bachand, and Brian A Bergamaschi. 2009. “High-frequency *in situ* Optical Measurements during a Storm Event: Assessing Relationships between Dissolved Organic Matter, Sediment Concentrations, and Hydrologic Processes.” *Journal of Geophysical Research: Biogeosciences* 114 (G4).

Sawakuchi, Henrique O, Vania Neu, Nicholas D Ward, Maria de Lourdes C Barros, Aline M Valerio, William Gagne-Maynard, Alan C Cunha, Diani F S Less, Joel E M Diniz, and Daimio C Brito. 2017. “Carbon Dioxide Emissions along the Lower Amazon River.” *Frontiers in Marine Science* 4: 76.

Seegers, Bridget N, Richard P Stumpf, Blake A Schaeffer, Keith A Loftin, and P Jeremy Werdell. 2018. “Performance Metrics for the Assessment of Satellite Data Products: An Ocean Color Case Study.” *Optics Express* 26 (6): 7404–22.

Shi, Kun, Yunlin Zhang, Guangwei Zhu, Xiaohan Liu, Yongqiang Zhou, Hai Xu, Boqiang Qin, Ge Liu, and Yunmei Li. 2015. “Long-Term Remote Monitoring of Total Suspended Matter Concentration in Lake Taihu Using 250 m MODIS-Aqua Data.” *Remote Sensing of Environment* 164: 43–56.

Shi, Wei, and Menghua Wang. 2009. “An Assessment of the Black Ocean Pixel Assumption for MODIS SWIR Bands.” *Remote Sensing of Environment* 113 (8): 1587–97.

Slade, Wayne H, Emmanuel Boss, Giorgio Dall’Olmo, M Rois Langner, James Loftin, Michael J Behrenfeld, Collin Roesler, and Toby K Westberry. 2010. “Underway and Moored Methods for Improving Accuracy in Measurement of Spectral Particulate Absorption and Attenuation.” *Journal of Atmospheric and Oceanic Technology* 27 (10): 1733–46.

Smith, Val H. 2003. “Eutrophication of Freshwater and Coastal Marine Ecosystems a Global Problem.” *Environmental Science and Pollution Research* 10 (2): 126–39.

Spyrakos, Evangelos, Ruth O’Donnell, Peter D Hunter, Claire Miller, Marian Scott, Stefan G H Simis, Claire Neil, Claudio C F Barbosa, Caren E Binding, and Shane Bradt. 2018. “Optical Types of Inland and Coastal Waters.” *Limnology and Oceanography* 63 (2): 846–70.

Sriwongsitanon, Nutchanart, Kritsanat Surakit, and Sansarith Thianpopirug. 2011. “Influence of Atmospheric Correction and Number of Sampling Points on the Accuracy of Water Clarity Assessment Using Remote Sensing Application.” *Journal of Hydrology* 401 (3–4): 203–20.

Stadler, Philipp, Luke C Loken, John T Crawford, Paul J Schramm, Kirsti Sorsa, Catherine Kuhn, Domenico Savio, Robert G Striegl, David Butman, and Emily H Stanley. 2018. “Spatial Patterns of Enzymatic Activity in Large Water Bodies: Ship-Borne Measurements of Beta-D-Glucuronidase Activity as a Rapid Indicator of Microbial Water Quality.” *The Science of the Total Environment* 651 (Pt 2): 1742–52.

Sterckx, S, S Knaeps, Susanne Kratzer, and K Ruddick. 2015. “SIMilarity Environment Correction (SIMEC) Applied to MERIS Data over Inland and Coastal Waters.” *Remote Sensing of Environment* 157: 96–110.

Sun, Deyong, Chuanmin Hu, Zhongfeng Qiu, Jennifer P Cannizzaro, and Brian B Barnes. 2014.

"Influence of a Red Band-Based Water Classification Approach on Chlorophyll Algorithms for Optically Complex Estuaries." *Remote Sensing of Environment* 155: 289–302.

Team, R Core. 2017. "R: A Language and Environment for Statistical Computing." Vienna, Austria.: R Foundation for Statistical Computing.

Tebbs, E J, J J Remedios, and D M Harper. 2013. "Remote Sensing of Chlorophyll-*a* as a Measure of Cyanobacterial Biomass in Lake Bogoria, a Hypertrophic, Saline–Alkaline, Flamingo Lake, Using Landsat ETM+." *Remote Sensing of Environment* 135: 92–106.

Turner, P.A., T.J. Griffis, J.M. Baker, X. Lee, J.T. Crawford, L.C. Loken, and R.T. Venterea. 2016. "Regional-Scale Controls on Dissolved Nitrous Oxide in the Upper Mississippi River." *Geophysical Research Letters*, April.

USGS. 2018. "Landsat 8 Surface Reflectance Code Product Guide."

Valente, André, Shubha Sathyendranath, Vanda Brotas, Steve Groom, Michael Grant, Malcolm Taberner, David Antoine, et al. 2016. "A Compilation of Global Bio-Optical *in situ* Data for Ocean-Colour Satellite Applications." *Earth System Science Data* 8 (1): 235–52.

Valerio, Aline, Milton Kampel, Vincent Vantrepotte, Nicholas Ward, Henrique Sawakuchi, Diani Fernanda, Diani Less, et al. 2017. "Assessment of Remote Sensing Empirical Algorithms to Retrieve Colored Dissolved Organic Matter in the Lower Amazon River." In *XVIII Proceedings of Brazilian Symposium on Remote Sensing*. Santos, SP: Brazilian Symposium on Remote Sensing - SBSR.

Vanhellemont, Q, and K Ruddick. 2015. "Advantages of High Quality SWIR Bands for Ocean Colour Processing: Examples from Landsat-8." *Remote Sensing of Environment*.

———. 2016. "Acolite for Sentinel-2: Aquatic Applications of MSI Imagery." In *Proceedings of the Living Planet Symposium*, edited by L. Ouwehand, ESA-SP Volume 740, ISBN: 978-

92-9221-305-3, 55. Prague, Czech Republic.

Vanhellemont, Quinten, and Kevin Ruddick. 2014. “Turbid Wakes Associated with Offshore Wind Turbines Observed with Landsat 8.” *Remote Sensing of Environment* 145: 105–15.

———. 2018. “Atmospheric Correction of Metre-Scale Optical Satellite Data for Inland and Coastal Water Applications.” *Remote Sensing of Environment* 216: 586–97.

Vermote, Eric, Chris Justice, Martin Claverie, and Belen Franch. 2016. “Preliminary Analysis of the Performance of the Landsat 8/OLI Land Surface Reflectance Product.” *Remote Sensing of Environment* 185: 46–56.

Vörösmarty, Charles J, Peter B McIntyre, Mark O Gessner, David Dudgeon, Alexander Prusevich, Pamela Green, Stanley Glidden, Stuart E Bunn, Caroline A Sullivan, and C Reidy Liermann. 2010. “Global Threats to Human Water Security and River Biodiversity.” *Nature* 467 (7315): 555.

Wang, Menghua. 2010. “Atmospheric Correction for Remotely-Sensed Ocean-Colour Products.” *Reports and Monographs of the International Ocean-Colour Coordinating Group (IOCCG)*.

Wang, Menghua, and Wei Shi. 2006. “Cloud Masking for Ocean Color Data Processing in the Coastal Regions.” *IEEE Transactions on Geoscience and Remote Sensing* 44 (11): 3105–96.

———. 2007. “The NIR-SWIR Combined Atmospheric Correction Approach for MODIS Ocean Color Data Processing.” *Optics Express* 15 (24): 15722–33.

Wang, Menghua, Wei Shi, and Lide Jiang. 2012. “Atmospheric Correction Using Near-Infrared Bands for Satellite Ocean Color Data Processing in the Turbid Western Pacific Region.” *Optics Express* 20 (2): 741–53.

Ward, Nicholas D, Thomas S Bianchi, Henrique O Sawakuchi, William Gagne-Maynard, Alan C Cunha, Daimio C Brito, Vania Neu, Aline Matos Valerio, Rodrigo Silva, and Alex V Krusche. 2016. “The Reactivity of Plant-derived Organic Matter and the Potential Importance of Priming Effects along the Lower Amazon River.” *Journal of Geophysical Research: Biogeosciences*.

Ward, Nicholas D, Henrique O Sawakuchi, and Jeffrey E Richey. 2018. “The Amazon River’s Ecosystem—Where Land Meets the Sea.” Eos, Transactions American Geophysical Union (Online) 99.PNNL-SA-128535 (2018). Water, U N. 2009. “Water in a Changing World, United Nations World Water Development Report 3.” *World Water Assessment Programme*.

Werdell, P Jeremy, and Sean W Bailey. 2005. “An Improved In-Situ Bio-Optical Data Set for Ocean Color Algorithm Development and Satellite Data Product Validation.” *Remote Sensing of Environment* 98 (1): 122–40.

Werdell, P Jeremy, Lachlan I W McKinna, Emmanuel Boss, Steven G Ackleson, Susanne E Craig, Watson W Gregg, Zhongping Lee, Stéphane Maritorena, Collin S Roesler, and Cécile S Rousseaux. 2018. “An Overview of Approaches and Challenges for Retrieving Marine Inherent Optical Properties from Ocean Color Remote Sensing.” *Progress in Oceanography*.

Werdell, P Jeremy, Christopher W Proctor, Emmanuel Boss, Thomas Leeuw, and Mustapha Ouhssain. 2013. “Underway Sampling of Marine Inherent Optical Properties on the Tara Oceans Expedition as a Novel Resource for Ocean Color Satellite Data Product Validation.” *Methods in Oceanography* 7: 40–51.

Whitehead, P G, R L Wilby, R W Battarbee, M Kernan, and Andrew John Wade. 2009. “A

Review of the Potential Impacts of Climate Change on Surface Water Quality." *Hydrological Sciences Journal* 54 (1): 101–23.

Woodcock, Curtis E, Richard Allen, Martha Anderson, Alan Belward, Robert Bindschadler, Warren Cohen, Feng Gao, Samuel N Goward, Dennis Helder, and Eileen Helmer. 2008. "Free Access to Landsat Imagery." *Science* 320 (5879): 1011.

Zhang, Hankui K, David P Roy, Lin Yan, Zhongbin Li, Haiyan Huang, Eric Vermote, Sergii Skakun, and Jean-Claude Roger. 2018. "Characterization of Sentinel-2A and Landsat-8 Top of Atmosphere, Surface, and Nadir BRDF Adjusted Reflectance and NDVI Differences." *Remote Sensing of Environment*.

2.7 APPENDIX A

This appendix holds supplemental text, figures and tables for Chapter 2.

2.7.1 *Inland water remote sensing*

The R_{rs} estimates resulting from atmospheric correction are a fundamental input for bio-optical models. Over the past three decades, a wide variety of universally applicable remote sensing algorithms have been developed to retrieve Chl-*a* and turbidity from remote sensing reflectance (Odermatt et al. 2012; C. R. McClain 2009; O'Reilly et al. 1998). To date, standardized high quality science products derived from such algorithms have yet to be developed for optically complex waters (Matthews 2011; Zheng and DiGiacomo 2017), although commercial products are available (Heege et al. 2014).

The free public availability of L8 and S2 data has led to an increase in studies over mesotrophic to eutrophic lakes (Dörnhöfer et al. 2018) productive coastal and estuarine waters (Snyder et al. 2017), CDOM-rich Estonian lakes (Kutser et al. 2016; Toming et al. 2016) and sediment-laden river plumes in the Northern Adriatic Sea (Brando et al. 2015). L8 has been used to map suspended matter, Chl-*a* and trophic state on an oligotrophic tropical reservoir (Bernardo et al. 2016; Watanabe et al. 2015) and to model CDOM and water clarity in Midwest USA lakes (Olmanson et al. 2016). Lobo et al. (2015) used L8 to model total suspended sediment in Brazil's turbid Tapajos river, yet overall applications in rivers are sparse.

2.7.2 *Atmospheric correction*

The SWIR approach has been successfully implemented in both SeaDAS (Wang et al. 2009) and ACOLITE (Vanhellemont & Ruddick 2015) across a range of turbidities (Ho et al. 2017; Liu et al. 2017; Atsushi Matsuoka et al. 2017). SWIR-corrected L8 estimates have shown good

agreement with SeaWiFs and MODIS-derived R_{rs} (Franz et al. 2015). While the SWIR-only method has produced valid retrievals in turbid waters (Martins et al. 2017; Ody et al. 2016), Pahlevan et al. (2017a) suggests the S2 SWIR bands, when used alone, can yield noisy and negative retrievals in the blue and red channels because of the low signal-to-noise ratio and insensitivity to variability in aerosol type over aquatic systems.

2.7.3 *Retrieval algorithms*

Chlorophyll-*a* was estimated using the NASA Ocean Color Biology Processing groups standard approach for Landsat 8 of the OC3 algorithm, which was implemented in both SeaDAS and ACOLITE. The algorithm is a fourth order polynomial based on the O'Reilly band ratio algorithm OCx that takes the reflectance in the blue (443 > 482 nm) and green (560 nm) bands as inputs:

$$log_{10}(chla) = a_o + \sum_{i=1}^{4} * a_i * (log_{10}(\frac{R_{rs}(\lambda_{blue})}{R_{rs}\lambda_{(green)}}))^i \quad \text{(A1-S1)}$$

where

$a_0 = 0.2412$, $a_1 = -2.0546$, $a_2 = 1.1776$, $a_3 = -0.5538$, $a_4 = 0.4570$.

The same approach was used for Sentinel-2. These coefficients were developed using the NASA bio-Optical Marine Algorithm Dataset (NOMAD) (Werdell and Bailey 2005) and validation statistics from the SeaWiFS Bio-Optical Archive and Storage System (SeaBASS) for Landsat-8 and Sentinel-2 are pending (Jeremy Werdell, personal communication).

Turbidity was estimated using the red band using a semi-empirical retrieval algorithm derived from the red band.

$$T = \frac{A * \rho_w}{1 - \rho_w - C} \quad FNU \quad \text{(A1-S2)}$$

where ρ_w is the water-leaving radiance reflectance, A = 289.29 g and C = 0.1686 as described in

(Vanhellemont and Ruddick 2014).

Table 2.5 Mission and sensor characteristics for Landsat-8 OLI and Sentinel-2 MSI. Both sensors possess a 12-bit radiometric quantization allowing for much higher signal-to-noise ratios than previous Landsat missions.

Sensor	Agency	Launch Date	Bands	Revisit	Coverage and Swath (km)	GSD (m)*
Landsat-8 Operational Land Imager (OLI)	NASA and USGS (USA)	Feb 11, 2013 - Present	9 spectral bands (413 - 1.375 nm)	16 days	Global, 170 X 185	30m†
Sentinel-2A/B Multispectral Imager (MSI)	ESA (Europe)	Sentinel-2A: June 23, 2015 - Present Sentinel-2B: March 7, 2017 - Present	13 spectral bands (443 - 2202 nm)	2-5 days	Global, 290 X 300	10m‡

** Ground sampling distance (GSD)*

† GSD in visible and near-infrared bands; 15m (panchromatic band) 100m (TIRS bands 10-11)

‡ GSD in visible and near-infrared bands; 20m (shortwave infrared) 60m (atmospheric correction band)

Table 2.6 Key differences in processor options used by this study. Note the level of customization ranges for each processor and that this table is not meant to be exhaustive of the parameterization schemes for each correction but rather to highlight major differences relevant for inland water remote sensing. Also, the table describes the specific settings used in this study; some of the components are customizable while others are hard-coded into the processor. For example, it is not possible to implement a BRDF correction in LaSRC or ACOLITE but the correction can be turned on and off for SeaDAS. In contrast, epsilon in ACOLITE can be fixed by tile or by scene for this band combination. Note the LaSRC correction produces surface reflectance, which can be compared to remote sensing reflectance by dividing by π sr-1.

Atmospheric Correction Component	LaSRC*	SeaDAS (l2gen)	ACOLITE**
Bands	Blue/Red	NIR-SWIR	NIR-SWIR***
Rayleigh Correction	6SV (Vermote et al., 2006)	Refined Rayleigh computation (Wang 2005)	6SV (Vermote et al., 2016)
Aerosol Estimation	parameters assigned from standard dynamic aerosol model, "Urban Clean", no black pixel assumption	epsilon (ε) from Rayleigh-corrected NIR/SWIR reflectance. The epsilon is used to query LUTs of aerosol models developed from AERONET (Ahmad 2010)	fixed aerosol epsilon (ε) derived from the Rayleigh-corrected reflectance in the NIR-SWIR
Aerosol Assignment	per pixel	smoothed to minimize noise (7X7 for Landsat-8, 6X6 for Sentinel-2)	fixed by scene
Sun & sky glint	includes sun glint	standard glint correction modeled from environmental conditions such as windspeed and pressure (Wang and Bailey 2001)	addresses glint, clouds and land by masking Rayleigh-corrected reflectances above > 0.0215 in the 1609 nm SWIR band (Vanhellemont & Ruddick 2015)
Adjacency affects	No corrections for adjacency effects	No corrections for adjacency effects	No corrections for adjacency effects
BRDF Correction	No BRDF correction	Turned off over turbid waters	No BRDF correction

*See Vermote et al. (2016) and citations within for full descriptions.
** Processing options described fully in Vanhellemont and Ruddick (2015; Vanhellemont and Ruddick (2014; Vanhellemont and Ruddick (2016).

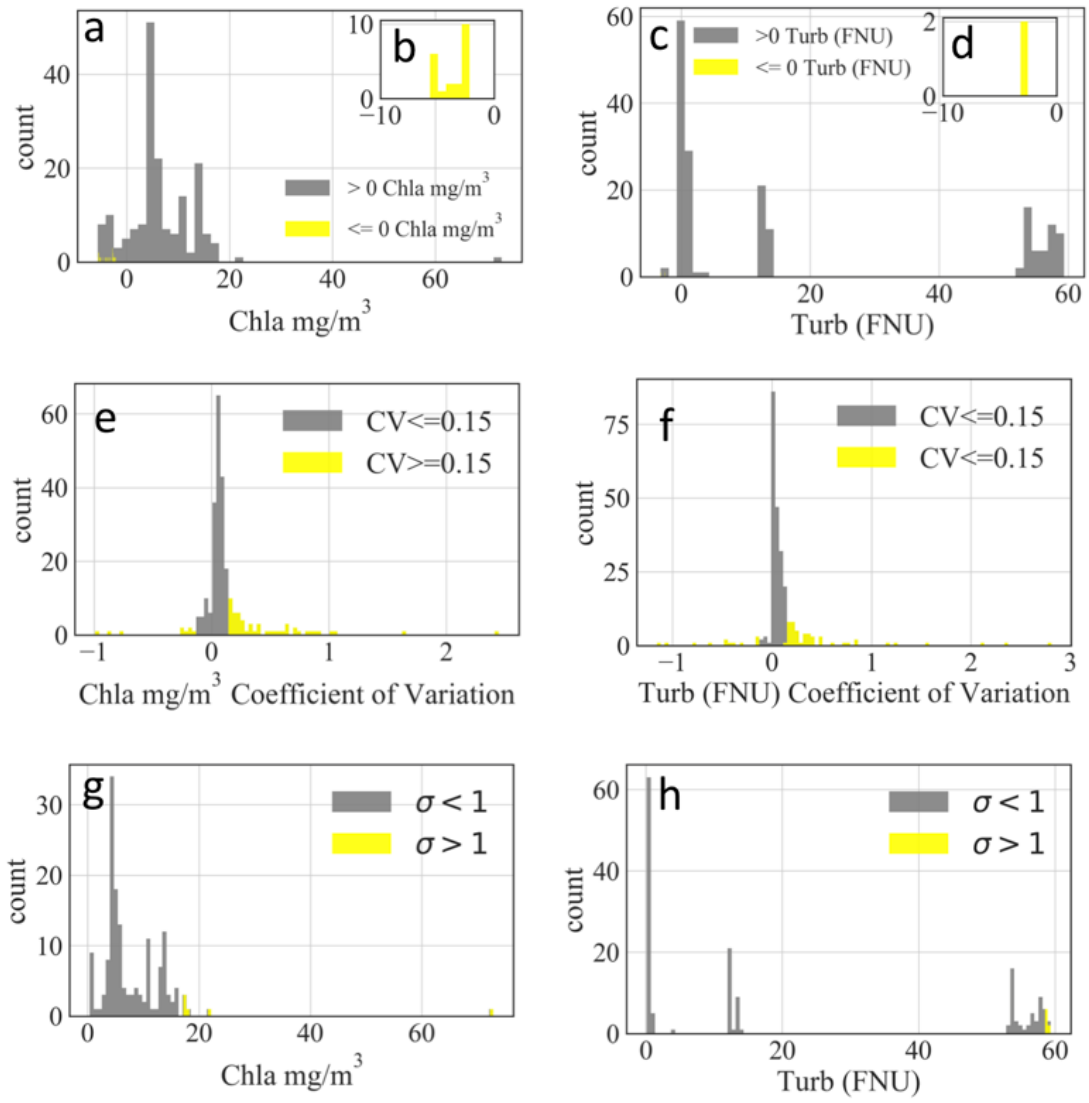

Figure 2.11. Additional quality control as recommended by Bailey and Werdell (2006) enacted upon the chlorophyll-*a* (left column) and turbidity (right column) data before match-up analysis.

Chapter 3. SATELLITE AND AIRBORNE REMOTE SENSING OF GROSS PRIMARY PRODUCTIVITY IN BOREAL ALASKAN LAKES

Kuhn et al., 2020. Environmental Research Letters. 430, 59-77.

3.1 INTRODUCTION

Northern high latitudes are warming at twice the global average rate (Overland et al. 2018), driving widespread changes to terrestrial ecosystem structure and function (Pastick et al., 2019; Wang et al., 2019), including to gross primary productivity (GPP) (Myneni et al., 1997; Beck and Goetz 2011; Goetz et al., 2005;). GPP is the rate primary producers convert inorganic carbon to biomass via photosynthetic pathways. Quantifying GPP can provide crucial insights into ecosystem functioning by establishing rates of food web carbon (C) uptake and energy flows.

Satellite remote sensing is a means to observe freshwater ecosystems at global scales. Satellite indices for productivity have been well-established for terrestrial (Tucker 1979; Pettorelli et al. 2005) and marine (Antoine et al., 1996; Lee et al., 2015) systems from the red and near-infrared bands. While inland water remote sensing research has accelerated (Palmer, Kutser, and Hunter 2015; Mouw et al. 2017; Matthews 2011; Dörnhöfer and Oppelt 2016; Topp et al. 2020), a comprehensive approach to efficiently map the spatial distribution of GPP for shallow lakes, which are globally abundant and concentrated in high northern latitudes (Downing et al. 2006), has yet to emerge.

Past lake productivity studies used an approach adopted from oceanography that assumes phytoplankton drive GPP. Indices based on blue and green reflectance (Morel and Prieur 1977) are calculated to estimate phytoplankton biomass, which then drives net primary productivity models (Behrenfeld et al. 2005; Shuchman et al. 2013). Studies have primarily been limited to large water bodies (Bergamino et al. 2010; Deng et al. 2017; Shuchman et al. 2013; Yousef et al. 2014; Fahnenstiel et al. 2016; Kauer et al. 2015) and the method has even been applied for large (> 1 km) lakes worldwide (Sayers et al. 2015). This model relies on the assumption that there is no influence from bottom-reflectance (i.e. that lakes are optically-deep).

However, worldwide 99% of all lakes are small (Verpoorter et al. 2014; Downing et al. 2006) and average lake depth globally has been estimated to only be 3.9 m (Messager et al. 2016). For these globally abundant small (< 1 km) and shallow lakes (< 10 m), the current method neglects benthic and littoral contributions to GPP from macrophytes and attached algae. Incorporating both benthic and pelagic processes into lake GPP models is crucial because macrophyte GPP rates exceed all other ecological communities including phytoplankton (Robert G Wetzel 2001) and can contribute 65 – 98% of ecosystem production in shallow lakes (Rautio and Vincent 2006; Jeppesen et al. 1998).

A remote sensing method for mapping GPP is needed that can integrate phytoplankton and macrophytes. This is especially relevant for the shallow lakes that dominate northern latitudes because of their potential relevance to carbon cycling and aquatic food webs (Raymond et al. 2013; Stanley and del Giorgio 2018; Wik et al. 2016). The majority of shallow water remote sensing studies have focused on deriving bathymetry and fractional cover of aquatic vegetation (Kutser et al. 2020). New field-based methods have emerged that account for contributions from phytoplankton and macrophytes in lakes (Bogard et al. 2017) but remote

sensing techniques have not caught up despite repeated calls for consistent, global inland water quality products (Malthus et al., 2012) and the increasing availability of high-resolution satellite imagery.

This study describes a new approach for quantifying shallow lake GPP using high-resolution (<10 m) remote sensing and field measurements. We combine field observations of GPP derived from oxygen isotopes with high-resolution satellite imagery to estimate shallow lake GPP. We then assess this approach using independently collected field data and test the model across platforms. We also measured *in situ* properties including turbidity and absorbance to rule out their influence on results. Linking bottom-up field measurements of lake properties with top-down remote sensing provides a novel method to link in-lake ecosystem processes with spatially explicit data to investigate ecosystem function across arctic and boreal lakes.

3.2 Data and Methods

3.2.1 *Study Area and Field Campaign Overview*

The Yukon Flats Basin is an extensive, 33,000 km^2 complex of low-lying lakes and wetlands inside the Yukon River Basin (Figure 3.1). Dry, cold and underlain by discontinuous permafrost (Minsley et al., 2012; Rey et al., 2019), the region's continental sub-arctic climate has an annual average temperature of ~ -3 °C (Chen et al. 2014) with short, ice-free summers (April/May - Sept/Oct) (Gallant 1995). Over 30,000 lakes dot this semi-arid landscape (Heglund and Jones 2003). Despite abundant surface water, the area receives very little precipitation (250 mm) and lake water balances are dominated by evaporation (Anderson et al. 2013, 2019). Lakes are on the whole shallow and macrophyte-rich; historical surveys demonstrated that lake bottoms are carpeted with up to 80% coverage of aquatic vegetation (Glesne 1986).

Study lakes (n = 7) representative of the region were carefully selected based on results from historical surveys (Heglund and Jones 2003; Halm and Guldager 2013; Halm and Griffith 2014) and a 2016 field study (Bogard et al. 2019) to represent a gradient taking into

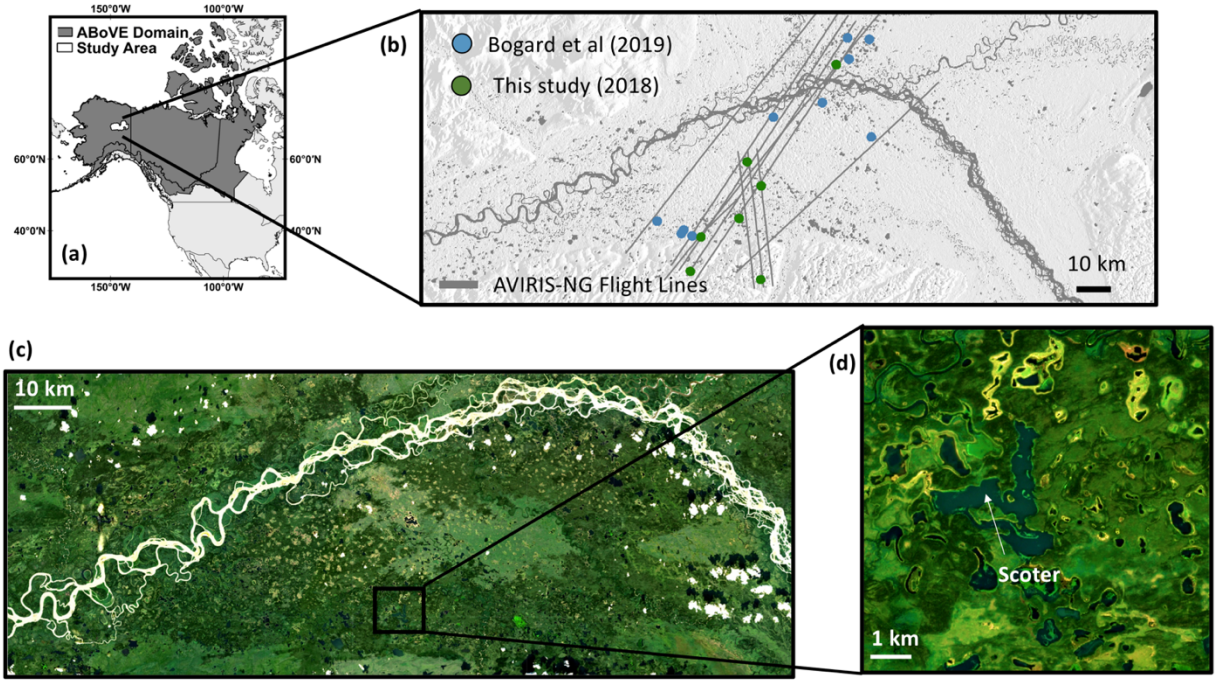

consideration depth, pH, DOC concentration, chlorophyll-*a* and CDOM absorption (Appendix B, Table 3.4)

Figure 3.1. (a) Field site location in interior Alaska (b) Yukon Flats lakes sampled in 2016 (n = 17, in blue) and repeated in 2018 (n = 7, in green) field campaigns with AVIRIS-NG flight lines shown in grey (c) Yukon Flats landscape shown in natural color from Sentinel-2 tiles (Table 3.5) collected on July 22, 2018 (d) Close-up of example study lake (Scoter) shown in Sentinel-2 natural color. The white arrow indicates where sample was collected on lake.

Lakes were sampled by boat and/or floatplane (Figure 3.1a-b) during a 2018 field campaign conducted as part of the National Aeronautics and Space Administration's (NASA) Arctic-Boreal Vulnerability Experiment (ABoVE) for a suite of parameters (Section 3.3.2, Appendix B, 3.6.1).

Table 3.1 Sampling dates, coordinates and physical properties of study lakes sampled *in situ* in July 2018 for GPP, reflectance, dissolved organic matter composition and chlorophyll-*a* among others (Section 3.2.2).

	Latitude	Longitude	Date Sampled	Depth (m)	Surface Area (km^2)
Boot (B)	66.07404	146.27066	7/18/18	22.0	0.73
Canvasback (CB)	66.38303	146.35489	7/19/18	1.4	2.83
Greenpepper (GP)	66.09209	146.73557	7/18/18	10.3	0.97
Ninemile (NM)	66.18285	146.66376	7/17/18	1.8	3.33
Scoter (SC)	66.24241	146.39896	7/17/18	4.5	4.56
YF17 (Y17)	66.32072	146.27431	7/17/18	1.6	1.75
YF20 (Y20)	66.63715	145.77278	7/17/18	1.3	0.59

3.2.2 Field and laboratory methods for lake GPP and color

Detailed chemical and optical measurements were collected from the center of each lake as well as *in situ* surface reflectance (R_s). Lake GPP was estimated using an oxygen isotope ($\delta^{18}O$) mass balance approach adapted from (Quay et al., 1995; Bocaniov et al., 2012) as described in Bogard (2017) and Appendix B, 3.6.1. For clarity, GPP derived from $\delta^{18}O$ field measurements will be referred to hereafter as *in situ* GPP in contrast to satellite-derived GPP.

Turbidity, chromophoric dissolved organic matter (CDOM) absorbance and phytoplankton chlorophyll-*a* were also measured to determine their influence, if any, on lake color. CDOM is the proportion of dissolved organic matter that absorbs strongly in ultraviolet and visible wavelengths (detailed methods in Appendix B, 3.6.1).

3.2.3 Satellite observations of lake color

The launch of commercial small satellites with daily return times and the increasing availability of hyperspectral imagery through large-scale campaigns such as NASA ABoVE has sparked interest in finer spatiotemporal analysis. In this study, we capitalize on the strengths of three different satellites: Landsat-8, Sentinel-2 and CubeSats (Planet, Inc). The sensors on-board Landsat-8 (L8), Sentinel-2 (S2) and PlanetScope (PS) all possess bands in the visible and near-infrared (VNIR) with varying spatial and temporal resolutions (Figure 3.2). We also incorporate hyperspectral airborne imagery from AVIRIS-NG (Figure 3.2).

a

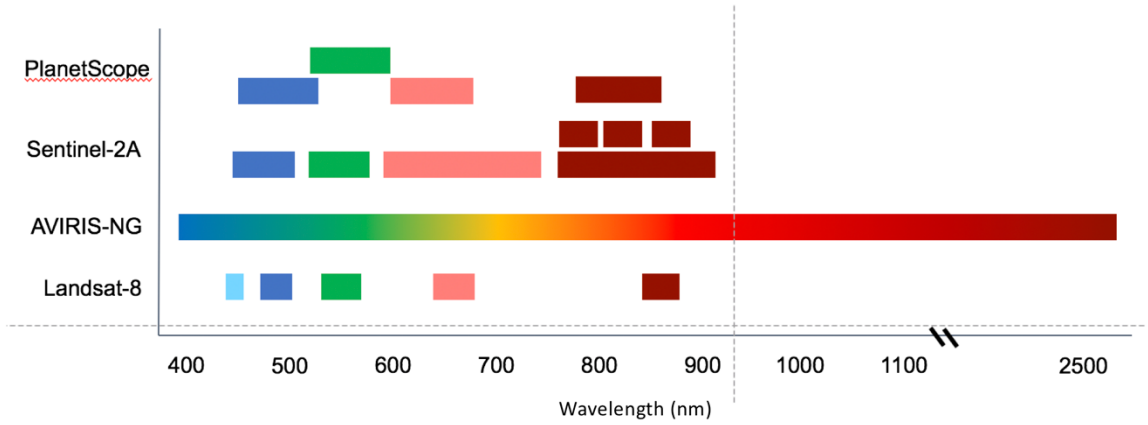

b

Craft	Sensor	Provider	Sensor Altitude (km)	Ground Sampling Distance
PlanetScope	CubeSat 3U	Planet Labs, Inc	475 km	3.0 m (approximate)
Sentinel-2 A/B	Multispectral Instrument (MSI)	European Space Agency (Europe)	786 km	10m (visible & near-infrared) 20m (shortwave infrared) 60m (atmospheric correction)
ERS-2	AVIRIS-NG	NASA Jet Propulsion Laboratory (JPL)	11km at high altitude, 1.9km at low altitude	4 to 20 m at altitude (4 to 20 km)
Landsat-8	Operational Land Imager (OLI)	National Aeronautics and Space Administration (NASA) (USA)	705 km	30m (visible & near-infrared) 15m (panchromatic & cirrus)

Figure 3.2. (a) Bandpass wavelengths (nm) in the visible bands and near-infrared for each sensor used in this study. The colors show the electromagnetic spectrum from blue (~400 nm) to near-infrared (dark red, > 700 nm). (b) Mission specifications for satellite and airborne imagery used in this study.

As part of the ABoVE campaign, AVIRIS-NG imagery was acquired on July 22, 2018. Level-2 (L2) atmospherically corrected Rs (Bue et al. 2015) was downloaded from https://avirisng.jpl.nasa.gov/dataportal/. Sentinel-2 acquisitions were identified and downloaded from the U.S. Geological Survey Earth Explorer (https://earthexplorer.usgs.gov/) and atmospherically corrected using the Land Surface Reflectance Code (LaSRC) (Vermote et al. 2016). Sentinel-2 images were also corrected using the Dark Spectrum Fitting (DSF) algorithm available in ACOLITE (Python Version 20190326.0), which is an open-source atmospheric

correction tested successfully in coastal waters (Vanhellemont 2019). PlanetScope Level-2 products were identified using the Planet Labs API (Planet 2017) and a cloud-native, scalable workflow called SWEEP (John et al. 2019). No cloud-free Landsat overpasses occurred during or close in time to field operations.

To utilize long-term Landsat records, we also calculated Landsat growing season composites, which are the per-pixel median greenness over the growing season (June, July and August). A common remote sensing tool used to quantify terrestrial productivity (Roy et al. 2010), growing season composites provide a continuous, stable record of seasonal lake color. While Landsat overpasses are infrequent (16 days) compared to Planet (~ daily), the Landsat program has the longest global record of Earth observation with acquisitions initiated in the mid-1980s (Lymburner et al. 2016), making it a powerful tool for historical analysis. For L8 composites, Collection 1 Level 2 R_s was accessed using Google Earth Engine. To generate seasonal composites, per-pixel median greenness was calculated from all cloud-free images acquired during the growing season (June 1 – Sep 30) over the study area. With the exception of ACOLITE, all reflectance products described above are derived using 6SV-based approaches (E Vermote et al. 2006). For brevity only those results are shown in the main text, but ACOLITE results are given in Appendix B (Figure 3.7, Figure 3.8, Table 3.6)

3.2.4 *In situ* surface reflectance validation data

In order to verify *in situ* lake color, R_s (350 - 2500 nm) was measured at each lake center in 2018 (n = 7) using an ASD FieldSpec 4 High Resolution Spectroradiometer (3 and 8 nm resolution in VNIR and SWIR) (Appendix B, 3.6.2). Above-water, *in situ* lake R_s was collected 3 - 5 days prior to overpasses because same-day *in situ* validation was not possible due to weather delays.

3.2.5 Combining field and satellite observations

Lake color was extracted for each sampling location from PlanetScope, Sentinel-2, Landsat-8 and AVIRIS scenes for each lake (n = 7) using Google Earth Engine (Gorelick et al. 2017b). A 3 X 3 pixel-wise box centered on field GPS coordinates was drawn for each lake and the median R_s within each box was extracted from the image in order to reduce bias introduced by spatial sampling (Pahlevan et al. 2016). In the case of scenes overlapping above a site, the median value between scenes was extracted. Since sampling was done at lake centers, all selected pixels were open water. A restrictive F-mask filter was also used to confirm selected pixels were water (Zhu et al., 2015). Lake color from each respective platform was then regressed against *in situ* GPP (n = 7) using a reduced major axis (RMA) type II regression (Python package plyr2, (Haëntjens 2018)). This same workflow was also used to extract lake color from Landsat seasonal composites (Section 3.2.3) for the 2016 samples (n = 24). The regression model was used to create satellite-derived maps of GPP by taking the regression equation derived from the GPP ~ greenness relationship observed in the 2018 field campaign and applying it on a per-pixel basis to Sentinel-2 imagery using the green band as the model input.

3.2.6 Comparing surface reflectance across sensors

In order to make hyperspectral lake color comparable to multi-spectral observations, *in situ* and AVIRIS-NG reflectance was spectrally convolved to Sentinel-2 wavelengths as in (Pahlevan et al. 2017):

$$R_s(\lambda_j) = \frac{\sum_{i=1}^{n} R_{rs}(\lambda_i) \text{ X } RSR\ (\lambda_i)}{\sum_{i=1}^{n} R_{rs}(\lambda_i)} \quad \text{(Eq. 3.1)}$$

where:

$R_s(\lambda_j)$: band center wavelength

RSR: spectral response factor

n: total number of hyperspectral band centers (i)

Median absolute percent different (MAPD) was used to compare sensor Rs:

$$\text{MAPD} = \text{median}\left(\text{abs}\left(\frac{x-y}{x}\right)\right) * 100 \quad \text{(Eq. 3.2)}$$

where x is sensor 1 and y is sensor 2. For decadal time series analysis (Figure 3.5), the non-parametric Mann-Kendall estimator and Sen's Slope were used to determine whether there was a positive or negative trend in lake greenness and its significance. Thiel-Sen Slope was calculated using the Scipy Python-based scientific computing package (Virtanen et al. 2020) and significance of the slope was determined using a Mann-Kendall test (Hirsch et al., 1982).

3.3 Results and Discussion

3.3.1 *In situ* lake GPP

In situ median GPP rates (

Table 3.2) were high at 9.72 mg O_2 m^{-2} d^{-1} and spanned a wide range (interquartile range = 6.25 to 10.50 O_2 m^{-2} d^{-1}). *In situ* GPP is on the same order of magnitude as other free-water techniques estimating GPP (Solomon et al. 2013). The rates observed here are higher than more dilute and often deeper boreal lakes (Ask et al., 2012; Deininger et al., 2017) and are consistent with the high productivity observed in shallow, macrophyte-rich lakes found in the northwestern Siberia lowlands (Manasypov et al. 2014) and shallow lakes in the Mackenzie Delta (Squires et al., 2009; Tank et al., 2009).

3.3.2 Controls on lake color

Other influences on lake color must be ruled out in order to avoid applying this empirical method over-ambitiously. To this end, we characterized variables (

Table 3.2) known to influence lake color, including phytoplankton pigments, CDOM and turbidity (Aurin and Dierssen 2012). We observed relatively low phytoplankton biomass based on HPLC Chl-*a* pigment analysis (median = 3.4 m^{-1}, interquartile range = 2.4 – 5.9 µg L^{-1}) (

Table 3.2). Overall, this is consistent with a previous study of 129 Yukon Flats lakes (Appendix B, Table 3.4) showing Chl-*a* was lower than expected based on nutrient availability (Heglund and Jones 2003). The relatively clear waters and high GPP observed here in the presence of low phytoplankton biomass suggest macrophyte production is driving lake GPP (Genkai-Kato et al. 2012). One exception was YF17, where field observations of a bloom were confirmed by high HPLC-derived Chl-*a* (83.3 µg L^{-1})

Table 3.2 Limnological conditions for Yukon Flats sites sampled in 2018. Values given represent the means and, when more than two replicates were collected, standard deviations of the replicates are given as well.

	pH	Turbidity (FNU)	Chl-*a* (µg L^{-1})	GPP (g O_2 m^{-2} d^{-1})	a440 (m^{-1})	DOC (mg L^{-1})
Boot (B)	8.31	0.54	2.7 ± 0.05	3.0	1.2 ± 0.12	19.2± 0.21
Canvasback (CB)	9.55	0.96	2.26 ± 0.01	10.7	2.41 ± 0.17	29.83 ± 0.22
Greenpepper (GP)	9.02	0.96	4.1 ± 0.04	6.2	0.42 ± 0.03	32.82 ± 0.40
Ninemile (NM)	9.46	< 0	6.5 ± 0.00	9.7	1.09 ± 0.31	27.64 ± 0.07
Scoter (SC)	8.93	< 0	7.1 ± 0.05	6.3	0.47 ± 0.20	19.46 ± 0.08
YF17 (Y17)	9.82	35	83.3± 0.33	14.6	2.42 ± 0.59	35.65 ± 0.54
YF20 (Y20)	10.24	< 0	1.26 ± 0.4	10.3	1.09 ± 0.83	10.17 ± 0.14

The majority of lakes were shallow (median depth of 1.6 m) (Table 3.1), with light extending to epiphytic periphyton and aquatic macrophytes. One lake was >10 m deep; the depth, low GPP and low Chl-*a* (Table 3.2) of this lake provided an end-point representative of the gradient in the area. Other studies have established that submerged and floating macrophytes reflect in the green (560 nm) and near-infrared (850 – 880 nm) (Silva et al., 2008; Oyama et al., 2015; Palmer et al., 2015; Dogliotti et al., 2018). The shallow depths of these relatively clear lakes, as inferred by low turbidities (< 1 FNU in most cases) could allow signals from macrophytes and periphyton to reach the surface (Mobley et al., 2010). Given the low Chl-*a*, low turbidities and the observed presence of macrophytes within the water column we suggest that overall, phytoplankton production is not a significant component of the optical signature.

A second influence on lake color is absorption of light by CDOM. CDOM can interfere with the remote sensing of GPP in two ways. CDOM absorbs green light, so high CDOM has the direct effect of masking green light reflected from photosynthetic pigments (Carder et al. 1989). Indirectly, CDOM can shade out aquatic producers, thus having the ecological impact of reducing GPP (Ask et al., 2012; Seekell et al., 2015). In order to rule out this influence, CDOM data were collected at each site. CDOM values (Table 3.2) in sampled lakes were low (a_{440}, median = 1.13 m^{-1}, interquartile range = 0.78 - 1.82 m^{-1}), showing that lakes are relatively clear despite their high DOC (10.2 to 25.6 mg L^{-1}) (Table 3.2). Our findings are consistent with other studies in semi-arid aquatic ecosystems (Osburn et al. 2011; Bogard et al. 2019; Kellerman et al. 2019) that show low CDOM despite high DOC. While coupling between DOC and CDOM has been demonstrated at global scales (Massicotte et al. 2017), CDOM-DOC decoupling in these semi-arid landscapes is hypothesized to result from decreased hydrologic connectivity which

reduces terrestrial organic carbon subsidies as aromatic carbon compounds to aquatic ecosystems, resulting in clearer lakes than otherwise expected (Johnston et al. 2020).

Finally, lake color can be influenced by scattering from sediment during periods of hydrologic connectivity to surface waters or during lake turnover. However, turbidity across lakes was low (< 1 FNU) (Table 3.2) with the exception of YF17, where the previously noted algal bloom drove turbidity up to 35 FNU. Taken together, these results indicate the clear and shallow nature of these macrophyte-rich lakes creates favorable conditions for the remote sensing of benthic properties.

3.3.3 Linking *in situ* GPP to Sentinel-2 lake color

Lake color from satellite and airborne sensors was regressed against 2018 *in situ* GPP (mg O_2 m^{-2} d^{-1}) (n = 7), revealing a strong, positive correlation between greenness and GPP (Figure 3.3a, p-value < 0.05). We then applied this regression pixel-wise to Sentinel-2 imagery to create spatially explicit GPP maps (Figure 3.3b-c, p-value < 0.05) for each lake. Modeled, S2 GPP ranged from 3.9 ± 1.14 mg O_2 m^{-2} d^{-1} in the deep, upland Boot Lake to 14.21 ± 6.42 mg O_2 m^{-2} d^{-1} in shallow, eutrophic YF17.

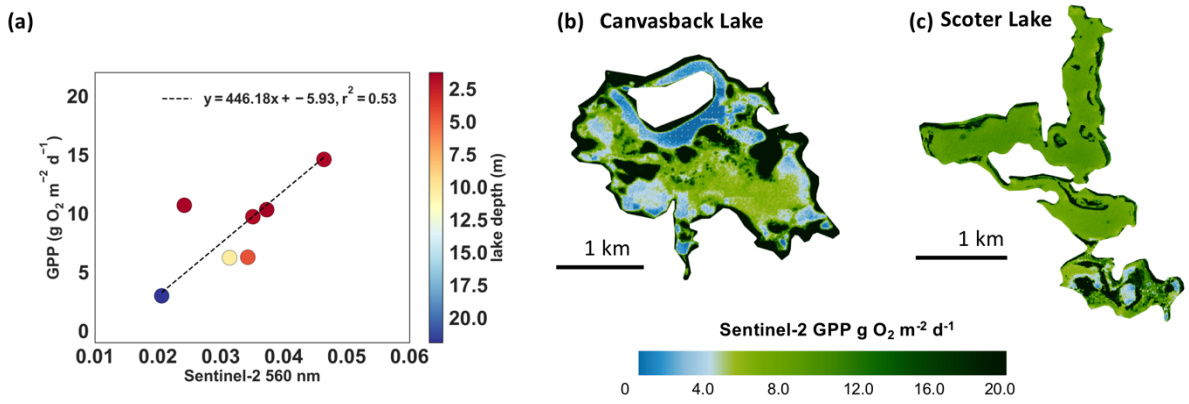

Figure 3.3. (a) Scatterplot showing the relationship between GPP measured *in situ* in 2018 and greenness as derived from Sentinel-2 surface reflectance (~560 nm) for July 2018 lake samples (n = 7). The equation shown in Figure 3.3a was then applied per pixel to the Sentinel-2 imagery, resulting in spatially-explicit maps of GPP. Examples of these resulting GPP maps modeled from satellite imagery are shown for two of the study lakes: (b) Canvasback Lake and (c) Scoter Lake. The color bar indicates the range of values for modeled GPP derived by applying the equation in Figure 3.3a to each Sentinel-2 pixel.

3.3.4 Independent evaluation with Landsat-8

The relationship between remotely sensed greenness and *in situ* productivity was then evaluated using a separate dataset from a 2016 field campaign that had been withheld for independent testing (Figure 3.4). As same-week images were not available, we instead regressed seasonal L8 composites against 2018 (n = 7) and 2016 *in situ* GPP (n = 17) (Bogard et al., 2019). The correlation between greenness and *in situ* GPP was maintained across both models.

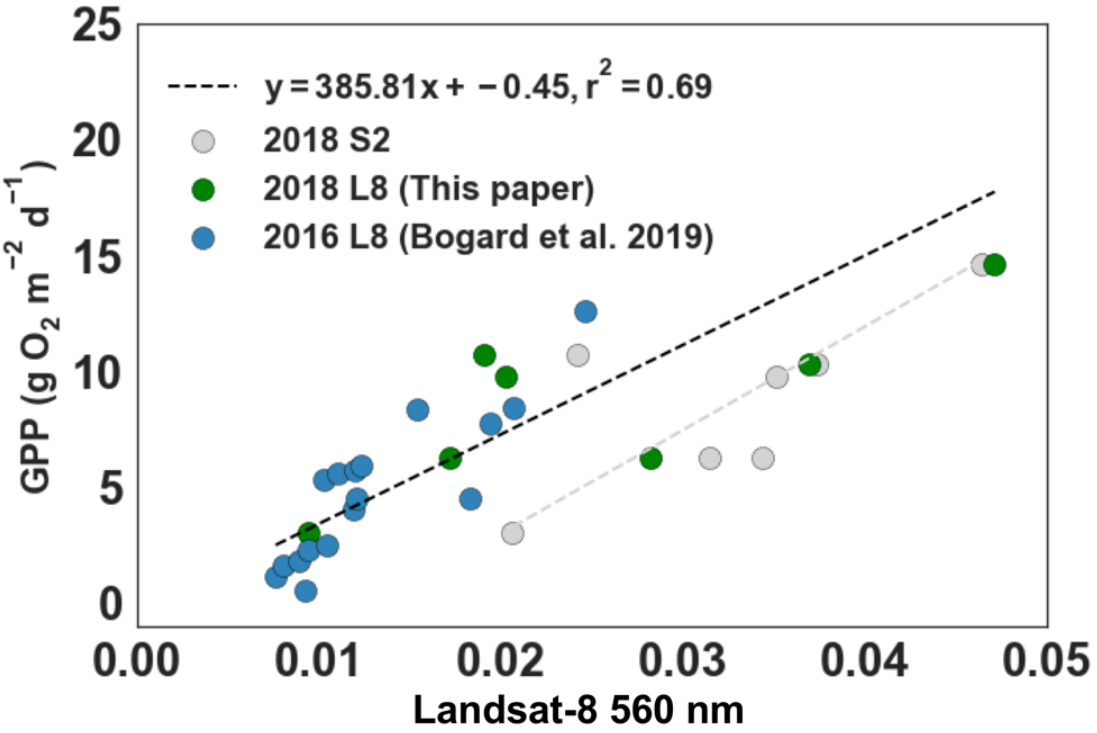

Figure 3.4. (a) Scatter plot using L8 composites (R_s; 560 nm) and *in situ* GPP from 2016 and 2018 (g O_2 m^{-2} d^{-1}) (n = 24). The 2016 *in situ* GPP is the average of June and September; 2018 *in situ* GPP was collected once during July. The 2016 (shown in blue, n = 17) and 2018 (shown in green, n = 7) R_s was calculated from June – September composites (see text for full description). The S2 model from Figure 3.1d (n= 7) is shown in grey for comparison. L8 regression model and coefficients of determination (r^2) are given in inset. Scene IDs can be found in Table 3.5.

The L8 seasonal composites produced a slightly stronger relationship (type 2 major axis regression: y = 385.81x – 0.45; r^2 = 0.69; p = 2.60 x 10^{-4}, n = 24) than the Sentinel-2 same-week model. This likely results from the smoothing of short-term variability from the composite and the relative stability of oxygen pools (Bogard et al. 2017) in these shallow lakes on seasonal

scales. The separate models provide an independent check against each other, further substantiating the robustness of this approach across sensors and years.

The use of Landsat allows us to tap into the powerful historical imagery available through the Landsat archive in order to detect decadal (Wang et al., 2014; Lymburner et al., 2016) and seasonal (Kallio et al. 2008) trends in lake color. Lake greenness computed for Scoter Lake Figure 3.5 showed a decline from 1984 – 2018. Field studies suggest that declines in greenness could result from increased CDOM absorption resulting from thermokarst processes for lakes with higher absorption (Wauthy et al. 2018), increases in depth (Duguay and Lafleur 2003), or increased sediment loading during periods of surface water connectivity (Vonk et al. 2015). Subsequent research combining these techniques with paleolimnology (Pienitz et al., 1999; Bouchard et al., 2017) and radiocarbon (Rühland et al., 2003) data has the potential to unveil past lake processes, although more testing is required to establish mechanistic links between these processes and lake color across more diverse ecosystems.

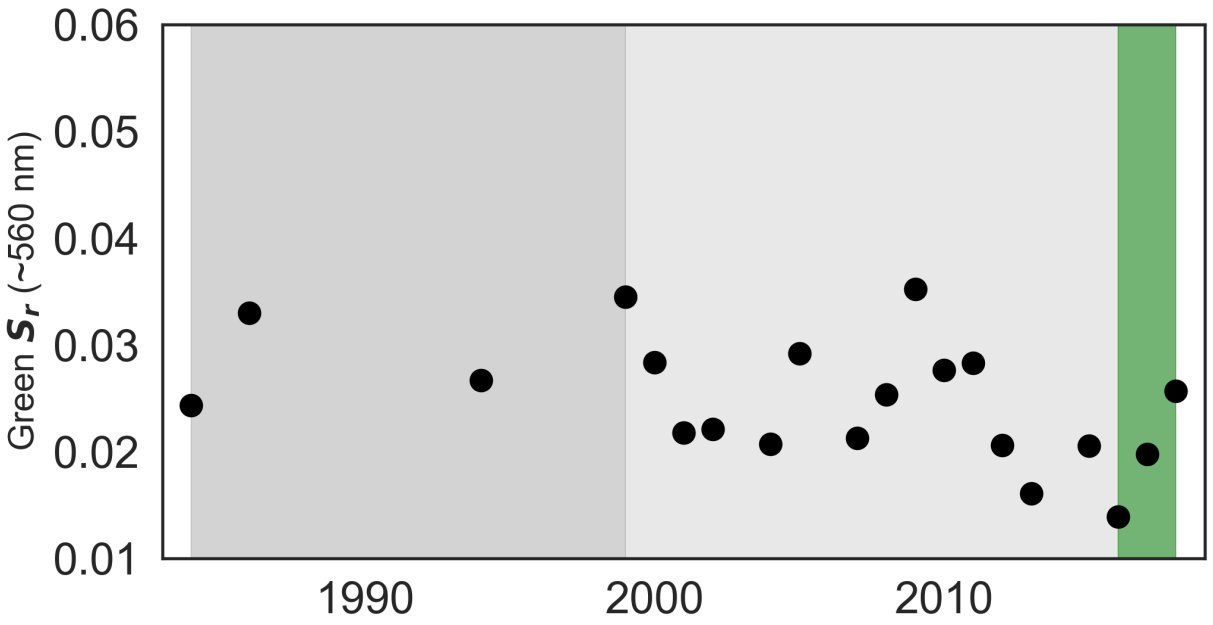

Figure 3.5. Landsat time series of greenness for Scoter Lake. Black dots represent median growing season greenness at the sampling location. The red line is the Thiel-Sen slope (y = -0.00023x + 0.61, p-value = 0.01) with the p-value from the Mann Kendall significance test given top left. Dark and light grey shading depicts launch of Landsat-5 and Landsat-7. After Landsat-7 launch two Landsat sensors have continuously been in orbit. Green shading represents time period of ABoVE field campaigns.

3.3.5 AVIRIS-NG, PlanetScope and *in situ* Rs

Surface reflectance from different sensors showed the greatest agreement in the green band. Using high-resolution PlanetScope and AVIRIS-NG R_s (Appendix B, Table 3.5), Sentinel-2 and *in situ* R_s (Figure 3.6, Appendix B, Figure 3.7, Figure 3.8), we compared R_s and respective model performance using 2018 *in situ* GPP. Analyzing agreement between the blue, green, red

and NIR bands, we found the best agreement in the green (MAPD median = 29%, interquartile range 8 - 53%) (Appendix B, Figure 3.7, Figure 3.8, text 3.6.3, text 3.6.4).

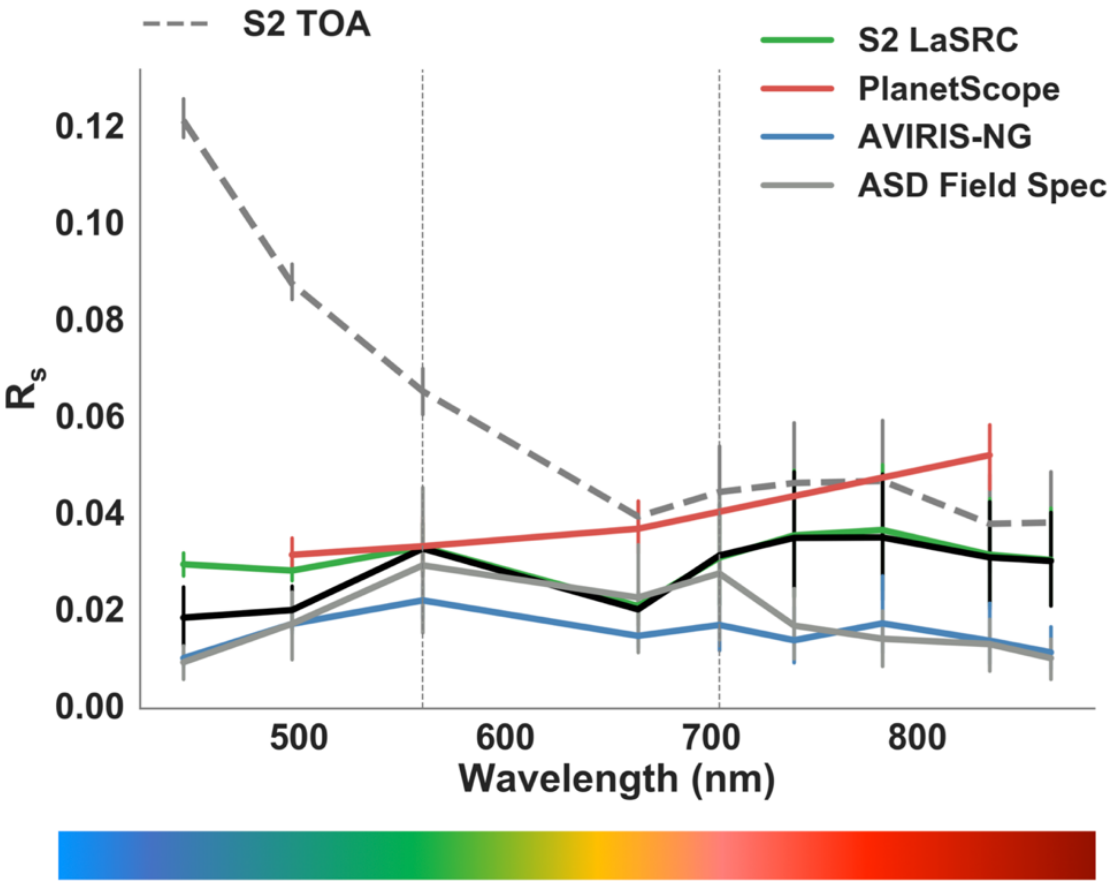

Figure 3.6. Surface reflectance (R_s) represented as the median and interquartile range (25%, 75%) of 2018 lakes. Dashed vertical grey lines show the wavelengths used to model GPP at 560 nm (green) and 704 nm (red-edge). S2 TOA spectra given for context. Extended discussion of differences given in Appendix B (Figure 3.7, Figure 3.8, text 3.6.3, text 3.6.4). It is important to note ASD measurements (Table 3.1 for dates) were collected prior to airborne (July 22) and satellite (PlanetScope, July 23; Sentinel-2, July 22) measurements.

Green R_s is less subject to inter-sensor differences (Pahlevan et al. 2018) and calibration errors between Landsat sensors (Vogelmann et al. 2016). S2's green R_s has been successfully

ground-truthed over small thermokarst lakes and ponds by Freitas et al. (2019) and green R_s is also less impacted than NIR by particulates (Wang and Philpot 2007). Green R_s also has the major advantage of being measured by almost every spectral remote sensing platform, dating back to early Landsat (Dwyer et al. 2018) and including the upcoming Plankton Aerosol, Cloud, Ocean Ecosystem (PACE) Mission (Werdell et al. 2019). Finally, previous studies have shown greenness covaries with both phytoplankton (O'Reilly et al. 1998; O'Reilly and Werdell 2019) and macrophytes (Hestir et al. 2015). In light of the larger disagreements between sensors detected in the NIR (Appendix B, 3.6.4) these results suggest that green R_s may be a stable, sensor-agnostic quantity suitable for GPP modeling across a range of spectral, spatial and temporal resolutions.

3.3.6 GPP model results for green and red-edge bands across sensors

In every platform considered by this study, *in situ* GPP (mg O_2 m^{-2} d^{-1}) corresponded with greenness (Table 3.3, Appendix B, Figure 3.9, Figure 3.10). The strongest correlation was between *in situ* GPP and *in situ* R_s ($r^2 = 0.68$; p-value <0.05) and CubeSat R_s ($r^2 = 0.78$; p-value <0.05). This could be due to two factors. First, *in situ* R_s was collected simultaneous to *in situ* GPP, in contrast to the overpasses 2-5 days later. However, unlike dynamic river and coastal systems, processes in these lakes vary on seasonal and annual scales. For example, high-frequency daily observations of dissolved oxygen collected from May to September (Bogard et al. 2019) show consistently positive rates of net production driven by intense plant growth was sustained throughout most of the growing season. Johnston et al (2020) also showed diel dissolved organic matter composition and optical properties changed minimally over a 3-day period. A second reason for the stronger performance of PlanetScope and the *in situ* sensor could be because of their finer spatial resolution relative to other sensors (10 – 30 m).

Table 3.3. Regression results between July 2018 Rs and *in situ* GPP fitted using a Type II regression model using the green (560 nm) and the red-edge (704 nm) bands from each sensor. The empty row results from PlanetScope lacking a red-edge band. All p-values were < 0.05 (Appendix B, Table 3.6) and individual scatterplots are provided in Appendix B (Figure 3.9, Figure 3.10)

	Green (~560 nm)			Red-edge (~704 nm)		
	Slope	Intercept	r^2	Slope	Intercept	r^2
S2 TOA	478.91	-22.46	0.30	478.91	-22.46	0.56
S2 LaSRC	446.18	-5.93	0.53	446.18	-5.93	0.62
PlanetScope	413.39	-6.65	0.78	NA	NA	NA
AVIRIS-NG	607.19	-4.51	0.40	607.19	-4.51	0.74
ASD Field Spec	146.86	4.43	0.68	146.86	4.43	0.80

While restricting the time difference between field and satellite observations can improve model uncertainty in dynamic river systems (Kuhn et al., 2019), albeit time differences of up to 3 to 5 days have been used successfully in several lake studies (Kloiber et al., 2002; Chipman et al., 2004; Olmanson et al., 2008; Boucher et al., 2018). Shorter time differences are ideal, yet given the temporal stability of the dissolved oxygen pool and water color over several days in these lakes, we are confident these results are representative and provide important insights, particularly given the lack of comparisons of surface reflectance over inland waters (Maciel et al. 2020).

A second advantage of Sentinel-2 over Landsat-8 is the addition of red-edge bands suitable for mapping vegetation. An even stronger correlation than with greenness was observed between GPP and the red-edge band (704 nm) (Table 3.3). Models improved by an average of 16% (Table 3.3) due to the strong red-edge reflectance of macrophytes. This suggests that, when available, red-edge bands may be the strongest candidate for modeling GPP in these shallow lake ecosystems whose GPP is driven by both macrophytes and phytoplankton. This finding has implications for future missions as red-edge bands with narrower bandpasses are increasingly being added to, for example, Planet Lab's next-generation Dove satellites. While the green band is suitable for historic analysis, these findings encourage red-edge based algorithm development due to the strong signal in these shallow arctic and boreal lakes.

The correlation between green and NIR bands with *in situ* GPP across sensors and sites indicates their potential as a simple GPP proxy for shallow lakes with low turbidity and CDOM. For context, global ocean models typically only explain 40% of water-column-integrated primary production (Siegel et al. 2001). The strength of this relationship between lake color and *in situ* GPP for both 2016 and 2018 datasets suggest potential for the development of a remote sensing modeling framework for shallow lake GPP.

3.4 CONCLUSIONS

This study provides evidence of a simple empirical relationship between lake color and GPP for shallow, relatively clear boreal lakes using *in situ* field data paired with remote sensing. We use a novel approach that pairs oxygen isotopes with satellite imagery. Both techniques integrate pelagic and benthic processes from phytoplankton and macrophytes in shallow waters (Wetzel and Hough 1972; Jackson 2003). Summertime CO_2 drawdown in shallow lakes has been

linked to macrophyte growth, highlighting the potentially important role of macrophytes in lake carbon cycling (Tank et al., 2009; Vesterinen et al., 2016). Shallow lakes are abundant worldwide and therefore the ability to integrate benthic and pelagic GPP is crucial for capturing whole ecosystem GPP.

In terrestrial systems, NDVI has been widely adopted as a useful, albeit imperfect, proxy for vegetation biomass (Rouse 1974). NDVI has transformed our understanding of landscape change in remote northern regions (Goetz et al., 2005; Ju and Masek 2016; Jia et al., 2003; Sulla-Menashe et al., 2018; Bhatt et al., 2013), yet no such metric has been adopted for shallow lakes. This study provides initial evidence of the green band as a potential simple index for mapping GPP in shallow, light-filled, and highly productive northern lakes. We then confirmed this relationship using Landsat-8 and compare results from other sensors including AVIRIS-NG and PlanetScope. This study demonstrates green and red-edge bands from Sentinel-2, Landsat-8, AVIRIS-NG and PlanetScope can be used to map GPP when constrained with appropriate field data. More detailed *in situ* measurements of lake color and biogeochemistry across optically diverse systems are needed to further test this finding. Advances in field data collection needs to be prioritized for algorithm development across the circumpolar north.

In the Yukon Flats, warming and thawing has led to lake area decline (Jepsen et al. 2013; Jepsen et al. 2016). Surveying all 30,000 lakes in this region is not feasible yet the area is predicted to undergo drastic hydrologic changes linked to increasing permafrost thaw (Walvoord and Striegl 2007; Walvoord et al. 2012). Our findings suggest further work developing remote sensing algorithms for GPP could advance lake monitoring at scales useful for climate science and ecosystem management.

3.5 REFERENCES

Anderson, Lesleigh, Jean Birks, Jennifer Rover, and Nikki Guldager. 2013. "Controls on Recent Alaskan Lake Changes Identified from Water Isotopes and Remote Sensing." *Geophysical Research Letters* 40 (13): 3413–18.

Anderson, Lesleigh, Mary Edwards, Mark D. Shapley, Bruce P. Finney, and Catherine Langdon. 2019. "Holocene Thermokarst Lake Dynamics in Northern Interior Alaska: The Interplay of Climate, Fire, and Subsurface Hydrology." *Frontiers in Earth Science* 7 (53).

Antoine, David, Jean-Michel André, and André Morel. 1996. "Oceanic Primary Production: 2. Estimation at Global Scale from Satellite (Coastal Zone Color Scanner) Chlorophyll." *Global Biogeochemical Cycles* 10 (1): 57–69.

Ask, Jenny, Jan Karlsson, and Mats Jansson. 2012. "Net Ecosystem Production in Clear-water and Brown-water Lakes." *Global Biogeochemical Cycles* 26 (1).

Aurin, Dirk A, and Heidi M Dierssen. 2012. "Advantages and Limitations of Ocean Color Remote Sensing in CDOM-Dominated, Mineral-Rich Coastal and Estuarine Waters." *Remote Sensing of Environment* 125: 181–97.

Beck, Pieter S A, and Scott J Goetz. 2011. "Satellite Observations of High Northern Latitude Vegetation Productivity Changes between 1982 and 2008: Ecological Variability and Regional Differences." *Environmental Research Letters* 6 (4): 45501.

Behrenfeld, Michael J, Emmanuel Boss, David A Siegel, and Donald M Shea. 2005. "Carbon-based Ocean Productivity and Phytoplankton Physiology from Space." *Global Biogeochemical Cycles* 19 (1).

Bergamino, N, S Horion, S Stenuite, Y Cornet, S Loiselle, P.-D. Plisnier, and J-P. Descy. 2010. "Spatio-Temporal Dynamics of Phytoplankton and Primary Production in Lake Tanganyika

Using a MODIS Based Bio-Optical Time Series." *Remote Sensing of Environment* 114 (4): 772–80. https://doi.org/https://doi.org/10.1016/j.rse.2009.11.013.

Bhatt, Uma, Donald Walker, Martha Raynolds, Peter Bieniek, Howard Epstein, Josefino Comiso, Jorge Pinzon, et al. 2013. "Recent Declines in Warming and Vegetation Greening Trends over Pan-Arctic Tundra." *Remote Sensing* 5 (9): 4229–54.

Bocaniov, Serghei A, Sherry L Schiff, and Ralph E H Smith. 2012. "Plankton Metabolism and Physical Forcing in a Productive Embayment of a Large Oligotrophic Lake: Insights from Stable Oxygen Isotopes." *Freshwater Biology* 57 (3): 481–96.

Bogard, Matthew J., Catherine Kuhn, Sarah Ellen Johnston, Robert G. Striegl, Gordon W. Holtgrieve, Mark M. Dornblaser, Robert G.M. Spencer, Kimberly P. Wickland, and David E. Butman. 2019. "Negligible Cycling of Terrestrial Carbon in Many Lakes of the Arid Circumpolar Landscape." *Nature Geoscience* 12 (3): 180–85.

Bogard, Matthew J, Dominic Vachon, Nicolas F St- Gelais, and Paul A Del Giorgio. 2017. "Using Oxygen Stable Isotopes to Quantify Ecosystem Metabolism in Northern Lakes." *Biogeochemistry* 133 (3): 347–64.

Bouchard, Frédéric, Lauren A. MacDonald, Kevin W. Turner, Joshua R. Thienpont, Andrew S. Medeiros, Boris K. Biskaborn, Jennifer Korosi, Roland I. Hall, Reinhard Pienitz, and Brent B. Wolfe. 2017. "Paleolimnology of Thermokarst Lakes: A Window into Permafrost Landscape Evolution." *Arctic Science* 3 (2): 91–117.

Boucher, Jonah, Kathleen C Weathers, Hamid Norouzi, and Bethel Steele. 2018. "Assessing the Effectiveness of Landsat 8 Chlorophyll-*a* Retrieval Algorithms for Regional Freshwater Monitoring." *Ecological Applications* 28 (4): 1044–54.

Bue, Brian D, David R Thompson, Michael L Eastwood, Robert O Green, Bo-Cai Gao, Didier

Keymeulen, Charles M Sarture, Alan S Mazer, and Huy H Luong. 2015. “Real-Time Atmospheric Correction of AVIRIS-NG Imagery.” *IEEE Trans. Geoscience and Remote Sensing* 53 (12): 6419–28.

Carder, Kendall L, Robert G Steward, George R Harvey, and Peter B Ortner. 1989. “Marine Humic and Fulvic Acids: Their Effects on Remote Sensing of Ocean Chlorophyll.” *Limnology and Oceanography* 34 (1): 68–81.

Chen, Min, Joel C Rowland, Cathy J Wilson, Garrett L Altmann, and Steven P Brumby. 2014. “Temporal and Spatial Pattern of Thermokarst Lake Area Changes at Yukon Flats, Alaska.” *Hydrological Processes* 28 (3): 837–52.

Chipman, Jonathan W, Thomas M Lillesand, Jeffrey E Schmaltz, Jill E Leale, and Mark J Nordheim. 2004. “Mapping Lake Water Clarity with Landsat Images in Wisconsin, USA.” *Canadian Journal of Remote Sensing* 30 (1): 1–7.

Deininger, Anne, Carolyn L Faithfull, and A-K Bergström. 2017. “Phytoplankton Response to Whole Lake Inorganic N Fertilization along a Gradient in Dissolved Organic Carbon.” *Ecology* 98 (4): 982–94.

Deng, Yubing, Yunlin Zhang, Deping Li, Kun Shi, and Yibo Zhang. 2017. “Temporal and Spatial Dynamics of Phytoplankton Primary Production in Lake Taihu Derived from Modis Data.” *Remote Sensing* 9 (3): 195.

Dogliotti, Ana, Juan Gossn, Quinten Vanhellemont, and Kevin Ruddick. 2018. “Detecting and Quantifying a Massive Invasion of Floating Aquatic Plants in the Río de La Plata Turbid Waters Using High Spatial Resolution Ocean Color Imagery.” *Remote Sensing* 10 (7): 1140.

Dörnhöfer, Katja, and Natascha Oppelt. 2016. “Remote Sensing for Lake Research and Monitoring–Recent Advances.” *Ecological Indicators* 64: 105–22.

Downing, John A, Y T Prairie, J J Cole, C M Duarte, L J Tranvik, Robert G Striegl, W H McDowell, Pirkko Kortelainen, N F Caraco, and J M Melack. 2006. “The Global Abundance and Size Distribution of Lakes, Ponds, and Impoundments.” *Limnology and Oceanography* 51 (5): 2388–97.

Duguay, C R, and P M Lafleur. 2003. “Determining Depth and Ice Thickness of Shallow Sub-Arctic Lakes Using Space-Borne Optical and SAR Data.” *International Journal of Remote Sensing* 24 (3): 475–89.

Dwyer, John, David Roy, Brian Sauer, Calli Jenkerson, Hankui Zhang, and Leo Lymburner. 2018. “Analysis Ready Data: Enabling Analysis of the Landsat Archive.” *Remote Sensing* 10 (9): 1363.

Fahnenstiel, Gary L, Michael J Sayers, Robert A Shuchman, Foad Yousef, and Steven A Pothoven. 2016. “Lake-Wide Phytoplankton Production and Abundance in the Upper Great Lakes: 2010–2013.” *Journal of Great Lakes Research* 42 (3): 619–29.

Freitas, Pedro, Gonçalo Vieira, João Canário, Diogo Folhas, and Warwick F Vincent. 2019. “Identification of a Threshold Minimum Area for Reflectance Retrieval from Thermokarst Lakes and Ponds Using Full-Pixel Data from Sentinel-2.” *Remote Sensing* 11 (6): 657.

Gallant, Alisa L. 1995. *Ecoregions of Alaska*. US Government Printing Office.

Genkai-Kato, Motomi, Yvonne Vadeboncoeur, Lone Liboriussen, and Erik Jeppesen. 2012. “Benthic–Planktonic Coupling, Regime Shifts, and Whole-lake Primary Production in Shallow Lakes.” *Ecology* 93 (3): 619–31.

Glesne, Reed S. 1986. “Fairbanks Fishery Resources Progress Report Number FY86–2.” Fairbank, AK.

Goetz, Scott J, Andrew G Bunn, Gregory J Fiske, and R A Houghton. 2005. “Satellite-Observed

Photosynthetic Trends across Boreal North America Associated with Climate and Fire Disturbance." *Proceedings of the National Academy of Sciences* 102 (38): 13521–25.

Gorelick, Noel, Matt Hancher, Mike Dixon, Simon Ilyushchenko, David Thau, and Rebecca Moore. 2017. "Google Earth Engine: Planetary-Scale Geospatial Analysis for Everyone." *Remote Sensing of Environment* 202: 18–27.

Haëntjens, Nils. 2018. "Plyr2 0.1.0." PyPi. https://pypi.org/project/pylr2/.

Halm, Douglas R, and Brad Griffith. 2014. "Water-Quality Data from Lakes in the Yukon Flats, Alaska, 2010-2011." US Geological Survey.

Halm, Douglas R, and Nikki Guldager. 2013. "Water-Quality Data of Lakes and Wetlands in the Yukon Flats, Alaska, 2007–2009." US Geological Survey.

Heglund, Patricia J., and John R. Jones. 2003. "Limnology of Shallow Lakes in the Yukon Flats National Wildlife Refuge, Interior Alaska." *Lake and Reservoir Management* 19 (2): 133–40.

Hestir, Erin Lee, Vittorio E Brando, Mariano Bresciani, Claudia Giardino, Erica Matta, Paolo Villa, and Arnold G Dekker. 2015. "Measuring Freshwater Aquatic Ecosystems: The Need for a Hyperspectral Global Mapping Satellite Mission." *Remote Sensing of Environment* 167: 181–95.

Hirsch, Robert M, James R Slack, and Richard A Smith. 1982. "Techniques of Trend Analysis for Monthly Water Quality Data." *Water Resources Research* 18 (1): 107–21.

Jackson, Leland J. 2003. "Macrophyte-Dominated and Turbid States of Shallow Lakes: Evidence from Alberta Lakes." *Ecosystems* 6 (3): 213–23.

Jeppesen, Erik, Torben L Lauridsen, Timo Kairesalo, and Martin R Perrow. 1998. "Impact of Submerged Macrophytes on Fish-Zooplankton Interactions in Lakes." In *The Structuring*

Role of Submerged Macrophytes in Lakes, 91–114. Springer.

Jepsen, S M, C I Voss, Michelle Ann Walvoord, J R Rose, B J Minsley, and B D Smith. 2013. "Sensitivity Analysis of Lake Mass Balance in Discontinuous Permafrost: The Example of Disappearing Twelvemile Lake, Yukon Flats, Alaska (USA)." *Hydrogeology Journal* 21 (1): 185–200.

Jepsen, Steven M, Michelle A Walvoord, Clifford I Voss, and Jennifer Rover. 2016. "Effect of Permafrost Thaw on the Dynamics of Lakes Recharged by Ice-jam Floods: Case Study of Yukon Flats, Alaska." *Hydrological Processes* 30 (11): 1782–95.

Jia, Gensuo J., Howard E. Epstein, and Donald A. Walker. 2003. "Greening of Arctic Alaska, 1981-2001." *Geophysical Research Letters* 30 (20).

John, Aji, Krstiina Ausmees, Kathleen Muenzen, Catherine Kuhn, and Amanda Tan. 2019. "SWEEP: Accelerating Scientific Research Through Scalable Serverless Workflows." In *UCC '19 Companion: IEEE/ACM 12th International Conference on Utility and Cloud Computing Companion Proceedings*. Auckland, New Zealand. https://www.ucc-conference.org/.

Johnston, Sarah Ellen, Robert G. Striegl, Matthew J. Bogard, Mark M. Dornblaser, David E. Butman, Anne Kellerman, Kimberly Wickland, David C. Podgorski, and Robert G. M. Spencer. 2020. "Hydrologic Connectivity Determines Dissolved Organic Matter Biogeochemistry in Northern High-Latitude Lakes." *Limnology and Oceanography*, no. 0: 1–16.

Ju, Junchang, and Jeffrey G Masek. 2016. "The Vegetation Greenness Trend in Canada and US Alaska from 1984–2012 Landsat Data." *Remote Sensing of Environment* 176: 1–16.

Kallio, Kari, Jenni Attila, Pekka Härmä, Sampsa Koponen, Jouni Pulliainen, Ulla-Maija

Hyytiäinen, and Timo Pyhälahti. 2008. “Landsat ETM+ Images in the Estimation of Seasonal Lake Water Quality in Boreal River Basins.” *Environmental Management* 42 (3): 511–22.

Kauer, Tuuli, Tiit Kutser, Helgi Arst, Thomas Danckaert, and Tiina Nõges. 2015. “Modelling Primary Production in Shallow Well Mixed Lakes Based on MERIS Satellite Data.” *Remote Sensing of Environment* 163: 253–61.

Kellerman, Anne M, Ana Arellano, David C Podgorski, Ellen E Martin, Jonathan B Martin, Kelly M Deuerling, Thomas S Bianchi, and Robert G M Spencer. 2019. “Fundamental Drivers of Dissolved Organic Matter Composition across an Arctic Effective Precipitation Gradient.” *Limnology and Oceanography* 10: 1–18.

Kloiber, Steven M, Patrick L Brezonik, Leif G Olmanson, and Marvin E Bauer. 2002. “A Procedure for Regional Lake Water Clarity Assessment Using Landsat Multispectral Data.” *Remote Sensing of Environment* 82 (1): 38–47.

Kuhn, C., A. de Matos Valerio, N. Ward, L. Loken, H.O. Sawakuchi, M. Kampel, J. Richey, et al. 2019. “Performance of Landsat-8 and Sentinel-2 Surface Reflectance Products for River Remote Sensing Retrievals of Chlorophyll-*a* and Turbidity.” *Remote Sensing of Environment* 224.

Kutser, Tiit, John Hedley, Claudia Giardino, Chris Roelfsema, and Vittorio E. Brando. 2020. “Remote Sensing of Shallow Waters – A 50 Year Retrospective and Future Directions.” *Remote Sensing of Environment* 240 (April): 111619.

Lee, Zhongping, John Marra, Mary Jane Perry, and Mati Kahru. 2015. “Estimating Oceanic Primary Productivity from Ocean Color Remote Sensing: A Strategic Assessment.” *Journal of Marine Systems* 149: 50–59.

Lymburner, Leo, Elizabeth Botha, Erin Hestir, Janet Anstee, Stephen Sagar, Arnold Dekker, and Tim Malthus. 2016. “Landsat 8: Providing Continuity and Increased Precision for Measuring Multi-Decadal Time Series of Total Suspended Matter.” *Remote Sensing of Environment* 185: 108–18.

Maciel, Daniel Andrade, Evlyn Márcia Leão De Moraes Novo, Cláudio Clemente Faria Barbosa, Vitor Souza Martins, Rogério Flores Júnior, Afonso Henrique Oliveira, Lino Augusto Sander De Carvalho, and Felipe De Lucia Lobo. 2020. “Evaluating the Potential of CubeSats for Remote Sensing Reflectance Retrieval over Inland Waters.” *International Journal of Remote Sensing* 41 (7): 2807–17.

Malthus, Tim J, Erin L Hestir, Arnold G Dekker, and Vittorio E Brando. 2012. “The Case for a Global Inland Water Quality Product.” In *2012 IEEE International Geoscience and Remote Sensing Symposium*, 5234–37. IEEE.

Manasypov, Rinat M, O S Pokrovsky, S N Kirpotin, and L S Shirokova. 2014. “Thermokarst Lake Waters across the Permafrost Zones of Western Siberia.” *The Cryosphere* 8 (4): 1177–93.

Massicotte, Philippe, Eero Asmala, Colin Stedmon, and Stiig Markager. 2017. “Global Distribution of Dissolved Organic Matter along the Aquatic Continuum: Across Rivers, Lakes and Oceans.” *Science of the Total Environment* 609: 180–91.

Matthews, Mark William. 2011. “A Current Review of Empirical Procedures of Remote Sensing in Inland and Near-Coastal Transitional Waters.” *International Journal of Remote Sensing* 32 (21): 6855–99.

Messager, Mathis Loïc, Bernhard Lehner, Günther Grill, Irena Nedeva, and Oliver Schmitt. 2016. “Estimating the Volume and Age of Water Stored in Global Lakes Using a Geo-

Statistical Approach." *Nature Communications* 7: 13603.

Minsley, Burke J., Jared D. Abraham, Bruce D. Smith, James C. Cannia, Clifford I. Voss, M. Torre Jorgenson, Michelle A. Walvoord, et al. 2012. "Airborne Electromagnetic Imaging of Discontinuous Permafrost." *Geophysical Research Letters* 39 (2): n/a-n/a.

Mobley, C, E Boss, and C Roesler. 2020. *NASA Ocean Optics Web Book*. Edited by NASA grant NNX14AQ49G. 2020th ed. Creative Commons. http://www.oceanopticsbook.info/view/references/publications.

Morel, Anclré, and Louis Prieur. 1977. "Analysis of Variations in Ocean Color." *Limnology and Oceanography*.

Mouw, Colleen B, Nick J Hardman-Mountford, Séverine Alvain, Astrid Bracher, Robert J W Brewin, Annick Bricaud, Aurea M Ciotti, Emmanuel Devred, Amane Fujiwara, and Takafumi Hirata. 2017. "A Consumer's Guide to Satellite Remote Sensing of Multiple Phytoplankton Groups in the Global Ocean." *Frontiers in Marine Science* 4: 41.

Myneni, Ranga B, C D Keeling, Compton J Tucker, Ghassem Asrar, and Ramakrishna R Nemani. 1997. "Increased Plant Growth in the Northern High Latitudes from 1981 to 1991." *Nature* 386 (6626): 698.

O'Reilly, John E, Stephane Maritorena, B Greg Mitchell, David A Siegel, Kendall L Carder, Sara A Garver, Mati Kahru, and Charles McClain. 1998. "Ocean Color Chlorophyll Algorithms for SeaWiFS." *Journal of Geophysical Research: Oceans* 103 (C11): 24937–53.

O'Reilly, John E, and P Jeremy Werdell. 2019. "Chlorophyll Algorithms for Ocean Color Sensors-OC4, OC5 & OC6." *Remote Sensing of Environment* 229: 32–47.

Olmanson, Leif G, Marvin E Bauer, and Patrick L Brezonik. 2008. "A 20-Year Landsat Water Clarity Census of Minnesota's 10,000 Lakes." *Remote Sensing of Environment* 112 (11):

4086–97.

Osburn, Christopher L, Courtney R Wigdahl, Sherilyn C Fritz, and Jasmine E Saros. 2011. "Dissolved Organic Matter Composition and Photoreactivity in Prairie Lakes of the US Great Plains." *Limnology and Oceanography* 56 (6): 2371–90.

Overland, J E, Edward Hanna, I Hanssen-Bauer, S-J Kim, J E Walsh, M Wang, U S Bhatt, and R L Thoman. 2018. "Surface Air Temperature." *Arctic Report Card*.

Overland, J E, and M Wang. 2005. "The Arctic Climate Paradox: The Recent Decrease of the Arctic Oscillation." *Geophysical Research Letters* 32 (6).

Oyama, Yoichi, Bunkei Matsushita, and Takehiko Fukushima. 2015. "Distinguishing Surface Cyanobacterial Blooms and Aquatic Macrophytes Using Landsat/TM and ETM+ Shortwave Infrared Bands." *Remote Sensing of Environment* 157: 35–47.

Pahlevan, N, B Smith, C Binding, and D M O'Donnell. 2017. "Spectral Band Adjustments for Remote Sensing Reflectance Spectra in Coastal/Inland Waters." *Optics Express* 25 (23): 28650–67.

Pahlevan, Nima, Sundarabalan Balasubramanian, Sudipta Sarkar, and Bryan Franz. 2018. "Toward Long-Term Aquatic Science Products from Heritage Landsat Missions." *Remote Sensing* 10 (9): 1337.

Pahlevan, Nima, Sudipta Sarkar, and Bryan A. Franz. 2016. "Uncertainties in Coastal Ocean Color Products: Impacts of Spatial Sampling." *Remote Sensing of Environment* 181 (August): 14–26.

Palmer, Stephanie C.J., Tiit Kutser, and Peter D. Hunter. 2015. "Remote Sensing of Inland Waters: Challenges, Progress and Future Directions." *Remote Sensing of Environment* 157 (February): 1–8.

Pastick, Neal J, M Torre Jorgenson, Scott J Goetz, Benjamin M Jones, Bruce K Wylie, Burke J Minsley, Hélène Genet, Joseph F Knight, David K Swanson, and Janet C Jorgenson. 2019. "Spatiotemporal Remote Sensing of Ecosystem Change and Causation across Alaska." *Global Change Biology* 25 (3): 1171–89.

Pettorelli, Nathalie, Jon Olav Vik, Atle Mysterud, Jean-Michel Gaillard, Compton J Tucker, and Nils Chr Stenseth. 2005. "Using the Satellite-Derived NDVI to Assess Ecological Responses to Environmental Change." *Trends in Ecology & Evolution* 20 (9): 503–10.

Pienitz, Reinhard, John P Smol, and Glen M MacDonald. 1999. "Paleolimnological Reconstruction of Holocene Climatic Trends from Two Boreal Treeline Lakes, Northwest Territories, Canada." *Arctic, Antarctic, and Alpine Research* 31 (1): 82–93.

Planet. 2017. "Planet Application Program Interface: In Space for Life on Earth." San Francisco. https://api.planet.com.

Quay, P D, J E Richey, A H Devol, R Benner, and B R Forsberg. 1995. "The 18O: 16O of Dissolved Oxygen in Rivers and Lakes in the Amazon Basin: Determining the Ratio of Respiration to Photosynthesis Rates in Freshwaters." *Limnology and Oceanography* 40 (4): 718–29.

Rautio, Milla, and Warwick F Vincent. 2006. "Benthic and Pelagic Food Resources for Zooplankton in Shallow High-latitude Lakes and Ponds." *Freshwater Biology* 51 (6): 1038–52.

Raymond, Peter A, Jens Hartmann, Ronny Lauerwald, Sebastian Sobek, Cory McDonald, Mark Hoover, David Butman, et al. 2013. "Global Carbon Dioxide Emissions from Inland Waters." *Nature* 503 (7476): 355–59.

Rey, David M, Michelle Walvoord, Burke Minsley, Jennifer Rover, and Kamini Singha. 2019.

"Investigating Lake-Area Dynamics across a Permafrost-Thaw Spectrum Using Airborne Electromagnetic Surveys and Remote Sensing Time-Series Data in Yukon Flats, Alaska." *Environmental Research Letters* 14 (2): 25001.

Rouse, J W. 1974. "Monitoring the Vernal Advancement of Retrogradation of Natural Vegetation, NASA/GSFG, Type III." *Final Report* 371.

Roy, David P, Junchang Ju, Kristi Kline, Pasquale L Scaramuzza, Valeriy Kovalskyy, Matthew Hansen, Thomas R Loveland, Eric Vermote, and Chunsun Zhang. 2010. "Web-Enabled Landsat Data (WELD): Landsat ETM+ Composited Mosaics of the Conterminous United States." *Remote Sensing of Environment* 114 (1): 35–49.

Rühland, Kathleen, Alisha Priesnitz, and John P Smol. 2003. "Paleolimnological Evidence from Diatoms for Recent Environmental Changes in 50 Lakes across Canadian Arctic Treeline." *Arctic, Antarctic, and Alpine Research* 35 (1): 110–23.

Sayers, Michael J, Amanda G Grimm, Robert A Shuchman, Andrew M Deines, David B Bunnell, Zachary B Raymer, Mark W Rogers, Whitney Woelmer, David H Bennion, and Colin N Brooks. 2015. "A New Method to Generate a High-Resolution Global Distribution Map of Lake Chlorophyll." *International Journal of Remote Sensing* 36 (7): 1942–64.

Seekell, David A., Jean-François Lapierre, Jenny Ask, Ann-Kristin Bergström, Anne Deininger, Patricia Rodríguez, and Jan Karlsson. 2015. "The Influence of Dissolved Organic Carbon on Primary Production in Northern Lakes." *Limnology and Oceanography* 60 (4): 1276–85.

Shuchman, Robert A, Michael Sayers, Gary L Fahnenstiel, and George Leshkevich. 2013. "A Model for Determining Satellite-Derived Primary Productivity Estimates for Lake Michigan." *Journal of Great Lakes Research* 39: 46–54.

Siegel, D A, T K Westberry, M C O'brien, N B Nelson, A F Michaels, J R Morrison, A Scott, E

A Caporelli, J C Sorensen, and S Maritorena. 2001. “Bio-Optical Modeling of Primary Production on Regional Scales: The Bermuda BioOptics Project.” *Deep Sea Research Part II: Topical Studies in Oceanography* 48 (8–9): 1865–96.

Silva, Thiago S F, Maycira P F Costa, John M Melack, and Evlyn M L M Novo. 2008. “Remote Sensing of Aquatic Vegetation: Theory and Applications.” *Environmental Monitoring and Assessment* 140 (1–3): 131–45.

Solomon, Christopher T, Denise A Bruesewitz, David C Richardson, Kevin C Rose, Matthew C Van de Bogert, Paul C Hanson, Timothy K Kratz, Bret Larget, Rita Adrian, and Brenda Leroux Babin. 2013. “Ecosystem Respiration: Drivers of Daily Variability and Background Respiration in Lakes around the Globe.” *Limnology and Oceanography* 58 (3): 849–66.

Squires, Margaret M, Lance F W Lesack, Robert E Hecky, Stephanie J Guildford, Patricia Ramlal, and Scott N Higgins. 2009. “Primary Production and Carbon Dioxide Metabolic Balance of a Lake-Rich Arctic River Floodplain: Partitioning of Phytoplankton, Epipelon, Macrophyte, and Epiphyton Production among Lakes on the Mackenzie Delta.” *Ecosystems* 12 (5): 853–72.

Stanley, Emily H, and Paul A del Giorgio. 2018. “Toward an Integrative, Whole Network Approach to C Cycling of Inland Waters.” *Limnology and Oceanography Letters* 3 (3): 39–40.

Sulla-Menashe, Damien, Curtis E Woodcock, and Mark A Friedl. 2018. “Canadian Boreal Forest Greening and Browning Trends: An Analysis of Biogeographic Patterns and the Relative Roles of Disturbance versus Climate Drivers.” *Environmental Research Letters* 13 (1): 14007.

Tank, Suzanne E, Lance F W Lesack, and Raymond H Hesslein. 2009. “Northern Delta Lakes as

Summertime CO 2 Absorbers within the Arctic Landscape." *Ecosystems* 12 (1): 144–57.

Topp, Simon N, Tamlin M Pavelsky, Daniel Jensen, Marc Simard, and Matthew R V Ross. 2020. "Research Trends in the Use of Remote Sensing for Inland Water Quality Science: Moving Towards Multidisciplinary Applications." *Water* 12 (1): 169.

Tucker, Compton J. 1979. "Red and Photographic Infrared Linear Combinations for Monitoring Vegetation." *Remote Sensing of Environment* 8 (2): 127–50.

Vanhellemont, Quinten. 2019. "Adaptation of the Dark Spectrum Fitting Atmospheric Correction for Aquatic Applications of the Landsat and Sentinel-2 Archives." *Remote Sensing of Environment* 225: 175–92.

Vermote, E, D Tanré, J L Deuzé, M Herman, J J Morcrette, and S Y Kotchenova. 2006. "Second Simulation of a Satellite Signal in the Solar Spectrum-Vector (6SV)." *6S User Guide Version* 3: 1–55.

Vermote, Eric, Chris Justice, Martin Claverie, and Belen Franch. 2016. "Preliminary Analysis of the Performance of the Landsat 8/OLI Land Surface Reflectance Product." *Remote Sensing of Environment* 185: 46–56.

Verpoorter, Charles, Tiit Kutser, David A Seekell, and Lars J Tranvik. 2014. "A Global Inventory of Lakes Based on High-resolution Satellite Imagery." *Geophysical Research Letters* 41 (18): 6396–6402.

Vesterinen, Jussi, Shawn P Devlin, Jari Syväranta, and Roger I Jones. 2016. "Accounting for Littoral Primary Production by Periphyton Shifts a Highly Humic Boreal Lake towards Net Autotrophy." *Freshwater Biology* 61 (3): 265–76.

Virtanen, Pauli, Ralf Gommers, Travis E Oliphant, Matt Haberland, Tyler Reddy, David Cournapeau, Evgeni Burovski, Pearu Peterson, Warren Weckesser, and Jonathan Bright.

2020. “SciPy 1.0: Fundamental Algorithms for Scientific Computing in Python.” *Nature Methods*, 1–12.

Vogelmann, James E., Alisa L. Gallant, Hua Shi, and Zhe Zhu. 2016. “Perspectives on Monitoring Gradual Change across the Continuity of Landsat Sensors Using Time-Series Data.” *Remote Sensing of Environment* 185 (November): 258–70.

Vonk, J. E., S. E. Tank, W. B. Bowden, I. Laurion, W. F. Vincent, P. Alekseychik, M. Amyot, et al. 2015. “Reviews and Syntheses: Effects of Permafrost Thaw on Arctic Aquatic Ecosystems.” *Biogeosciences* 12 (23): 7129–67.

Walvoord, Michelle A, and Robert G Striegl. 2007. “Increased Groundwater to Stream Discharge from Permafrost Thawing in the Yukon River Basin: Potential Impacts on Lateral Export of Carbon and Nitrogen.” *Geophysical Research Letters* 34 (12).

Walvoord, Michelle A, Clifford I Voss, and Tristan P Wellman. 2012. “Influence of Permafrost Distribution on Groundwater Flow in the Context of Climate-driven Permafrost Thaw: Example from Yukon Flats Basin, Alaska, United States.” *Water Resources Research* 48 (7).

Wang, Chi-Kuei, and William D Philpot. 2007. “Using Airborne Bathymetric Lidar to Detect Bottom Type Variation in Shallow Waters.” *Remote Sensing of Environment* 106 (1): 123–35.

Wang, Jida, Yongwei Sheng, and Tak Shun D Tong. 2014. “Monitoring Decadal Lake Dynamics across the Yangtze Basin Downstream of Three Gorges Dam.” *Remote Sensing of Environment* 152: 251–69.

Wang, Jonathan A, Damien Sulla-Menashe, Curtis E Woodcock, Oliver Sonnentag, Ralph F Keeling, and Mark A Friedl. 2019. “Extensive Land Cover Change Across Arctic-Boreal

Northwestern North America from Disturbance and Climate Forcing." *Global Change Biology* 26 (2): 807-822.

Wauthy, Maxime, Milla Rautio, Kirsten S Christoffersen, Laura Forsström, Isabelle Laurion, Heather L Mariash, Sari Peura, and Warwick F Vincent. 2018. "Increasing Dominance of Terrigenous Organic Matter in Circumpolar Freshwaters Due to Permafrost Thaw." *Limnology and Oceanography Letters* 3 (3): 186–98.

Wellman, Tristan P, Clifford I Voss, and Michelle A Walvoord. 2013. "Impacts of Climate, Lake Size, and Supra-and Sub-Permafrost Groundwater Flow on Lake-Talik Evolution, Yukon Flats, Alaska (USA)." *Hydrogeology Journal* 21 (1): 281–98.

Werdell, P Jeremy, Michael J Behrenfeld, Paula S Bontempi, Emmanuel Boss, Brian Cairns, Gary T Davis, Bryan A Franz, Ulrik B Gliese, Eric T Gorman, and Otto Hasekamp. 2019. "The Plankton, Aerosol, Cloud, Ocean Ecosystem Mission: Status, Science, Advances." *Bulletin of the American Meteorological Society* 100 (9): 1775–94.

Wetzel, R G, and R A Hough. 1972. "Productivity and the Role of Aquatic Macrophytes in Lakes: An Assessment." Michigan State Univ., Hickory Corners. WK Kellogg Biological Station. https://www.osti.gov/servlets/purl/4639975.

Wetzel, Robert G. 2001. *Limnology: Lake and River Ecosystems*. Gulf Professional Publishing.

Wik, Martin, Ruth K. Varner, Katey Walter Anthony, Sally MacIntyre, and David Bastviken. 2016. "Climate-Sensitive Northern Lakes and Ponds Are Critical Components of Methane Release." *Nature Geoscience* 9 (2): 99–105.

Yousef, Foad, W Charles Kerfoot, Robert Shuchman, and Gary Fahnenstiel. 2014. "Bio-Optical Properties and Primary Production of Lake Michigan: Insights from 13-Years of SeaWiFS Imagery." *Journal of Great Lakes Research* 40 (2): 317–24.

Zhu, Zhe, Shixiong Wang, and Curtis E Woodcock. 2015. “Improvement and Expansion of the Fmask Algorithm: Cloud, Cloud Shadow, and Snow Detection for Landsats 4–7, 8, and Sentinel 2 Images.” *Remote Sensing of Environment* 159: 269–77.

3.6 APPENDIX B

This section provides additional details on site selection, the satellite and airborne imagery used for the GPP model, and additional figures analyzing differences in remote sensing reflectance spectra. References can be found in Section 3.6.

Table 3.4. Range of limnological conditions documented in this study and previous work.

	This study overall	**Bogard et al (2019)**	**Halm & Guldager (2013)**	**Halm & Griffith (2014)**	**Heglund and Jones (2003)***	**Corcoran (2009)**	**Lewis (2014)**
Year Sampled	2018	2016	2007 - 2009	2010 - 2011	1985, 1986, 1987, 1989	2001 - 2003	2010 - 2012
Count (n)	7	21	144	122	129	13	14
Depth (m)	1.8 (1.5-7.4)	2.1 (1.53 - 4.38)			<2 m (<0.5 m - 0.6m)*		<2 m
Surface Area (km^2)	1.75 (0.85 – 3.08)		0.47 (0.21 – 0.92)	1.9 (1.2 – 3.1)	0.018 (<0.001 - 2.47)**	0.46 (0.006 - 0.5)	0.005 - 6*
pH	9.46 (8.98 – 9.69)	8.1 (7.55 - 8.68)	8.06 (8.05 – 9.22)	8.6 (7.7 – 9.2)	7.8 (5.9 - 10)**		
Turbidity (FNU)	0.54 (0 – 0.96)	0.75 (0 - 1.61)					
Chl-a ($\mu g\ L^{-1}$)		5.28 (3.91-9.70)			7.9 (0.5 - 115)**	11.13 +- 2.62*	1 - 25*
GPP ($g\ O_2\ m^{-2}\ d^{-1}$)	4.1 (2.7 – 7.2) 9.72 (6.25 - 10.50)	4.5 (2.3 - 2.2)					
a440 (m^{-1})	1.13 (0.78 - 1.8)	2.05 (1.28 - 3.22)					
a254 (m^{-1})	44 (38 - 51)	61.77 (44.14 - 78.92)	60.90 (43.98 - 88.25)	60.90 (44.8 - 90.1)			
DOC ($mg\ L^{-1}$)	27.64 (19.33 – 31.32)	26.91 (16.36 - 35.74)	30.5 (23.55 – 40.05)	32.7 (24.55 – 45.2)			

** anecdotal mean with full range*
**median and full range*
*** reported as stdev not IQR*
**full range*

Table 3.5. Satellite image IDs for tiles used in this analysis. Planet and Sentinel-2 scenes listed here were the acquisitions closest in time to field surveys (Table 3.1). For the 2018 campaign, no cloud-free data within 5 days were acquired so Landsat seasonal composites were used.

Sentinel-2 (July 22, 2018)	Landsat 2016 (Seasonal Composites)	Landsat 2018 (Seasonal Composites)
L1C_T06WVU_A016099_20180722T213530	LE07_L1TP_068013_20160713_20160831_01_T1	LE07_L1TP_068013_20180601_20180628_01_T1
L1C_T06WWU_A016099_20180722T213530	LE07_L1TP_068014_20160713_20160901_01_T1	LE07_L1TP_068013_20180617_20180715_01_T1
L1C_T06WWV_A016099_20180722T213530	LE07_L1TP_069013_20160704_20160831_01_T1	LE07_L1TP_068013_20180703_20180730_01_T1
	LE07_L1TP_069013_20160720_20160831_01_T1	LE07_L1TP_068014_20180601_20180628_01_T1
Planet (July 23, 2018)	LE07_L1TP_069014_20160618_20160901_01_T1	LE07_L1TP_068014_20180617_20180714_01_T1
20180723_204630_1021	LE07_L1TP_069014_20160704_20160831_01_T1	LE07_L1TP_068014_20180703_20180730_01_T1
20180723_204744_0f35	LE07_L1TP_069014_20160720_20160901_01_T1	LE07_L1TP_068014_20180719_20180816_01_T1
20180723_204628_1021	LE07_L1TP_070013_20160711_20160831_01_T1	LE07_L1TP_069013_20180608_20180705_01_T1
20180723_204743_0f35	LE07_L1TP_070013_20160727_20160831_01_T1	LE07_L1TP_069013_20180624_20180721_01_T1
20180723_204624_1021	LE07_L1TP_070014_20160625_20160901_01_T1	LE07_L1TP_069013_20180726_20180821_01_T1
20180723_204627_1021	LE07_L1TP_070014_20160711_20160831_01_T1	LE07_L1TP_069014_20180608_20180705_01_T1
20180723_204449_100c	LE07_L1TP_070014_20160727_20160831_01_T1	LE07_L1TP_069014_20180624_20180721_01_T1
20180722_204413_1033	LC08_L1TP_068013_20160603_20170223_01_T1	LE07_L1TP_069014_20180710_20180806_01_T1
20180723_204451_100c	LC08_L1TP_068013_20160619_20170221_01_T1	LE07_L1TP_069014_20180726_20180821_01_T1
20180722_204416_1033	LC08_L1TP_068013_20160705_20170223_01_T1	LE07_L1TP_070013_20180615_20180712_01_T1
20180722_204415_1033	LC08_L1TP_068013_20160721_20170221_01_T1	LE07_L1TP_070013_20180701_20180728_01_T1
20180723_204626_1021	LC08_L1TP_068014_20160603_20170223_01_T1	LE07_L1TP_070013_20180717_20180813_01_T1
20180723_204624_1021	LC08_L1TP_068014_20160705_20170223_01_T1	LE07_L1TP_070014_20180615_20180712_01_T1
20180723_204448_100c	LC08_L1TP_068014_20160721_20170221_01_T1	LE07_L1TP_070014_20180701_20180728_01_T1
20180722_204411_1033	LC08_L1TP_069013_20160610_20170220_01_T1	LE07_L1TP_070014_20180717_20180813_01_T1
20180723_191112_0f3d	LC08_L1TP_069013_20160626_20170222_01_T1	LC08_L1TP_068013_20180609_20180615_01_T1
20180723_204442_100c	LC08_L1TP_069013_20160712_20170222_01_T1	LC08_L1TP_068013_20180625_20180704_01_T1
20180723_204441_100c	LC08_L1TP_069013_20160728_20170221_01_T1	LC08_L1TP_068013_20180711_20180717_01_T1
20180722_204406_1033	LC08_L1TP_069014_20160610_20170220_01_T1	LC08_L1TP_068013_20180727_20180731_01_T1
	LC08_L1TP_069014_20160626_20170222_01_T1	LC08_L1TP_068014_20180609_20180615_01_T1
AVIRIS-NG	LC08_L1TP_069014_20160712_20170222_01_T1	LC08_L1TP_068014_20180625_20180704_01_T1
ang20180722t212222	LC08_L1TP_069014_20160728_20170221_01_T1	LC08_L1TP_068014_20180711_20180717_01_T1
ang20180722t214026	LC08_L1TP_070013_20160601_20170223_01_T1	LC08_L1TP_068014_20180727_20180731_01_T1
ang20180722t215812	LC08_L1TP_070013_20160617_20170222_01_T1	LC08_L1TP_069013_20180616_20180703_01_T1
ang20180722t221648	LC08_L1TP_070013_20160703_20170221_01_T1	LC08_L1TP_069013_20180702_20180717_01_T1
ang20180722t205755	LC08_L1TP_070013_20160719_20170223_01_T1	LC08_L1TP_069013_20180718_20180731_01_T1
ang20180722t204801	LC08_L1TP_070014_20160601_20170223_01_T1	LC08_L1TP_069014_20180616_20180703_01_T1
ang20180722t203748	LC08_L1TP_070014_20160617_20170222_01_T1	LC08_L1TP_069014_20180702_20180717_01_T1
	LC08_L1TP_070014_20160703_20170221_01_T1	LC08_L1TP_069014_20180718_20180731_01_T1
	LC08_L1TP_070014_20160719_20170223_01_T1	LC08_L1TP_070013_20180607_20180615_01_T1
		LC08_L1TP_070013_20180623_20180704_01_T1
		LC08_L1TP_070013_20180709_20180717_01_T1
		LC08_L1TP_070013_20180725_20180731_01_T1
		LC08_L1TP_070014_20180607_20180615_01_T1
		LC08_L1TP_070014_20180623_20180704_01_T1
		LC08_L1TP_070014_20180709_20180717_01_T1
		LC08_L1TP_070014_20180725_20180731_01_T1

3.6.1 *Extended Laboratory Methods*

Water temperature, pH and turbidity were measured on site using an EXO-2 multiparameter probe (Yellow Springs Instruments). Samples for dissolved organic carbon

(DOC, mg L^{-1}) and chromophoric dissolved organic matter (CDOM) were measured as in Johnston et al. (2019). CDOM absorbance was measured from 220 to 800 nm and reported as the absorption coefficient at 440 nm (a_{440}, m^{-1}) and 254 nm (a_{254}, m^{-1}). Phytoplankton pigments were collected from water samples filtered using Whatman GF/F filters with a 0.7 μm nominal pore size that were pre-combusted at 450 °C for > 5 hours before HPLC analysis as described in Van Heukelem and Thomas (2001).

At each site, point measurements of dissolved oxygen (DO) concentration, $\delta^{18}O$–DO and $\delta^{18}O$–H_2O were collected and used to calculate spatiotemporally integrated ecosystem GPP. $\delta^{18}O$–DO samples were processed on a ThermoFinnigan Delta V Plus isotope ratio mass spectrometer (IRMS) in continuous flow mode (Bogard et al. 2019). Stable isotope composition of water ($\delta^{18}O$–H_2O) was measured using an isotopic water analyzer (Picarro L2140-i).

3.6.2 *Extended Remote Sensing Methods*

The instrument has a 25° field of view and measures from 350 to 2500 nm. Measurements from 0.3 m above the water surface were collected at a fixed geometry with a solar zenith angle of 90 - 135° at 45° from the water surface to minimize glint as in Kuhn *et al.* (2019). When possible, sampling was done in direct sunlight during the brightest part of the day (8 AM - 1 PM) to coincide with local satellite overpass times. At each site, ten replicates each of the water surface (L_{sw}), a white Spectralon reference (L_{red}) panel, and the sky (L_{sky}) were collected in sequence (Valerio et al. 2017).

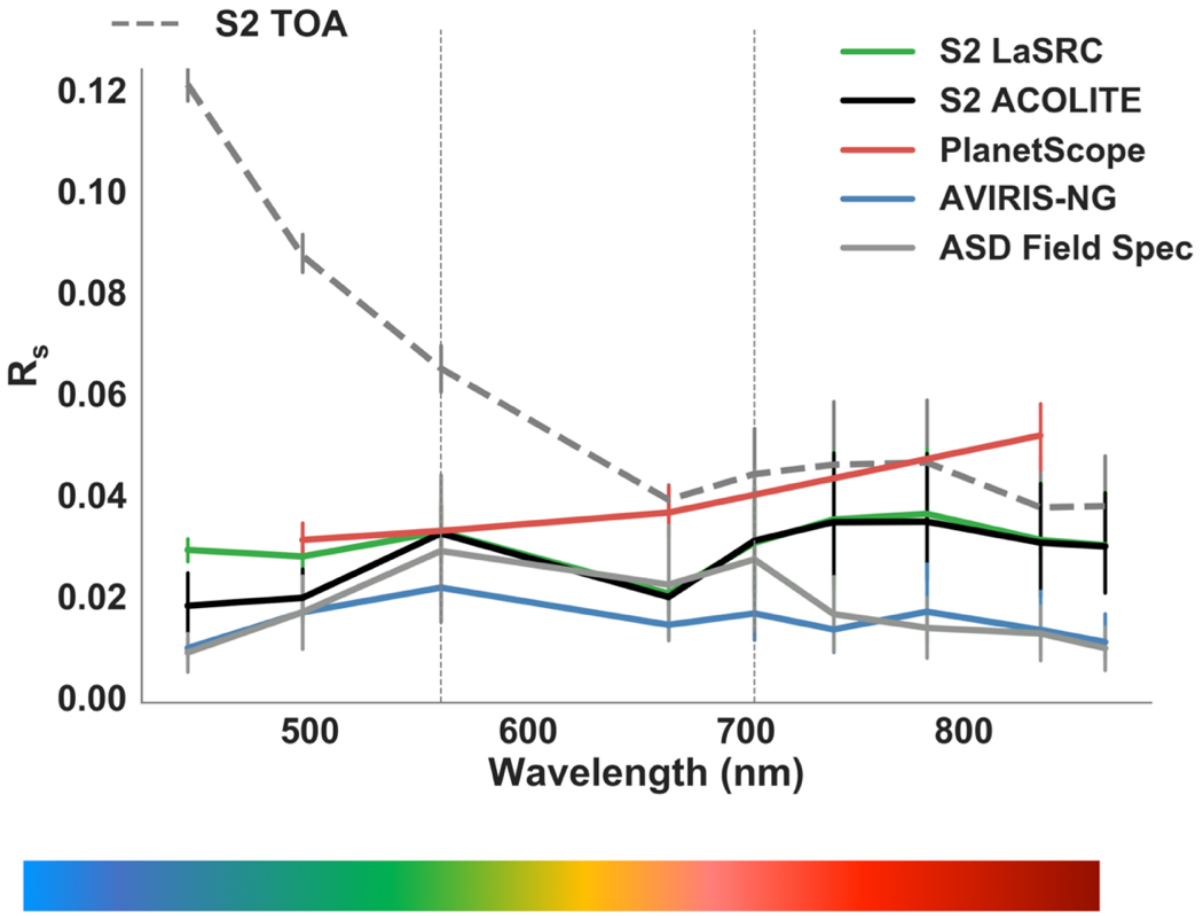

Figure 3.7. Surface reflectance for sensors tested in this study. Surface reflectance (R_s) represented as the median and interquartile range (25%, 75%) of 2018 lakes. Dashed vertical grey lines show the wavelengths used to model GPP (Table 3.2) at 560 nm (green) and 703 nm (red-edge). Top-of-atmosphere (TOA) spectra given for context.

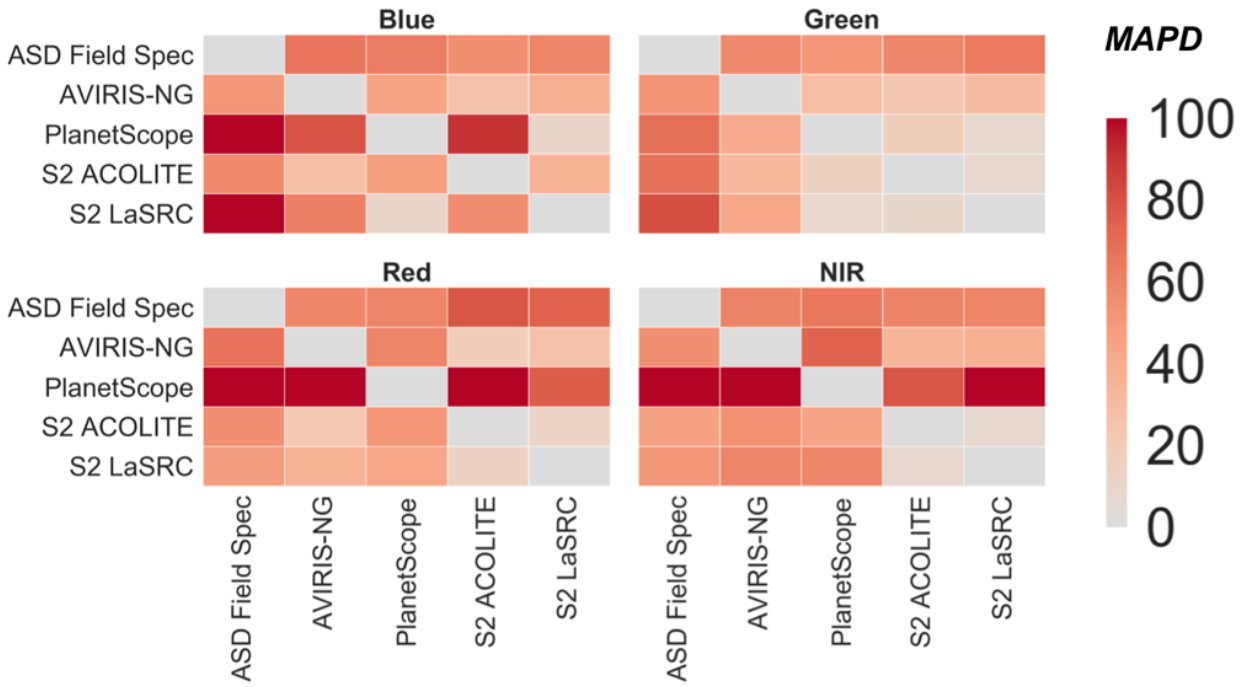

Figure 3.8. Mean Absolute Percent Difference in surface reflectance between each sensor for each band.

3.6.3 *Extended Results: Reflectance Inter-comparison*

Median visible to near-infrared R_s values (443.9 – 864.8 nm) were 0.014 (interquartile range = 0.0056 - 0.024), 0.012 (interquartile range = 0.009242 - 0.017), 0.021 (interquartile range = 0.017 - 0.034), and 0.025 (0.02-0.03) for the ASD Field Spec, AVIRIS-NG, Sentinel-2 corrected with ACOLITE (Python Version 20190326.0), and Sentinel-2 corrected with LaSRC, respectively. PlanetScope had the highest overall reflectance (median 0.035, interquartile range = 0.031 - 0.043).

The closest agreement (MAPD <1%) was observed between the two Sentinel-2 atmospheric corrections (ACOLITE versus LaSRC) (Appendix B, Figure 3.7) where surface reflectance values were very closely aligned with the exception of the blue bands (MAPD ~30%),

which are known to be the most sensitive to errors from atmospheric correction (Kuhn *et al.*, 2019). The least agreement (276% MAPD) was observed in between PlanetScope and AVIRIS-NG in the near-infrared bands (Appendix B, Figure 3.7), likely resulting from the much wider bandpass of Planet in the NIR.

R_s generally showed high values, with peaks in the green and NIR (Figure 3.6). *In situ* R_s was lower (< 0.015) across the visible to NIR (443.9 – 864.8 nm) than satellite *Rs* (> 0.02) likely resulting from residual scattering remaining after atmospheric correction (Kuhn *et al.*, 2019; Pahlevan *et al.*, 2019). *In situ* median NIR (835 nm) values were the comparable for the ASD (median = 0.012 interquartile range 0.005 – 0.02) and AVIRIS-NG (median = 0.013 interquartile range 0.01 – 0.04) and much lower than the satellite R_s. The agreement observed between airborne and *in situ Rs* further implies that *Rs* differences could be due to atmospheric correction.

We assessed how well any individual sensor performed overall relative to other sensors by averaging the MAPD for each sensor. The two Sentinel-2 surface reflectance products showed the lowest MAPD with each other and other sensors (LaSRC median = 28%, interquartile range 7 - 60%, ACOLITE: median = 25%, interquartile range = 8 - 60%). AVIRIS-NG and PlanetScope had higher and similar MAPDs (AVIRIS-NG: median = 48%, interquartile range = 27- 61%, PlanetScope: median = 44%, interquartile range = 9 - 60%). The PlanetScope MAPDs are comparable with Mean Absolute Percent Error (MAPE) values of 46% reported over turbid waters (Maciel et al. 2020).

The largest differences were observed between the field measurements and satellite platforms (median = 55%, interquartile range = 48 - 72%), which could be because the remote sensing acquisitions occurred a week after field measurements. While images were acquired on the closest cloud-free day possible coincident to field measurements, this lag between field and

satellite overpasses mean observations were acquired under different atmospheric and environmental conditions which no doubt contributed uncertainty.

3.6.4 *Extended Results: NIR*

Sensors disagreed the most in the NIR as indicated by a large MAPD (median 54%, interquartile range of 8 - 60%). Sentinel-2 NIR (835 nm) *Rs* ranged from a median of 0.038 (interquartile range 0.005 – 0.02) for TOA to slightly lower and similar values for LaSRC (median = 0.031 interquartile range 0.018 – 0.04) and ACOLITE (median = 0.031 interquartile range 0.016 – 0.041) after atmospheric correction. Planet had the highest NIR *Rs* (median = 0.05 interquartile range 0.04 – 0.06). High NIR and shortwave infrared (SWIR) R_s in these shallow, macrophyte-rich lakes contrasts sharply to the classic assumption of water as a "dark pixel" (Wang and Shi 2007b; Siegel et al. 2000). Greater disagreement in the NIR over water, and high R_s in the NIR, is consistent with other studies (Bernardo *et al.*, 2017; Wang *et al.*, 2019; Maciel *et al.*, 2019) and has implications for NIR use in atmospheric correction and water detection. Atmospheric corrections that rely on negligible NIR/SWIR R_s will overestimate aerosols. Therefore terrestrial approaches, or other techniques that allow for NIR/SWIR R_s, are likely a more appropriate choice for these systems (Bailey *et al.*, 2010; Vermote *et al.*, 2016; Vanhellemont, 2019).

Table 3.6. Model results for sensors tested in this study including ACOLITE.

	Green (~560 nm)				Red-edge (~703 nm)			
	Slope	*Intercept*	r^2	*p-value*	*Slope*	*Intercept*	r^2	*p-value*
S2 TOA	478.91	-22.46	0.30	0.000429	478.91	-22.46	0.56	0.000078
S2 LaSRC	446.18	-5.93	0.53	0.000104	446.18	-5.93	0.62	0.000219
S2 ACOLITE	391.77	-4.03	0.28	0.000378	391.77	-4.03	0.57	0.000278
PlanetScope	413.39	-6.65	0.78	0.000028	NA	NA	NA	
AVIRIS-NG	607.19	-4.51	0.40	0.000198	607.19	-4.51	0.74	0.000086
ASD Field Spec	146.86	4.43	0.68	0.001667	146.86	4.43	0.80	0.001823

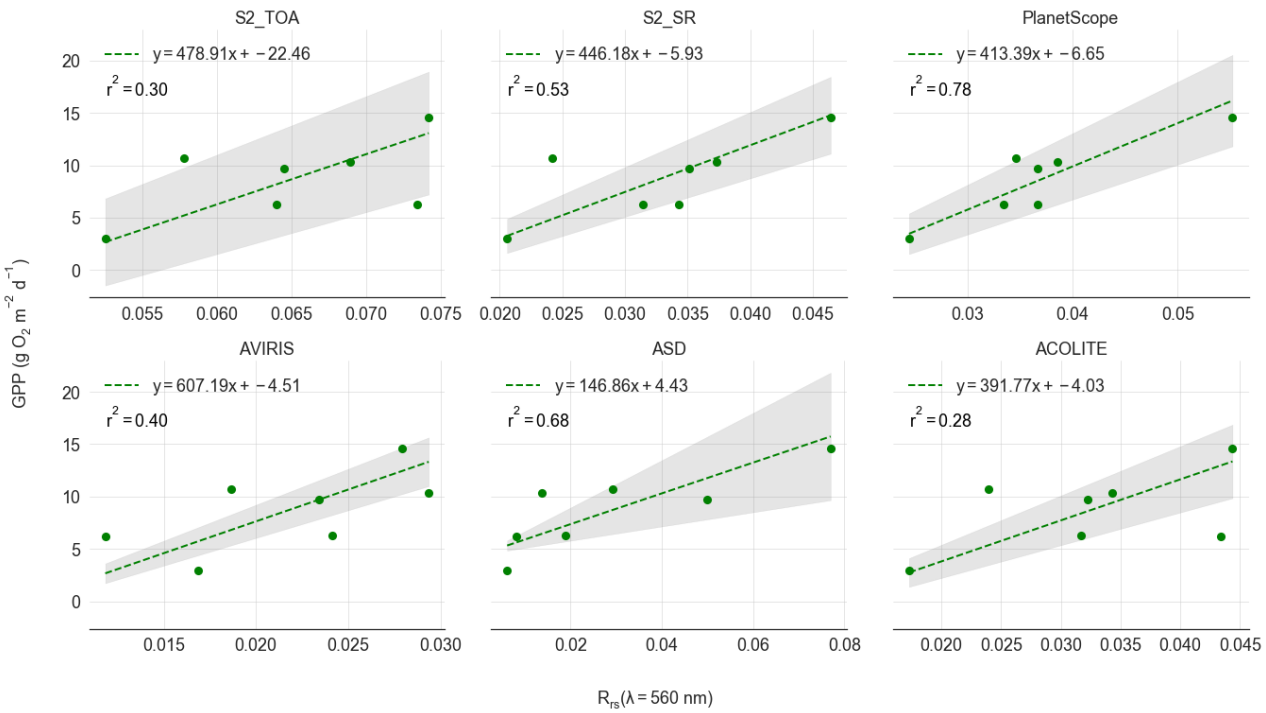

Figure 3.9. Correlation between *in situ* GPP (g O2 m-2 d-1) on the y-axis and lake color measured as reflectance (Rs) in the green (~ 560 nm) on the x-axis. The data points (green circles) in each subplot represents each of the 2018 study lakes (n = 7). The different subplots show lake color from each of the respective sensors considered in this study. The title above each subplot indicates which sensor's green Rs is being plotted on the x-axis. Regression model and coefficients of determination (r2) are given in inset.

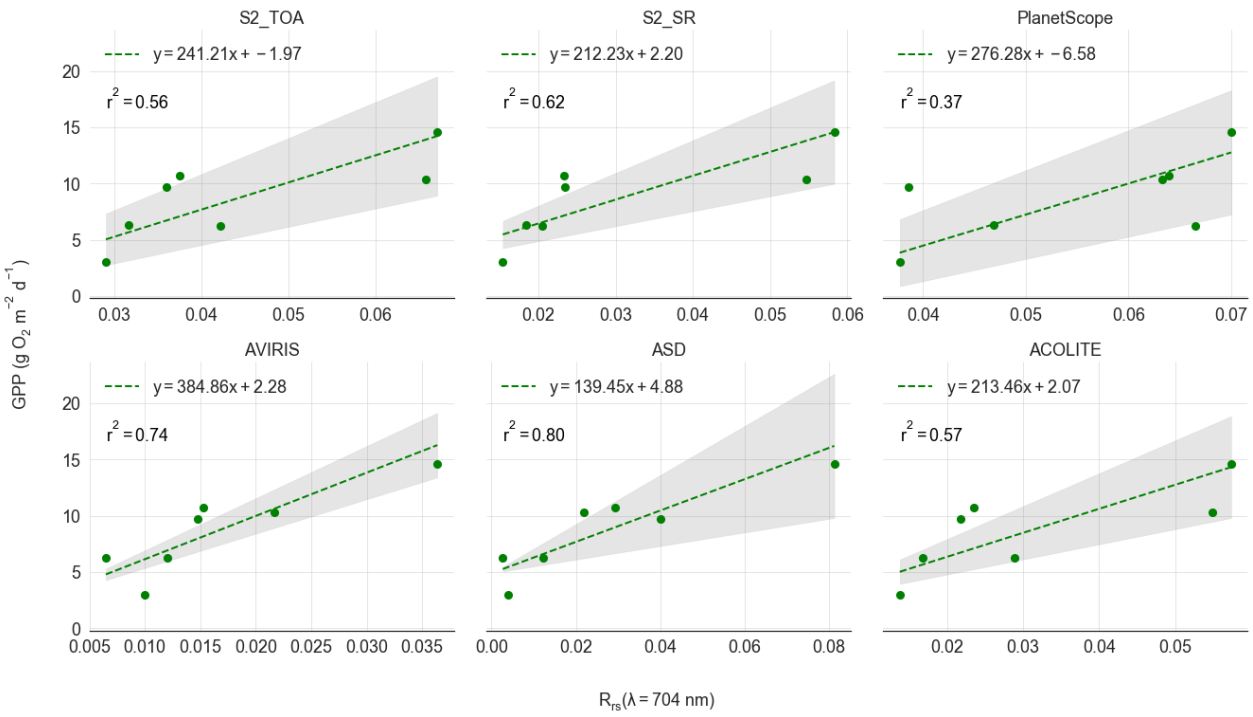

Figure 3.10 Correlation between *in situ* GPP (g O_2 m^{-2} d^{-1}) on the y-axis and lake color measured as reflectance (R_s) in the red-edge (~ 704 nm) on the x-axis. The data points (green circles) in each subplot represents each of the 2018 study lakes (n = 7). The different subplots show lake color from each of the respective sensors considered in this study. The title above each subplot indicates which sensor's red-edge R_s is being plotted on the x-axis. Regression model and coefficients of determination (r^2) are given in inset.

Chapter 4. DECLINING COLOR IN ARCTIC-BOREAL LAKES

Kuhn et al., 2021. *Proceedings of the National Academy*.

4.1 INTRODUCTION

Recent, widespread changes in arctic-boreal primary productivity linked to global climate change have been documented in terrestrial (Jia, Epstein, and Walker 2003; Bhatt et al. 2013; Ju and Masek 2016; Beck and Goetz 2011) and oceanic (Arrigo and van Dijken 2008; Lewis, van Dijken, and Arrigo 2020) ecosystems. Satellite records have enabled large-scale analysis, providing evidence of uneven changes in vegetation growth in tundra (Bhatt et al. 2013; Jia, Epstein, and Walker 2009; Ju and Masek 2016; Myneni et al. 1997; Pastick et al. 2019; Wang et al. 2019) and boreal ecosystems (Phoenix and Bjerke 2016; de Jong et al. 2011; Bhatt et al. 2013), as inferred from vegetation indices. Thus, satellite records have provided critical insight into long-term global change in remote arctic and boreal regions.

However, less attention has been paid to the large-scale changes in lake color, owing in part to the prevalence of small lakes, which were previously not detectable by earlier generations of satellites (Duncan et al. 2020). Lakes are abundant in permafrost landscapes (Verpoorter et al. 2014; Downing et al. 2006), supporting crucial ecosystem services such as wildlife habitat, biodiversity, nutrient and carbon (C) cycling, and recreation. The lack of pan-arctic studies of lake color is surprising because half of the world's total lake surface area is concentrated in arctic-boreal regions (Smith, Sheng, and MacDonald 2007), where permafrost thaw has been predicted to dramatically alter lake physical and optical properties (Vonk et al. 2015).

Evidence from field studies has suggested lake color is linked to primary productivity (Kuhn et al. 2020) and dissolved organic carbon concentrations, which in turn may be influenced

by terrestrial processes (Johnston et al. 2020). For example, shifts in terrestrial vegetation cover are hypothesized to influence lake ecological structure and function (Finstad et al. 2016). As the frequency and timing of spring thaw change, along with total annual precipitation, the magnitude and pathways of water moving within the landscape will impact the routing of terrestrial carbon into aquatic ecosystems. However, the responses of arctic-boreal lakes to changes in terrestrial ecosystems remains highly uncertain.

Lake color, as observed from space, offers a powerful approach for monitoring at large scales. Lake color has been used to infer properties relevant to carbon cycling, including lake clarity (Kloiber et al. 2002; Page, Olmanson, and Mishra 2019), phytoplankton stocks (Dierssen and Karl 2010b), and primary production (Kuhn et al. 2020; Sayers et al. 2015). Despite the fact that lake color has been designated an Essential Climate Variable by the Global Climate Observing System (GCOS) (Kirk 1994), analysis of pan-arctic trends in lake color remains limited. The majority of lake color studies have been conducted outside arctic and boreal regions (Topp et al. 2020), with most high northern latitude work focused on dissolved organic carbon dynamics (Kutser et al. 2015; Kutser 2012; Griffin et al. 2018; Olmanson, Bauer, and Brezonik 2008), single regions (Matsuoka et al. 2007) or on physical processes such as changes in inundation extent (Rover et al. 2012; L. Smith et al. 2005; Cooley et al. 2017; Chen et al. 2014; Watts et al. 2012). To date, no study has applied this approach to evaluate widespread trajectories of lake greenness, which has been shown to closely track rates of lake primary productivity in diverse northern lake ecosystems (Bogard et al. 2019; Kuhn et al. 2020).

Decades of field studies have led to the hypothesis that lake color is changing due to shifts in hydrology and climate (Monteith et al. 2007; Kritzberg 2017; de Wit et al. 2016). Here we explore this hypothesis at the continental scale and discuss our findings in the context of

physiochemical, biological, and hydrologic controls. To document trends in lake color, we analyze time series of lake greenness for over 400,000 of lakes in western North America's arctic-boreal zone. Using over 54 million observations from Landsat 5, 7, and 8, we generated seasonal composites of lake color from 1984 - 2019 for 542,934 lakes larger than 0.1 km^2 as a complement to existing studies on growing season greenness in terrestrial ecosystems. At each lake site, we first extracted a time series of lake greenness, defined as growing season surface reflectance (R_s, unitless) in the green band (~ 560 nm), and then calculated the overall trend in lake greenness (Δ Green R_s yr^{-1}) (see Methods). Ultimately, patterns of greenness were compared to historical changes in the landscape and climatic parameters known to influence lake productivity.

4.2 RESULTS

4.2.1 *Widespread, but spatiotemporally variable, declines in lake greenness*

Overall, lake greenness has declined in the last 35 years in North America's western arctic and boreal regions (Figure 4.1). Decadal trends and spatial patterns in annual growing season lake color (1984 – 2019) are presented in Figure 4.1. Taking all the lakes together, we found a significant negative trend in greenness (Mann Whitney trend test, Z=-2.88, P=3.8 X 10^{-3}, n = 472,889), calculated by creating a time series that reflects the average greenness of all lakes for each year (Figure 4.1b). Lake greening is rarer, contributing to less than 3% of observed trends, although in places where greening is observed the magnitude of the trend is higher (Figure 4.2).

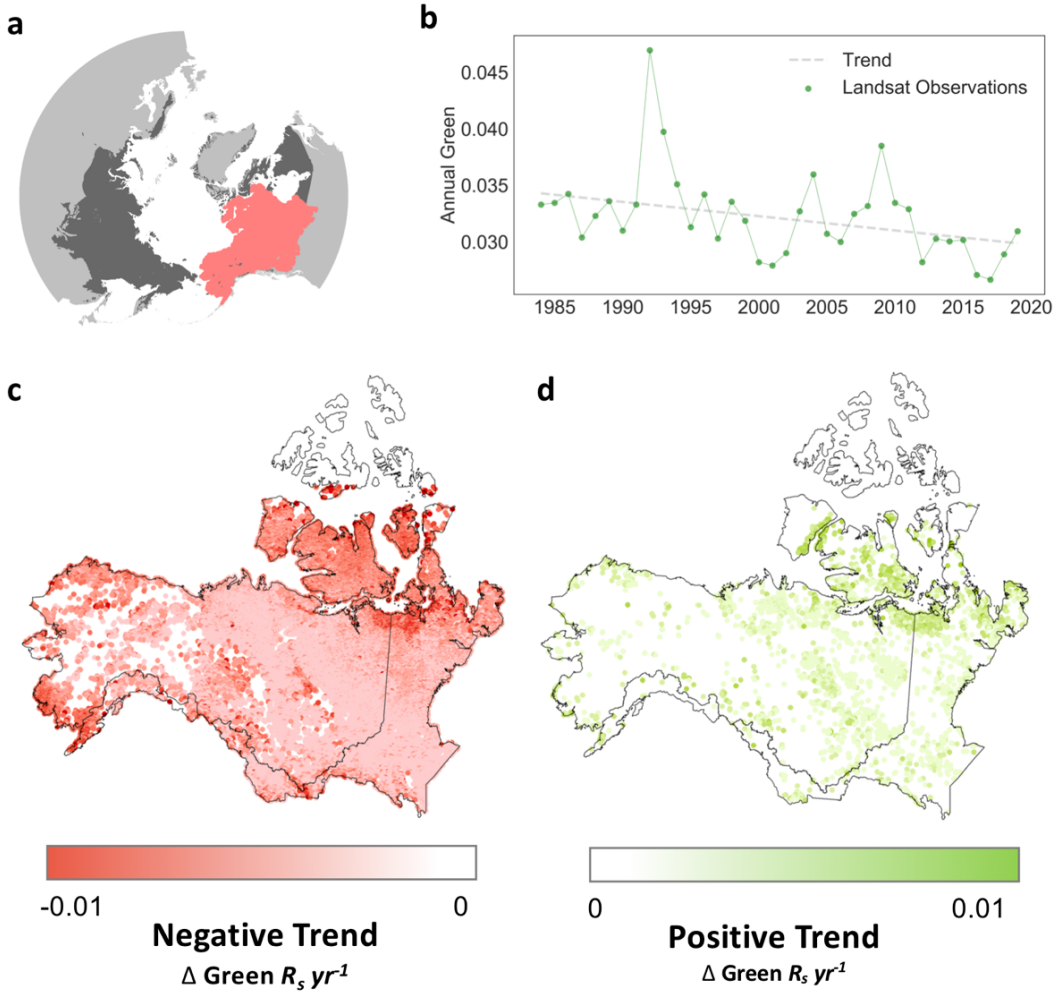

Figure 4.1. Spatiotemporal patterns in arctic and boreal lake color change from 1984 – 2019. a-d, Changes in lake greenness vary spatiotemporally and overall lake greenness declined 15% from 1984 -2019. a, Map showing the location of study lakes (red) and distribution of global circumpolar permafrost landscapes (dark grey). b, Time series of median greenness (R_s, unitless) for study lakes from Harmonized Landsat Collection 1 Surface Reflectance dataset (1984 – 2019) of study lakes (n = 472,889). Trend lines were calculated from lake time series using a robust Theil-Sen estimator. Trends in lake greenness (Δ Green R_s yr^{-1}) vary

spatiotemporally. Lakes with significant (P<0.05) negative c, and positive d, trends below 75 degrees N.

Calculating individual significance for each lake, 26% of lakes showed statistically significant (*P*<0.05) shifts in color, and spatiotemporal differences are revealed in Figure 4.1c,d. Of the lakes with significant trends, 97% show declining greenness. Lakes within the zone of continuous permafrost showed stronger negative trends (Figure 4.3). Significant differences existed between biomes (H=16,230, P<0.05, n=472,889) (Appendix C, Figure 4.9, Figure 4.10) Tundra, temperate grasslands, and shrub biomes showed similar and greater declines in greenness than forested biomes (Appendix C, Table 4.1, Table 4.2). Areas of particularly apparent rapid change are located in the Yukon-Kuskokwim (YK) Delta (Figure 4.1c), where studies have linked terrestrial browning to salt-kill from coastal flooding (Jorgenson, Frost, and Dissing 2018). Shrubification of previously barren tundra regions indicates that energy and nutrients are present enough to support more complex vegetation, which in turn can alter local energy budgets, impacting the rate of permafrost thaw (Pearson et al. 2013) and eventual transfer to aquatic ecosystems (Vonk et al. 2015).

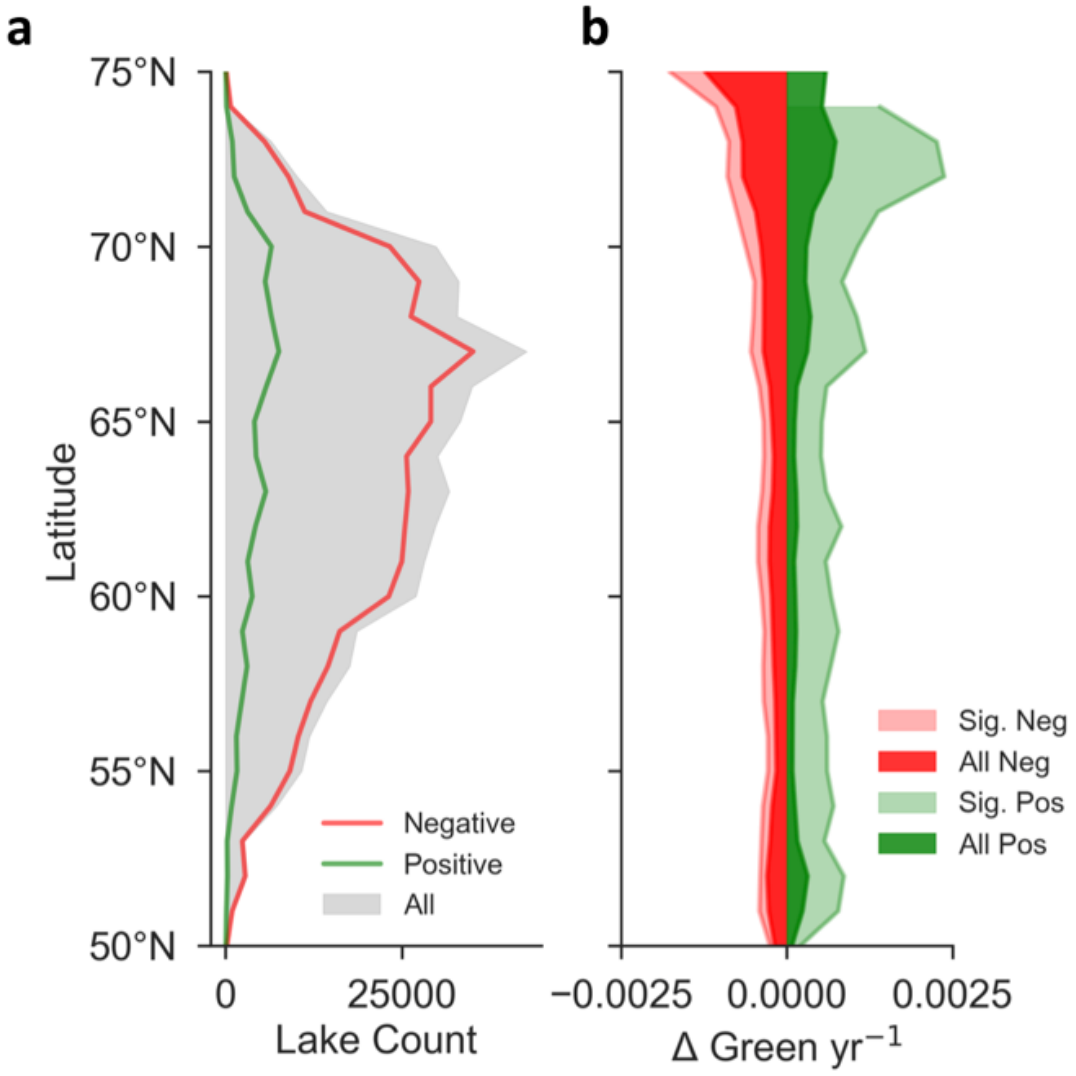

Figure 4.2. Latitudinal profiles of lake count and color. a, Distribution of study lakes by latitude b, greenness trend for all lakes (lighter colors), and significant lakes (darker colors). Plots were made by binning statistics by every 1° of latitude.

Taken together, these results show the greatest changes in lake greenness are concentrated in the shrub and tundra ecosystems underlain by continuous permafrost regions (Figure 4.1c, Figure 4.2). Negative trends in lake color observed here are supported by evidence of increased organic carbon export to lakes (Larsen, Andersen, and Hessen 2011; Williamson et

al. 2015), potentially due to thermokarst-activated flow paths between aquatic and terrestrial systems (Bring et al. 2016). Other factors shown to drive increased light absorption include warming and precipitation changes (Couture, Houle, and Gagnon 2012; Freeman et al. 2001; Tranvik and Jansson 2002; Weyhenmeyer, Prairie, and Tranvik 2014; de Wit et al. 2016), recovery from acidification (Monteith et al. 2007), altered biogeochemical interactions (Weyhenmeyer, Prairie, and Tranvik 2014) and changes in land use (Kritzberg 2017; Meyer-Jacob et al. 2015). Declines in color can impact the amount of light available for photosynthesis (Seekell et al. 2015), reducing productivity, and weakening the strength of the arctic carbon sink (Ask, Karlsson, and Jansson 2012).

However, changes in lake color are complex and may be driven by a combination of water column properties, bottom substrate, and lake depth (Lee et al. 2010). Our analysis indicates that shallow lakes are more vulnerable to changes in color. To assess the impact of depth, we compared trends between shallow (<10 m depth) and deeper (>10 m depth) lakes. Shallower lakes exhibited 34% greater declines in greenness than deeper lakes (Figure 4.3), and the difference was significant (Mann Whitney U test, W=560,284,235, P=1.43 X 10^{-30}, n = 469,990) compared to deeper lakes (>10 m, n = 2,899). Here, measures of lake depth have been estimated using a static geostatistical model conditioned on topography (Messager et al. 2016).

Assessing the impact of changes in lake depth on color would require multi-temporal lake depth estimates. Regional lake levels have been characterized using AirSWOT, an experimental airborne Ka-band radar interferometer (Pitcher et al. 2019). However, most pan-arctic studies have focused on changes in lake area and surface water extent (Smith et al. 2005; Riordan, Verbyla, and McGuire 2006; Roach et al. 2011; Rover et al. 2012; Watts et al. 2012), not on lake depth, precluding our ability to capture the historical change in lake water level or depth.

However, these results imply that shallower lakes may be undergoing more dramatic transformations.

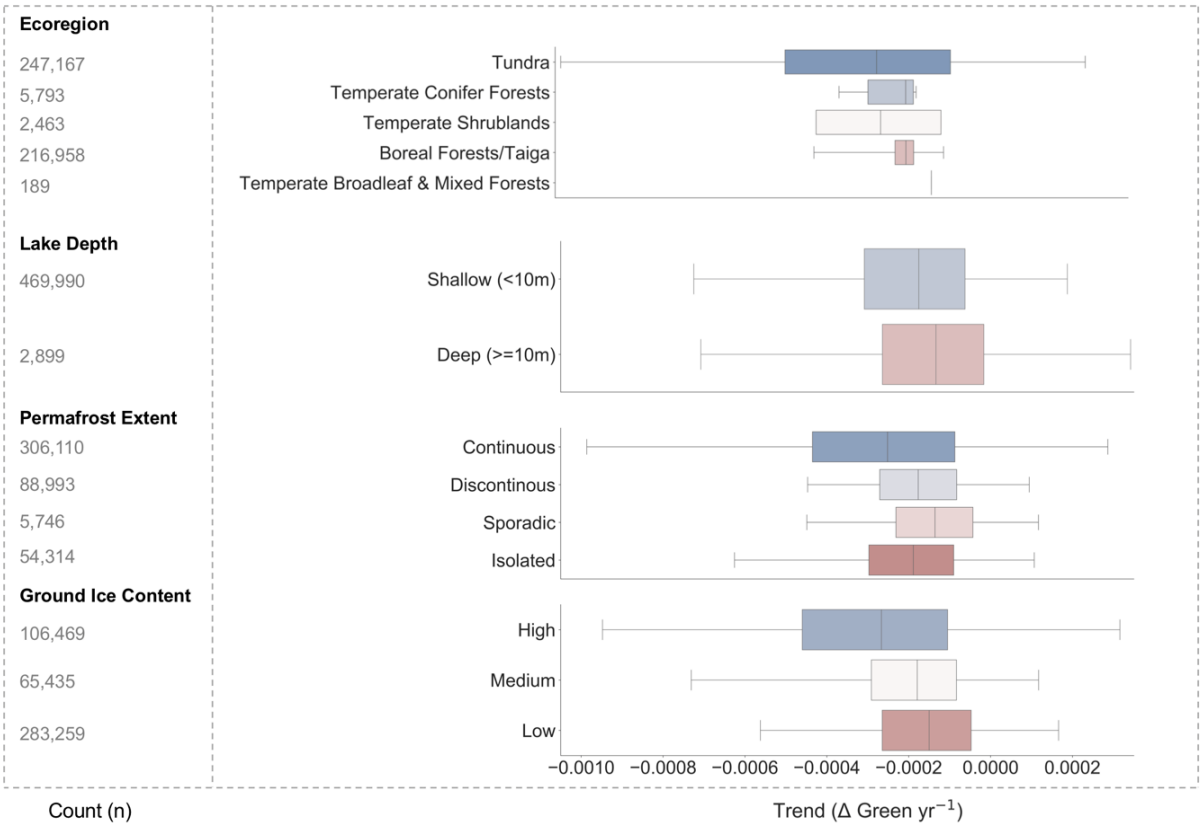

Figure 4.3. Greening trends binned by bioclimatic and physical controls on lake color. Boxplots showing lake greenness trend binned by a, ecoregion b, lake depth c, permafrost extent and d, ground ice content.

We implemented an extensive screening method to produce high-quality time series. The main sources of uncertainty in this analysis are discrepancies arising from using multiple generations of Landsat sensors and the correct identification of water pixels using Landsat's Quality Assessment Bands. To minimize uncertainty from using multiple Landsat sensors, we selected the green band, which has the lowest calibration errors across sensors (Vogelmann et al. 2016). Another possible bias is the fewer number of observations in the Landsat-5 archive due to downlink and data quality issues. Sparse Landsat-5 observations in the 1980s-90s can bias the

interpretation of trends. Our analysis showed that 93% of lakes had >20 years of data (Appendix C, Figure 4.8), and lakes with fewer than 10 years were excluded (see Methods). To assess bias introduced by using composites derived from multiple Landsat sensors, we calculated trends with and without harmonization coefficients (Roy et al. 2014) and found the overall trend remained negative and significant for both cases (Appendix C, Figure 4.11). A series of conservative filters (Appendix C, Figure 4.5) including Landsat's QA band and an independent water mask derived from the Global Surface Water Dataset (Pekel et al. 2016) were used to ensure analyzed pixels were not clouds, vegetation, or snow/ice (see Methods). These extra efforts were undertaken to provide evidence that the results were robust and free from potential systematic errors (Bailey and Werdell 2006b).

4.2.2 *Lake greenness declines most in warming and wetting regions*

The continental-scale shifts in lake color observed here appear to track regional changes in climatic conditions. To evaluate lake color trends in the context of climate conditions, we analyzed air temperature and precipitation trends using the ERA5 climate reanalysis dataset (Copernicus 2017) (Figure 4.4a-f). Consistent with other studies, the last three decades (1984 – 2019) are characterized by an overall rise in western North American arctic and boreal air temperatures (Overland et al. 2018) by 0.031°C (standard deviation = ± 0.028 °C) per year (Figure 4.4a), which is lower but on the same order of magnitude as estimates made using a process model for the time period of 1982 – 1998 (Lucht et al. 2002).

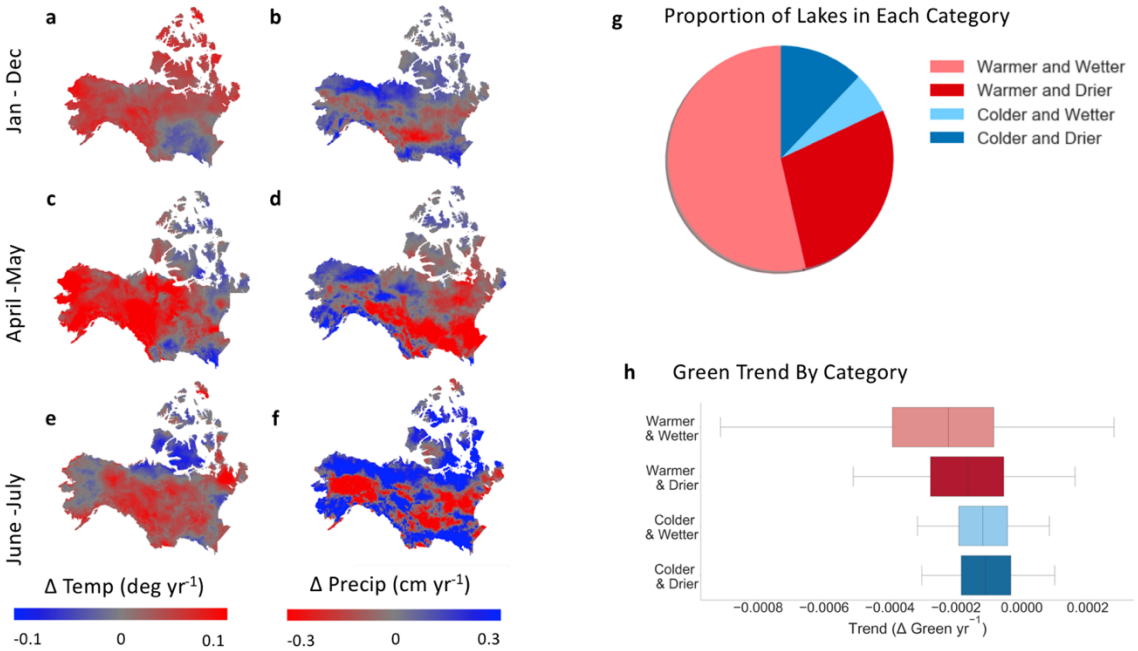

Figure 4.4. Climate trends. Overall trends in temperature (a, c, e) and precipitation (b, d, f) for annual (a, b), spring (c, d) and summer (e, f) time periods. The proportion of lakes whose basins are in each climate category (g). Boxplots of distributions of green trend by basin climate trend category calculated by basin for each lake using the GLCP dataset (see Materials and Methods) (h).

We then linked each lake to the climate reanalysis dataset by matching each lake to its smallest basin using the Global Lake Area, Climate, and Population (GLCP) Dataset (Labou et al. 2019) (see Materials & Methods). We calculated that 60% (n= 224,422) of lakes are located in wetter basins, and 40% (n = 152,603) of lakes are conversely in drier basins (see Appendix C, 4.6.1 for extended climate results). We separated temperature and precipitation trends into four categories: warmer and wetter, warmer and drier, colder and wetter, and colder and drier (Figure 4.4g). We found a significant difference in greening trends between these four categories (Kruskal-Wallis test, H= 21,326, P<0.05, n= 377,025) (Figure 4.4h). Lakes in warmer and wetter basins had a 2.5 times greater mean decline in green reflectance than lakes in colder and drier

basins (Figure 4.4h). This result is consistent with the current hypothesis that precipitation and permafrost warming are altering terrestrial-to-aquatic hydrologic connectivity. This impacts downstream delivery of terrestrial solutes, including organic carbon, to lakes (Fowler, Osburn, and Saros 2020; Johnston et al. 2020), which in turn could negatively influence primary productivity and further induce net heterotrophy (Hastie et al. 2016).

The decline in lake greenness under warmer and wetter conditions is likely caused by two linked mechanisms: (1) changes in terrestrial-to-aquatic hydrologic connectivity that impact the downstream delivery of terrestrial solutes and (2) higher dissolved organic carbon (DOC) concentrations resulting from increased lateral connectivity (Williamson et al. 2015), which in turn can shade out primary producers, weakening the strength CO_2 uptake (Thrane, Hessen, and Andersen 2014). Increased connectivity exerts a two-way influence on primary productivity. Increased terrestrial inputs can supply nutrients, thereby stimulating phytoplankton growth.

However, high concentrations of colored DOC can reduce light availability, shading out producers (Thrane, Hessen, and Andersen 2014). These findings suggest that in arctic and boreal lakes of western North America, the former mechanism is dominating. Declining light availability, as indicated by a decrease in the green reflectance of lakes, could be a symptom of a larger shift from clear-water systems dominated by benthic production to brown-water ecosystems that are net heterotrophic (Creed et al. 2018; Ask et al. 2009).

4.2.3 *Further implications*

The continental-scale shifts in lake greenness, and their links to large-scale climatic changes, are not necessarily surprising, since temperature and precipitation patterns have been shown to shape other lake properties, such as dissolved organic carbon concentrations (Weyhenmeyer and Karlsson 2009) and patterns of greenhouse gas emissions (Guo et al. 2020).

Yet our observations have several important implications for water quality, primary productivity, and greenhouse gas (GHG) emissions.

First, changes in color can impact lake surface temperatures (Wetzel and Likens 2000), which alters mixing regimes and lake stratification (Read and Rose 2013). Greater stratification can restrict nutrient upwelling and lower bottom-water oxygen concentrations, reducing both water quality and primary production (Woolway et al. 2019). Second, changes in lake greenness may have major implications for lake C storage and GHG emissions. Lake ecosystems are both sources and sinks of carbon (Denfeld et al. 2018; Tranvik et al. 2009; Bogard and del Giorgio 2016; Buffam et al. 2011; Cole et al. 2007), varying significantly between and within regions. This balance depends to varying degrees on rates of primary production, which have been linked to greenness (Bogard et al. 2019; Kuhn et al. 2020). Lakes that are less green may store less carbon in sediments because burial rates correlate with primary productivity (Mendonça et al. 2017).

Changes in greenness may also translate to changes in methane (CH_4) fluxes because productivity and CH_4 emissions are correlated (Schmidt and Conrad 1993; Larmola et al. 2004; Juutinen et al. 2009; Deemer et al. 2016). As a result of this relationship, surface reflectance has even been used as a proxy for methane concentration in Siberian rivers (Morozumi et al. 2019). However, relationships to carbon dioxide (CO_2) fluxes are more complicated because of hydrologic loading of external CO_2.

Another implication of this decline in greenness is a decrease in gross primary productivity (GPP). Previous work has established a relationship between airborne and satellite observations of arctic-boreal lake greenness and GPP (Kuhn et al. 2020). Using published relationships between Landsat greenness and *in situ* GPP, declines in greenness between the first

and last decades of this analysis translate to a drop in carbon uptake of 58 Tg C during growing season (see Materials & Methods, Appendix C, Table 4.4). These results cannot inform on net annual carbon fluxes because this analysis is constrained to a narrow window during the ice-free, growing season and therefore does not include under-ice or non-growing season dynamics. Field measurements across the entire year should be prioritized to fully constrain net annual carbon fluxes. However, our results indicate a potential 16% reduction in carbon uptake from declining gross primary productivity during the growing season, a finding that implies that the mechanism by which lakes take up carbon during the growing season is weakening.

4.3 Conclusion

In this study, we present the first comprehensive analysis of changing greenness for arctic and boreal lakes in western North America. Results show lakes with declines in greenness overwhelmingly outnumbered greening lakes and this trend occurs over a much larger region than previous large-scale studies of lake color (Monteith et al. 2007; Kritzberg et al. 2014).

As rising temperatures accelerate permafrost thaw, more soil organic carbon, and nutrients are expected to be released across terrestrial-aquatic interfaces (Larsen, Andersen, and Hessen 2011). Evidence increasingly indicates widespread, but spatially complex, changes in arctic and boreal terrestrial productivity (Myers-Smith et al. 2020). This in combination with vegetation transitions (McGowan et al. 2018) is predicted to have non-linear consequences for lake primary productivity (Solomon et al. 2013) and aquatic ecosystems more broadly. The decline in color documented here is consistent with the growing number of paleolimnological and biogeochemical field studies that show changes in light absorption resulting from altered terrestrial-aquatic connectivity (de Wit et al. 2016; Kritzberg et al. 2014; Finstad et al. 2016; Meyer-Jacob et al. 2019; Williamson et al. 2015; Thrane, Hessen, and Andersen 2014; Seekell et

al. 2015). These findings indicate changes in ecosystem structure and function that in turn impact lake carbon cycling dynamics, which are known to be globally significant (Raymond et al. 2013).

Many field studies, constricted by time and funding, trade-off between broad geographic coverage versus higher temporal resolution sampling. In contrast, satellite remote sensing used here encompasses a broad range of diverse geographies while simultaneously preserving high spatial resolution (< 100m). This balance ensures the trends detected are comprehensive, while also preserving the uneven change that can occur within and between regions. Our results show that declines in greenness are most evident in warmer and wetter ecosystems; providing additional support to the hypothesis that, in fact, hydrologic change is altering links between terrestrial and aquatic systems (Johnston et al. 2020). These findings warrant continued monitoring of high northern latitude lakes to characterize the significance of lake color change within the broader carbon cycling dynamics of Arctic and boreal landscapes. The boreal arctic is changing unevenly and we show that lakes are part of this uneven change.

4.4 Materials & Methods

The overall workflow for calculating growing season composites from 1989 – 2019 for each lake in this study is presented in Appendix C (Figure 4.5). Satellite remote sensing analyses were performed in Google Earth Engine (Gorelick et al. 2017b); statistics were calculated in Python (Virtanen et al. 2020) using a suite of packages and spatial joins were conducted in QGIS (Q. D. Team 2016). Data visualizations were created using all three platforms.

4.4.1 *Satellite Data*

The Landsat program offers the longest continuously-operating earth observation satellite record. Landsat Collection 1 Tier 1 scenes from Landsat 5 (n = 23,216), 7 (n = 36,123) and 8 (n = 16,903) were used. Surface reflectance scenes acquired over the study domain (Appendix C, Figure 4.6) (total n= 76,242 scenes) and accessed through Google Earth Engine (Pekel et al. 2016), a parallelized geospatial analysis platform featuring co-located storage and compute for large geospatial datasets, including the Landsat archive. The global coverage and analysis-ready Level 1 Surface Reflectance product (Vermote et al. 2016) has been shown to be suitable in previous studies for inland water color analysis including for lake clarity (Page, Olmanson, and Mishra 2019), chlorophyll-*a* and turbidity in rivers (Kuhn et al. 2019), and suspended sediment (Markert et al. 2018). Uncertainties stemming from orbital decay and radiometric intercalibration are noted, and the green band was selected as less influenced by remote sensing uncertainties relative to other bands (Pahlevan et al. 2018; Vogelmann et al. 2016).

4.4.2 *Satellite Imagery masking*

Clouds, cloud shadows, snow and ice were identified using the CFMask algorithm flags (Foga et al. 2017; Zhu and Woodcock 2012; Zhu, Wang, and Woodcock 2015) included in the Level 2 Pixel Quality Assessment band (Vermote et al. 2016). Additional thresholds were imposed to further mask clouds and cloud shadows using Landsat 8's aerosol band and haziness was filtered out using the atmospheric opacity bands (threshold of 0.3) (L5, L7). Saturated pixels were identified using the radsat_qa band (USGS 2018b) and scenes with low solar zenith angles (< 60°) were excluded to minimize glint (Pahlevan et al. 2014).

4.4.3 *Growing season composites*

Growing season greenness was calculated per-pixel as the median value during the peak growing season, which was defined June – July. Past work confirmed that this is the window of time in which maximum photosynthesis (Sulla-Menashe, Woodcock, and Friedl 2018; Miles, Miles, and Esau 2018) occurs with a minimum of interference from clouds and ice (Kuhn et al. 2020; Warner et al. 2018). This approach avoids uncertainties introduced by changes in the growing season length or seasonal phenology and was conservatively selected to restrict observations to the ice-free period (after June 1) and to avoid fall cloudiness (Appendix C, Figure 4.7) After filtering lakes to cloud-free observations, lakes were observed an average of 2.8 times each growing season, resulting in over 53 million observations total from 1984 – 2019. These observations were used to generate seasonal composites for each year for each lake (n = 584,596).

4.4.4 *Data sampling*

Growing season greenness for each lake was identified by sampling a 3-by-3 pixel area centered on each lake centroid calculated from HydroLAKES polygons within the study domain. The median, standard deviation and pixel count of the green band inside each 3-by-3 pixel box were calculated for each lake at the native scale of the Landsat green band (30m). Samples without a majority of valid pixels in the 3X3 pixel box ($n < 5$ out of 9) were discarded to further reduce influence from adjacent clouds or land (Kuhn et al. 2019). Growing season greenness for each lake for each year was then exported for visualization and statistical analysis. The dataset was further screened to exclude negative pixels (<1% of the dataset) and lakes with less than 10 years of data (2% of the dataset). To conservatively ensure that each observation was cloud-free and over water, a final filter using the Pixel QA (pixel_qa) band was imposed to identify only

lakes identified as cloud-free and water. Lake centroids were further intersected with the Global Surface Water Dataset (Pekel et al. 2016) and only those identified as having only permanent surface water (transition_class = 1) inside the 3X3 grid were maintained in the dataset.

4.4.5 *Time series analysis*

To assess changes in lake surface reflectance over time, we examined time series of summer (June-July) composites from 1984-2019. June and July were selected based on precedent in the literature (Miles, Miles, and Esau 2018; Sulla-Menashe, Woodcock, and Friedl 2018) and to avoid high cloud cover in August (Appendix C, Figure 4.7). The majority (70%) of lakes had over 30 years of observations available (Appendix C, Figure 4.8). Long-term trends in lake color over the four decades were analyzed as change in greenness per year (Δ green yr^{-1}) from 1984 – 2019. Trends were calculated using Theil-sen's Slope Estimator from the SciPy package (Jones, Oliphant, and Peterson 2001) and slopes were tested for significance using a Mann-Kendall test, which is designed to identify monotonic trends and is been widely used to identify terrestrial greening and browning trends (de Jong et al. 2011). This non-parametric approach accounts for gaps in observation years.

4.4.6 *Matching lakes to basins*

In order to calculate basin-level climate for each lake, lake basins were assigned using the harmonized Global Climate and Population (GLCP) Dataset (Labou et al. 2019). The GLCP offers basin-level climate and population data paired to the HydroLAKES dataset. Lakes were matched to basins using the HydroBASINS dataset (version 1.c format 1) which are basin polygons derived from the 15 arc-second resolution HydroSHEDS dataset. The HydroLAKES lake polygons used in this study, identified by a unique ID (hylak_id), and their corresponding

basin IDs were selected from the GLCP dataset. Level 12 basins only were selected as they hold the majority (83%) of lakes (Appendix C, Table 4.3) and to exclude artifacts in higher level basin assignments that are known problems in the GLCP (Labou et al. 2019). This step resulting in 30,902 unique basins being identified and used for climate analysis.

4.4.7 *Ecoregion and Permafrost Extent*

Ecoregions and biomes were assigned to each lake using the geographic boundaries given in the World Wildlife Fund Terrestrial Ecoregions (Olson et al. 2001) dataset (Appendix C, Figure 4.9). Ecoregions reflect distinct assemblages of flora and fauna that are in turn shaped by climate and landform. The 825 ecoregions and fourteen biomes featured in the WWF dataset were accessed from https://www.sciencebase.gov/catalog/item/508fece8e4b0a1b43c29ca22 as a polygon shapefile (WGS84 – EPSG:4326). Ecoregion and biome classifications were assigned using a spatial join between the WWF layer and HydroLAKES centroids. The majority (76%) of lakes were located in the Tundra or Boreal Forests/Taiga biomes with the remainder found in temperature conifer forests, temperature shrublands, or broadleaf and mixed forests.

Shapefiles of circumpolar permafrost extent and ground ice content (Brown et al. 1997) projected in Lambert Azimuthal Equal Area were downloaded from the National Snow and Ice Data Center (https://nsidc.org/data/ggd318) and re-projected to WGS-84. Lakes were assigned an ecoregion and permafrost extent by spatial joining the HydroLAKES centroids to the ecoregion and permafrost extent reprojected layers. Figure 4.3 shows results for the 472,889 lakes stratified by permafrost extent class, ground ice content, lake depth and biome classification.

4.4.8 *Climate reanalysis data*

Trends in temperature and precipitation were calculated from European Centre for Medium-range Weather Forecasts (ECMWF) fifth generation global atmospheric reanalysis data (ERA5) with a native spatial resolution of 0.25° X 0.25° degrees dating back to 1979 (Copernicus 2017). ERA5 data was released in 2019 and is freely available in Google Earth Engine and the Copernicus Climate Data Store. Studies have shown ERA5 to have satisfactory performance in accurately modeling storm surges (Dullaart et al. 2020), Canadian prairie climate (Betts, Chan, and Desjardins 2019), and global discharge reanalysis (Tarek, Brissette, and Arsenault 2019) compared to previous generations and other models. ERA5 monthly aggregated precipitation and temperature values were summarized annually and seasonally over the study domain. Summer (June, July and August) and spring (April, May, June) trends were identified by summarizing data using a Sen's slope estimator within those time periods by HUC 12 basin assigned using the GLCP.

4.4.9 *Gross Primary Productivity*

Declines in gross primary productivity (GPP) were calculated from the average greenness for the first (1984 – 1994) and last (2009 – 2019) decade using the relationship between Landsat growing season greenness and field measurements of GPP identified in Kuhn et al (2020) (Appendix C, Table 4.4). Average growing season GPP rates (g O_2 m^{-2} d^{-1}) were calculated for the first and last decade and multiplied by the length of growing season (n = 60 days) used in the remote sensing analysis. The resulting areal GPP (g O_2 m^{-2}) was then multiplied by the total lake area within the domain (417,152.40 km^2) to estimate the total change in O_2 (Tg) uptake between the two decades. Total lake area was calculated by summing the individual HydroLAKES lake area for lakes passing quality control. Photosynthetic uptake of carbon was calculated using the

carbon-oxygen photosynthetic quotient of 1.2 where for every 1 mole of oxygen produced, 1.2 moles of carbon are assimilated (Melack 1976).

4.5 REFERENCES

Arrigo, K, and G van Dijken. 2008. "Changes in Arctic Ocean Primary Production from 1998–2008."

Ask, Jenny, Jan Karlsson, and Mats Jansson. 2012. "Net Ecosystem Production in Clear-water and Brown-water Lakes." *Global Biogeochemical Cycles* 26 (1).

Ask, Jenny, Jan Karlsson, Lennart Persson, Per Ask, Pär Byström, and Mats Jansson. 2009. "Terrestrial Organic Matter and Light Penetration: Effects on Bacterial and Primary Production in Lakes." *Limnology and Oceanography* 54 (6): 2034–40.

Bailey, Sean W, and P Jeremy Werdell. 2006. "A Multi-Sensor Approach for the on-Orbit Validation of Ocean Color Satellite Data Products." *Remote Sensing of Environment* 102 (1–2): 12–23.

Beck, Pieter S A, and Scott J Goetz. 2011. "Satellite Observations of High Northern Latitude Vegetation Productivity Changes between 1982 and 2008: Ecological Variability and Regional Differences." *Environmental Research Letters* 6 (4): 45501.

Betts, Alan K, Darren Z Chan, and Raymond L Desjardins. 2019. "Near-Surface Biases in ERA5 over the Canadian Prairies." *Frontiers in Environmental Science* 7: 129.

Bhatt, Uma, Donald Walker, Martha Raynolds, Peter Bieniek, Howard Epstein, Josefino Comiso, Jorge Pinzon, et al. 2013. "Recent Declines in Warming and Vegetation Greening Trends

over Pan-Arctic Tundra." *Remote Sensing* 5 (9): 4229–54.

Bogard, Matthew J., Catherine Kuhn, Sarah Ellen Johnston, Robert G. Striegl, Gordon W. Holtgrieve, Mark M. Dornblaser, Robert G.M. Spencer, Kimberly P. Wickland, and David E. Butman. 2019. "Negligible Cycling of Terrestrial Carbon in Many Lakes of the Arid Circumpolar Landscape." *Nature Geoscience* 12 (3): 180–85.

Bogard, Matthew J, and Paul A del Giorgio. 2016. "The Role of Metabolism in Modulating CO2 Fluxes in Boreal Lakes." *Global Biogeochemical Cycles* 30 (10): 1509–25.

Bring, A., I. Fedorova, Y. Dibike, L. Hinzman, J. Mård, S. H. Mernild, T. Prowse, O. Semenova, S. L. Stuefer, and M. K. Woo. 2016. "Arctic Terrestrial Hydrology: A Synthesis of Processes, Regional Effects, and Research Challenges." *Journal of Geophysical Research G: Biogeosciences* 121 (3): 621–49.

Brown, Jerry, O J Ferrians Jr, J A Heginbottom, and E S Melnikov. 1997. *Circum-Arctic Map of Permafrost and Ground-Ice Conditions*. US Geological Survey Reston, VA. https://nsidc.org/data/ggd318.

Buffam, Ishi, Monica G Turner, Ankur R Desai, Paul C Hanson, James A Rusak, Noah R Lottig, Emily H Stanley, and Stephen R Carpenter. 2011. "Integrating Aquatic and Terrestrial Components to Construct a Complete Carbon Budget for a North Temperate Lake District." *Global Change Biology* 17 (2): 1193–1211.

Chen, Min, Joel C Rowland, Cathy J Wilson, Garrett L Altmann, and Steven P Brumby. 2014. "Temporal and Spatial Pattern of Thermokarst Lake Area Changes at Yukon Flats, Alaska." *Hydrological Processes* 28 (3): 837–52.

Cole, J. J., Y. T. Prairie, N. F. Caraco, W. H. McDowell, L. J. Tranvik, R. G. Striegl, C. M. Duarte, et al. 2007. "Plumbing the Global Carbon Cycle: Integrating Inland Waters into the

Terrestrial Carbon Budget." *Ecosystems* 10 (1): 172–85.

Cooley, Sarah W, Laurence C Smith, Leon Stepan, and Joseph Mascaro. 2017. "Tracking Dynamic Northern Surface Water Changes with High-Frequency Planet CubeSat Imagery." *Remote Sensing* 9 (12): 1306.

Copernicus. 2017. "ERA5: Fifth Generation of ECMWF Atmospheric Reanalyses of the Global Climate." 2017.

Couture, Suzanne, Daniel Houle, and Christian Gagnon. 2012. "Increases of Dissolved Organic Carbon in Temperate and Boreal Lakes in Quebec, Canada." *Environmental Science and Pollution Research* 19 (2): 361–71.

Creed, Irena F, Ann-Kristin Bergström, Charles G Trick, Nancy B Grimm, Dag O Hessen, Jan Karlsson, Karen A Kidd, Emma Kritzberg, Diane M McKnight, and Erika C Freeman. 2018. "Global Change-driven Effects on Dissolved Organic Matter Composition: Implications for Food Webs of Northern Lakes." *Global Change Biology* 24 (8): 3692–3714.

Deemer, Bridget R, John A Harrison, Siyue Li, Jake J Beaulieu, Tonya DelSontro, Nathan Barros, José F Bezerra-Neto, Stephen M Powers, Marco A dos Santos, and J Arie Vonk. 2016. "Greenhouse Gas Emissions from Reservoir Water Surfaces: A New Global Synthesis." *BioScience* 66 (11): 949–64.

Denfeld, Blaize A, Marcus Klaus, Hjalmar Laudon, Ryan A Sponseller, and Jan Karlsson. 2018. "Carbon Dioxide and Methane Dynamics in a Small Boreal Lake during Winter and Spring Melt Events." *Journal of Geophysical Research: Biogeosciences* 123 (8): 2527–40.

Dibike, Yonas, Terry Prowse, Tuomo Saloranta, and Roxanne Ahmed. 2011. "Response of Northern Hemisphere Lake-ice Cover and Lake-water Thermal Structure Patterns to a

Changing Climate." *Hydrological Processes* 25 (19): 2942–53.

Dierssen, Heidi M, and David M Karl. 2010. "Perspectives on Empirical Approaches for Ocean Color Remote Sensing of Chlorophyll in a Changing Climate." *Proceedings of the National Academy of Sciences* 107 (40): 17073–78.

Downing, John A, Y T Prairie, J J Cole, C M Duarte, L J Tranvik, Robert G Striegl, W H McDowell, Pirkko Kortelainen, N F Caraco, and J M Melack. 2006. "The Global Abundance and Size Distribution of Lakes, Ponds, and Impoundments." *Limnology and Oceanography* 51 (5): 2388–97.

Dullaart, Job C M, Sanne Muis, Nadia Bloemendaal, and Jeroen C J H Aerts. 2020. "Advancing Global Storm Surge Modelling Using the New ERA5 Climate Reanalysis." *Climate Dynamics* 54 (1–2): 1007–21.

Duncan, Bryan N, Lesley E Ott, James B Abshire, Ludovic Brucker, Mark L Carroll, James Carton, Josefino C Comiso, Emmanuel P Dinnat, Bruce C Forbes, and Alemu Gonsamo. 2020. "Space-Based Observations for Understanding Changes in the Arctic-Boreal Zone." *Reviews of Geophysics* 58 (1).

Finstad, Anders G, Tom Andersen, Søren Larsen, Koji Tominaga, Stefan Blumentrath, Heelen A de Wit, Hans Tømmervik, and Dag Olav Hessen. 2016. "From Greening to Browning: Catchment Vegetation Development and Reduced S-Deposition Promote Organic Carbon Load on Decadal Time Scales in Nordic Lakes'." *Scientific Reports*.

Foga, Steve, Pat L Scaramuzza, Song Guo, Zhe Zhu, Ronald D Dilley, Tim Beckmann, Gail L Schmidt, John L Dwyer, M Joseph Hughes, and Brady Laue. 2017. "Cloud Detection Algorithm Comparison and Validation for Operational Landsat Data Products." *Remote Sensing of Environment* 194: 379–90.

Fowler, Rachel A, Christopher L Osburn, and Jasmine E Saros. 2020. “Climate-Driven Changes in Dissolved Organic Carbon and Water Clarity in Arctic Lakes of West Greenland.” *Journal of Geophysical Research: Biogeosciences* 125 (2).

Freeman, C, C D Evans, D T Monteith, Brian Reynolds, and N Fenner. 2001. “Export of Organic Carbon from Peat Soils.” *Nature* 412 (6849): 785.

Gorelick, Noel, Matt Hancher, Mike Dixon, Simon Ilyushchenko, David Thau, and Rebecca Moore. 2017. “Google Earth Engine: Planetary-Scale Geospatial Analysis for Everyone.” *Remote Sensing of Environment* 202: 18–27.

Griffin, C G, J W McClelland, K E Frey, G Fiske, and R M Holmes. 2018. “Quantifying CDOM and DOC in Major Arctic Rivers during Ice-Free Conditions Using Landsat TM and ETM+ Data.” *Remote Sensing of Environment* 209: 395–409.

Guo, Mingyang, Qianlai Zhuang, Zeli Tan, Narasinha Shurpali, Sari Juutinen, Pirkko Kortelainen, and Pertti J. Martikainen. 2020. “Rising Methane Emissions from Boreal Lakes Due to Increasing Ice-Free Days.” *Environmental Research Letters* 15 (6).

Hastie, Adam Todd, Ronny Lauerwald, Gesa A Weyhenmeyer, Sebastian Sobek, Charles Verpoorter, and Pierre A G Regnier. 2016. “Carbon Dioxide Evasion from Boreal Lakes: Drivers, Variability and Revised Global Estimate.” *AGUFM* 2016: B24C-07.

Jansen, J, B F Thornton, M M Jammet, M Wik, A Cortés, T Friborg, S MacIntyre, and P M Crill. 2019. “Climate-Sensitive Controls on Large Spring Emissions of CH4 and CO2 From Northern Lakes.” *Journal of Geophysical Research: Biogeosciences* 124 (7): 2379–99.

Jia, Gensuo J., Howard E. Epstein, and Donald A. Walker. 2003. “Greening of Arctic Alaska, 1981-2001.” *Geophysical Research Letters* 30 (20). https://doi.org/10.1029/2003GL018268.

———. 2009. “Vegetation Greening in the Canadian Arctic Related to Decadal Warming.”

Journal of Environmental Monitoring 11 (12): 2231.

Johnston, Sarah Ellen, Robert G. Striegl, Matthew J. Bogard, Mark M. Dornblaser, David E. Butman, Anne Kellerman, Kimberly Wickland, David C. Podgorski, and Robert G. M. Spencer. 2020. "Hydrologic Connectivity Determines Dissolved Organic Matter Biogeochemistry in Northern High-Latitude Lakes." *Limnology and Oceanography*, no. 0: 1–16.

Jones, Eric, Travis Oliphant, and Pearu Peterson. 2001. "SciPy: Open Source Scientific Tools for Python."

Jong, Rogier de, Sytze de Bruin, Allard de Wit, Michael E Schaepman, and David L Dent. 2011. "Analysis of Monotonic Greening and Browning Trends from Global NDVI Time-Series." *Remote Sensing of Environment* 115 (2): 692–702.

Jorgenson, M Torre, Gerald V Frost, and Dorte Dissing. 2018. "Drivers of Landscape Changes in Coastal Ecosystems on the Yukon-Kuskokwim Delta, Alaska." *Remote Sensing* 10 (8): 1280.

Ju, Junchang, and Jeffrey G Masek. 2016. "The Vegetation Greenness Trend in Canada and US Alaska from 1984–2012 Landsat Data." *Remote Sensing of Environment* 176: 1–16.

Juutinen, Sari, M Rantakari, P Kortelainen, J T Huttunen, T Larmola, J Alm, J Silvola, and P J Martikainen. 2009. "Methane Dynamics in Different Boreal Lake Types."

Kirk, John T O. 1994. *Light and Photosynthesis in Aquatic Ecosystems*. Cambridge University Press Cambridge and New York.

Kloiber, Steven M, Patrick L Brezonik, Leif G Olmanson, and Marvin E Bauer. 2002. "A Procedure for Regional Lake Water Clarity Assessment Using Landsat Multispectral Data." *Remote Sensing of Environment* 82 (1): 38–47.

Kritzberg, Emma S. 2017. “Centennial-long Trends of Lake Browning Show Major Effect of Afforestation.” *Limnology and Oceanography Letters* 2 (4): 105–12.

Kritzberg, Emma S, Wilhelm Granéli, Jessica Björk, Christer Brönmark, Per Hallgren, Alice Nicolle, Anders Persson, and Lars-Anders Hansson. 2014. “Warming and Browning of Lakes: Consequences for Pelagic Carbon Metabolism and Sediment Delivery.” *Freshwater Biology* 59 (2): 325–36.

Kuhn, C., A. de Matos Valerio, N. Ward, L. Loken, H.O. Sawakuchi, M. Kampel, J. Richey, et al. 2019. “Performance of Landsat-8 and Sentinel-2 Surface Reflectance Products for River Remote Sensing Retrievals of Chlorophyll-*a* and Turbidity.” *Remote Sensing of Environment* 224: 108 - 118.

Kuhn, Catherine, Matthew Bogard, Sarah Ellen Johnston, Aji John, Eric F Vermote, Rob Spencer, Mark Dornblaser, Kimberly P Wickland, Robert G Striegl, and David Butman. accepted 2020. “Satellite and Airborne Remote Sensing of Gross Primary Productivity in Boreal Alaskan Lakes.” *Environmental Research Letters*.

Kutser, Tiit. 2012. “The Possibility of Using the Landsat Image Archive for Monitoring Long Time Trends in Coloured Dissolved Organic Matter Concentration in Lake Waters.” *Remote Sensing of Environment* 123 (August): 334–38.

Kutser, Tiit, Charles Verpoorter, Birgot Paavel, and Lars J. Tranvik. 2015. “Estimating Lake Carbon Fractions from Remote Sensing Data.” *Remote Sensing of Environment* 157 (February): 138–46.

Labou, Stephanie G, Michael F Meyer, Matthew R Brousil, Alli N Cramer, and Bradley T Luff. 2019. “Global Lake Area, Climate, and Population Dataset.” *Scientific Data* 7 (1): 1–12.

Larmola, Tuula, Jukka Alm, Sari Juutinen, Jari T Huttunen, Pertti J Martikainen, and Jouko

Silvola. 2004. “Contribution of Vegetated Littoral Zone to Winter Fluxes of Carbon Dioxide and Methane from Boreal Lakes.” *Journal of Geophysical Research: Atmospheres* 109 (D19).

Larsen, Søren, T O M Andersen, and Dag O Hessen. 2011. “Climate Change Predicted to Cause Severe Increase of Organic Carbon in Lakes.” *Global Change Biology* 17 (2): 1186–92.

Lee, ZhongPing, Chuanmin Hu, Brandon Casey, Shaoling Shang, Heidi Dierssen, and Robert Arnone. 2010. “Global Shallow—Water Bathymetry From Satellite Ocean Color Data.” *Eos, Transactions American Geophysical Union* 91 (46): 429–30.

Lewis, K M, G L van Dijken, and K R Arrigo. 2020. “Changes in Phytoplankton Concentration Now Drive Increased Arctic Ocean Primary Production.” *Science* 369 (6500): 198–202.

Lucht, Wolfgang, I Colin Prentice, Ranga B Myneni, Stephen Sitch, Pierre Friedlingstein, Wolfgang Cramer, Philippe Bousquet, Wolfgang Buermann, and Benjamin Smith. 2002. “Climatic Control of the High-Latitude Vegetation Greening Trend and Pinatubo Effect.” *Science* 296 (5573): 1687–89.

Markert, Kel N, Calla M Schmidt, Robert E Griffin, Africa I Flores, Ate Poortinga, David S Saah, Rebekke E Muench, Nicholas E Clinton, Farrukh Chishtie, and Kritsana Kityuttachai. 2018. “Historical and Operational Monitoring of Surface Sediments in the Lower Mekong Basin Using Landsat and Google Earth Engine Cloud Computing.” *Remote Sensing* 10 (6): 909.

Matsuoka, Atsushi, Yannick Huot, Koji Shimada, Sei-Ichi Saitoh, and Marcel Babin. 2007. “Bio-Optical Characteristics of the Western Arctic Ocean: Implications for Ocean Color Algorithms.” *Canadian Journal of Remote Sensing* 33 (6): 503–18.

McGowan, Suzanne, N John Anderson, Mary E Edwards, Emma Hopla, Viv Jones, Pete G

Langdon, Antonia Law, Nadia Solovieva, Simon Turner, and Maarten van Hardenbroek. 2018. “Vegetation Transitions Drive the Autotrophy–Heterotrophy Balance in Arctic Lakes.” *Limnology and Oceanography Letters* 3 (3): 246–55.

Melack, John M. 1976. “Primary Productivity and Fish Yields in Tropical Lakes.” *Transactions of the American Fisheries Society* 105 (5): 575–80.

Mendonça, Raquel, Roger A Müller, David Clow, Charles Verpoorter, Peter Raymond, Lars J Tranvik, and Sebastian Sobek. 2017. “Organic Carbon Burial in Global Lakes and Reservoirs.” *Nature Communications* 8 (1): 1–7.

Messager, Mathis Loïc, Bernhard Lehner, Günther Grill, Irena Nedeva, and Oliver Schmitt. 2016. “Estimating the Volume and Age of Water Stored in Global Lakes Using a Geo-Statistical Approach.” *Nature Communications* 7: 13603.

Meyer-Jacob, Carsten, Neal Michelutti, Andrew M Paterson, Brian F Cumming, Wendel (Bill) Keller, and John P Smol. 2019. “The Browning and Re-Browning of Lakes: Divergent Lake-Water Organic Carbon Trends Linked to Acid Deposition and Climate Change.” *Scientific Reports* 9 (1): 16676.

Meyer-Jacob, Carsten, Julie Tolu, Christian Bigler, Handong Yang, and Richard Bindler. 2015. “Early Land Use and Centennial Scale Changes in Lake-Water Organic Carbon Prior to Contemporary Monitoring.” *Proceedings of the National Academy of Sciences* 112 (21): 6579–84.

Miles, Martin W, Victoria V Miles, and Igor Esau. 2018. “Environmental Research Letters Varying Climate Response across the Tundra, Forest-Tundra and Boreal Forest Biomes in Northern West Siberia Varying Climate Response across the Tundra, Forest-Tundra and Boreal Forest Biomes in Northern West Siberia.”

Monteith, Donald T, John L Stoddard, Christopher D Evans, Heleen A de Wit, Martin Forsius, Tore Høgåsen, Anders Wilander, Brit Lisa Skjelkvåle, Dean S Jeffries, and Jussi Vuorenmaa. 2007. "Dissolved Organic Carbon Trends Resulting from Changes in Atmospheric Deposition Chemistry." *Nature* 450 (7169): 537–40.

Morozumi, Tomoki, Ryo Shingubara, Jun Murase, Shin Nagai, Hideki Kobayashi, Shinya Takano, Shunsuke Tei, Rong Fan, Trofim C Maximov, and Atsuko Sugimoto. 2019. "Usability of Water Surface Reflectance for the Determination of Riverine Dissolved Methane during Extreme Flooding in Northeastern Siberia." *Polar Science* 21: 186–94.

Myers-Smith, Isla H, Jeffrey T Kerby, Gareth K Phoenix, Jarle W Bjerke, Howard E Epstein, Jakob J Assmann, Christian John, Laia Andreu-Hayles, Sandra Angers-Blondin, and Pieter S A Beck. 2020. "Complexity Revealed in the Greening of the Arctic." *Nature Climate Change* 10 (2): 106–17.

Myneni, Ranga B, C D Keeling, Compton J Tucker, Ghassem Asrar, and Ramakrishna R Nemani. 1997. "Increased Plant Growth in the Northern High Latitudes from 1981 to 1991." *Nature* 386 (6626): 698.

Olmanson, Leif G, Marvin E Bauer, and Patrick L Brezonik. 2008. "A 20-Year Landsat Water Clarity Census of Minnesota's 10,000 Lakes." *Remote Sensing of Environment* 112 (11): 4086–97.

Olson, David M, Eric Dinerstein, Eric D Wikramanayake, Neil D Burgess, George V N Powell, Emma C Underwood, Jennifer A D'amico, Illanga Itoua, Holly E Strand, and John C Morrison. 2001. "Terrestrial Ecoregions of the World: A New Map of Life on EarthA New Global Map of Terrestrial Ecoregions Provides an Innovative Tool for Conserving Biodiversity." *BioScience* 51 (11): 933–38.

Overland, J E, Edward Hanna, I Hanssen-Bauer, S-J Kim, J E Walsh, M Wang, U S Bhatt, and R L Thoman. 2018. “Surface Air Temperature.” *Arctic Report Card*.

Page, Benjamin P., Leif G. Olmanson, and Deepak R. Mishra. 2019. “A Harmonized Image Processing Workflow Using Sentinel-2/MSI and Landsat-8/OLI for Mapping Water Clarity in Optically Variable Lake Systems.” *Remote Sensing of Environment* 231 (September): 111284.

Pahlevan, Nima, Sundarabalan Balasubramanian, Sudipta Sarkar, and Bryan Franz. 2018. “Toward Long-Term Aquatic Science Products from Heritage Landsat Missions.” *Remote Sensing* 10 (9): 1337.

Pahlevan, Nima, Zhongping Lee, Jianwei Wei, Crystal B Schaaf, John R Schott, and Alexander Berk. 2014. “On-Orbit Radiometric Characterization of OLI (Landsat-8) for Applications in Aquatic Remote Sensing.” *Remote Sensing of Environment* 154: 272–84.

Pastick, Neal J, M Torre Jorgenson, Scott J Goetz, Benjamin M Jones, Bruce K Wylie, Burke J Minsley, Hélène Genet, Joseph F Knight, David K Swanson, and Janet C Jorgenson. 2019. “Spatiotemporal Remote Sensing of Ecosystem Change and Causation across Alaska.” *Global Change Biology* 25 (3): 1171–89.

Pearson, Richard G, Steven J Phillips, Michael M Loranty, Pieter S A Beck, Theodoros Damoulas, Sarah J Knight, and Scott J Goetz. 2013. “Shifts in Arctic Vegetation and Associated Feedbacks under Climate Change.” *Nature Climate Change* 3 (7): 673.

Pekel, Jean-François, Andrew Cottam, Noel Gorelick, and Alan S Belward. 2016. “High-Resolution Mapping of Global Surface Water and Its Long-Term Changes.” *Nature*.

Phoenix, Gareth K, and Jarle W Bjerke. 2016. “Arctic Browning: Extreme Events and Trends Reversing Arctic Greening.” *Global Change Biology* 22 (9): 2960–62.

Pitcher, Lincoln H, Tamlin M Pavelsky, Laurence C Smith, Delwyn K Moller, Elizabeth H Altenau, George H Allen, Christine Lion, David Butman, Sarah W Cooley, and Jessica V Fayne. 2019. "AirSWOT InSAR Mapping of Surface Water Elevations and Hydraulic Gradients across the Yukon Flats Basin, Alaska." *Water Resources Research* 55 (2): 937–53.

Raymond, Peter A, Jens Hartmann, Ronny Lauerwald, Sebastian Sobek, Cory McDonald, Mark Hoover, David Butman, et al. 2013. "Global Carbon Dioxide Emissions from Inland Waters." *Nature* 503 (7476): 355–59.

Read, Jordan S, and Kevin C Rose. 2013. "Physical Responses of Small Temperate Lakes to Variation in Dissolved Organic Carbon Concentrations." *Limnology and Oceanography* 58 (3): 921–31.

Riordan, Brian, David Verbyla, and A David McGuire. 2006. "Shrinking Ponds in Subarctic Alaska Based on 1950–2002 Remotely Sensed Images." *Journal of Geophysical Research: Biogeosciences* 111 (G4).

Roach, Jennifer, Brad Griffith, Dave Verbyla, and Jeremy Jones. 2011. "Mechanisms Influencing Changes in Lake Area in Alaskan Boreal Forest." *Global Change Biology* 17 (8): 2567–83.

Rover, Jennifer, Lei Ji, Bruce K. Wylie, and Larry L. Tieszen. 2012. "Establishing Water Body Areal Extent Trends in Interior Alaska from Multi-Temporal Landsat Data." *Remote Sensing Letters* 3 (7): 595–604.

Roy, D P, M A Wulder, T R Loveland, Woodcock C.E., R G Allen, M C Anderson, D Helder, et al. 2014. "Landsat-8: Science and Product Vision for Terrestrial Global Change Research." *Remote Sensing of Environment* 145 (April): 154–72.

Sayers, Michael J, Amanda G Grimm, Robert A Shuchman, Andrew M Deines, David B Bunnell, Zachary B Raymer, Mark W Rogers, Whitney Woelmer, David H Bennion, and Colin N Brooks. 2015. "A New Method to Generate a High-Resolution Global Distribution Map of Lake Chlorophyll." *International Journal of Remote Sensing* 36 (7): 1942–64.

Schmidt, Ursula, and Ralf Conrad. 1993. "Hydrogen, Carbon Monoxide, and Methane Dynamics in Lake Constance." *Limnology and Oceanography* 38 (6): 1214–26.

Seekell, David A., Jean-François Lapierre, Jenny Ask, Ann-Kristin Bergström, Anne Deininger, Patricia Rodríguez, and Jan Karlsson. 2015. "The Influence of Dissolved Organic Carbon on Primary Production in Northern Lakes." *Limnology and Oceanography* 60 (4): 1276–85.

Smith, L, Y Sheng, G M MacDonald, and L D Hinzman. 2005. "Disappearing Arctic Lakes." *Science* 308 (5727): 1429.

Smith, Laurence C, Yongwei Sheng, and Glen M MacDonald. 2007. "A First Pan-Arctic Assessment of the Influence of Glaciation, Permafrost, Topography and Peatlands on Northern Hemisphere Lake Distribution." *Permafrost and Periglacial Processes* 18 (2): 201–8.

Solomon, Christopher T, Denise A Bruesewitz, David C Richardson, Kevin C Rose, Matthew C Van de Bogert, Paul C Hanson, Timothy K Kratz, Bret Larget, Rita Adrian, and Brenda Leroux Babin. 2013. "Ecosystem Respiration: Drivers of Daily Variability and Background Respiration in Lakes around the Globe." *Limnology and Oceanography* 58 (3): 849–66.

Sulla-Menashe, Damien, Curtis E Woodcock, and Mark A Friedl. 2018. "Canadian Boreal Forest Greening and Browning Trends: An Analysis of Biogeographic Patterns and the Relative Roles of Disturbance versus Climate Drivers." *Environmental Research Letters* 13 (1): 14007.

Tarek, Mostafa, François P Brissette, and Richard Arsenault. 2019. “Evaluation of the ERA5 Reanalysis as a Potential Reference Dataset for Hydrological Modeling over North-America.” *Hydrology and Earth System Sciences Discussions*, 1–35.

Team, QGIS Delopment. 2016. “QGIS Geographic Information System.” *Open Source Geospatial Foundation Project*.

Thrane, Jan-Erik, Dag O Hessen, and Tom Andersen. 2014. “The Absorption of Light in Lakes: Negative Impact of Dissolved Organic Carbon on Primary Productivity.” *Ecosystems* 17 (6): 1040–52.

Topp, Simon N, Tamlin M Pavelsky, Daniel Jensen, Marc Simard, and Matthew R V Ross. 2020. “Research Trends in the Use of Remote Sensing for Inland Water Quality Science: Moving Towards Multidisciplinary Applications.” *Water* 12 (1): 169.

Tranvik, L J, and M Jansson. 2002. “Terrestrial Export of Organic Carbon.” *Nature* 415 (6874): 861–62.

Tranvik, Lars J, John A Downing, James B Cotner, Steven A Loiselle, Robert G Striegl, Thomas J Ballatore, Peter Dillon, Kerri Finlay, Kenneth Fortino, and Lesley B Knoll. 2009. “Lakes and Reservoirs as Regulators of Carbon Cycling and Climate.” *Limnology and Oceanography* 54 (6part2): 2298–2314.

USGS. 2018. “Product Guide: LandsaT 4-7 Surface Reflectance (LEDAPS) Product Guide.” USGS USA.

Vermote, Eric, Chris Justice, Martin Claverie, and Belen Franch. 2016. “Preliminary Analysis of the Performance of the Landsat 8/OLI Land Surface Reflectance Product.” *Remote Sensing of Environment* 185: 46–56.

Verpoorter, Charles, Tiit Kutser, David A Seekell, and Lars J Tranvik. 2014. “A Global

Inventory of Lakes Based on High-resolution Satellite Imagery." *Geophysical Research Letters* 41 (18): 6396–6402.

Virtanen, Pauli, Ralf Gommers, Travis E Oliphant, Matt Haberland, Tyler Reddy, David Cournapeau, Evgeni Burovski, Pearu Peterson, Warren Weckesser, and Jonathan Bright. 2020. "SciPy 1.0: Fundamental Algorithms for Scientific Computing in Python." *Nature Methods*, 1–12.

Vogelmann, James E., Alisa L. Gallant, Hua Shi, and Zhe Zhu. 2016. "Perspectives on Monitoring Gradual Change across the Continuity of Landsat Sensors Using Time-Series Data." *Remote Sensing of Environment* 185 (November): 258–70.

Vonk, J. E., S. E. Tank, W. B. Bowden, I. Laurion, W. F. Vincent, P. Alekseychik, M. Amyot, et al. 2015. "Reviews and Syntheses: Effects of Permafrost Thaw on Arctic Aquatic Ecosystems." *Biogeosciences* 12 (23): 7129–67.

Wang, Jonathan A, Damien Sulla-Menashe, Curtis E Woodcock, Oliver Sonnentag, Ralph F Keeling, and Mark A Friedl. 2019. "Extensive Land Cover Change Across Arctic-Boreal Northwestern North America from Disturbance and Climate Forcing." *Global Change Biology* 26 (2): 807-822.

Warner, Kate A, Rachel A Fowler, Robert M Northington, Heera I Malik, Joan McCue, and Jasmine E Saros. 2018. "How Does Changing Ice-out Affect Arctic versus Boreal Lakes? A Comparison Using Two Years with Ice-out That Differed by More than Three Weeks." *Water* 10 (1): 78.

Watts, Jennifer D, John S Kimball, Lucas A Jones, Ronny Schroeder, and Kyle C McDonald. 2012. "Satellite Microwave Remote Sensing of Contrasting Surface Water Inundation Changes within the Arctic–Boreal Region." *Remote Sensing of Environment* 127: 223–36.

Wetzel, Robert G, and Gene E Likens. 2000. “Light and Temperature.” In *Limnological Analyses*, 15–32. Springer.

Weyhenmeyer, Gesa A, and Jan Karlsson. 2009. “Nonlinear Response of Dissolved Organic Carbon Concentrations in Boreal Lakes to Increasing Temperatures.” *Limnology and Oceanography* 54 (6part2): 2513–19.

Weyhenmeyer, Gesa A, Yves T Prairie, and Lars J Tranvik. 2014. “Browning of Boreal Freshwaters Coupled to Carbon-Iron Interactions along the Aquatic Continuum.” *PloS One* 9 (2).

Williamson, Craig E, Erin P Overholt, Rachel M Pilla, Taylor H Leach, Jennifer A Brentrup, Lesley B Knoll, Elizabeth M Mette, and Robert E Moeller. 2015. “Ecological Consequences of Long-Term Browning in Lakes.” *Scientific Reports* 5: 18666.

Wit, Heleen A. de, Salar Valinia, Gesa A. Weyhenmeyer, Martyn N. Futter, Pirkko Kortelainen, Kari Austnes, Dag O. Hessen, Antti Räike, Hjalmar Laudon, and Jussi Vuorenmaa. 2016. “Current Browning of Surface Waters Will Be Further Promoted by Wetter Climate.” *Environmental Science & Technology Letters* 3 (12): 430–35.

Woolway, R. Iestyn, Gesa A. Weyhenmeyer, Martin Schmid, Martin T. Dokulil, Elvira de Eyto, Stephen C. Maberly, Linda May, and Christopher J. Merchant. 2019. “Substantial Increase in Minimum Lake Surface Temperatures under Climate Change.” *Climatic Change*, May, 1–14.

Zhu, Zhe, Shixiong Wang, and Curtis E Woodcock. 2015. “Improvement and Expansion of the Fmask Algorithm: Cloud, Cloud Shadow, and Snow Detection for Landsats 4–7, 8, and Sentinel 2 Images.” *Remote Sensing of Environment* 159: 269–77.

Zhu, Zhe, and Curtis E Woodcock. 2012. “Object-Based Cloud and Cloud Shadow Detection in

Landsat Imagery." *Remote Sensing of Environment* 118: 83–94.

4.6 APPENDIX C

4.6.1 *Extended Results*

Our analysis shows more rapid warming in the spring (Figure 4.4c) relative to the summer (Figure 4.4e). Spring temperatures in the study region were warming twice as rapidly (0.04 °C ± 0.05 °C yr^{-1}) as summer (0.02 °C ± 0.03 °C yr^{-1}) but with greater spatial variability. For the lakes with associated basins (see Materials & Methods), our results show that 82% (n = 309,053) of lakes are located in warming basins. Warmer temperatures are predicted to shorten the duration of ice-cover (Dibike et al. 2011), which is a main driver of carbon dynamics (Jansen et al. 2019). Changes in precipitation show greater spatiotemporal variability (Figure 4.4g, Appendix C, Figure 4.12), with an overall net increase of 0.002 ± 0.03 cm yr^{-1} over the region on an annual basis. Spring and summer (Figure 4.4d,f) had comparably greater increases in precipitation of 0.008 ± 0.03 cm yr^{-1} and 0.007 ± 0.02 cm yr^{-1} respectively.

Supplemental Figures

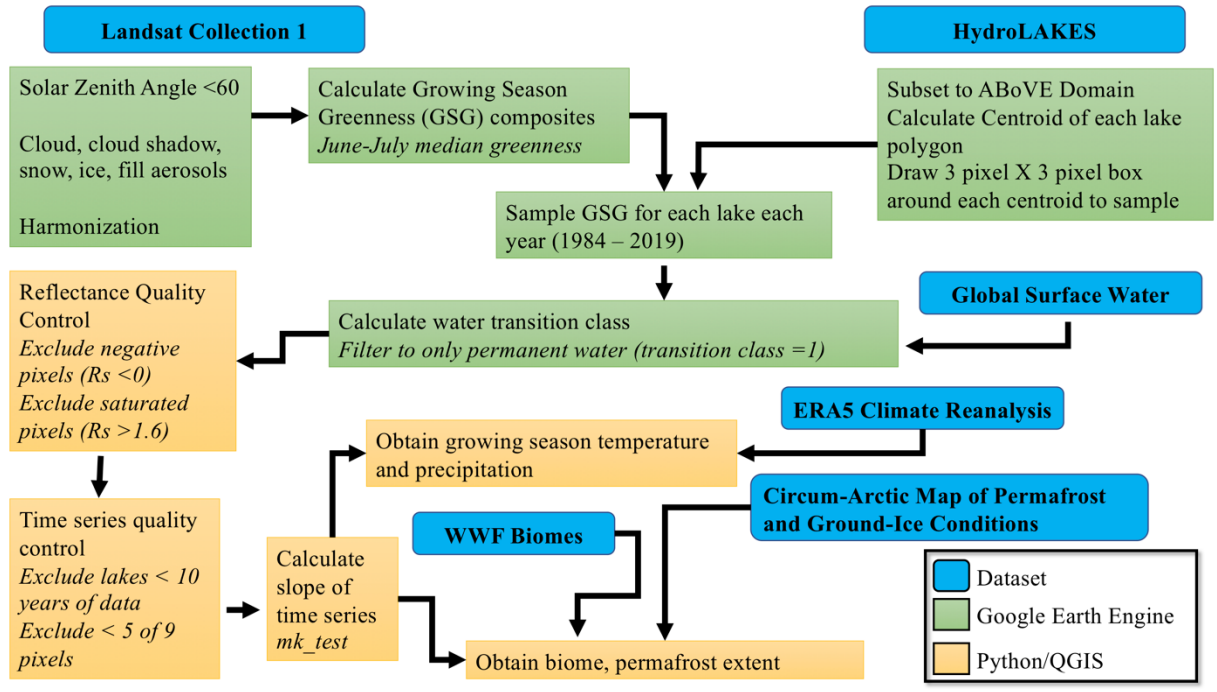

Figure 4.5. Workflow for Landsat time series analysis

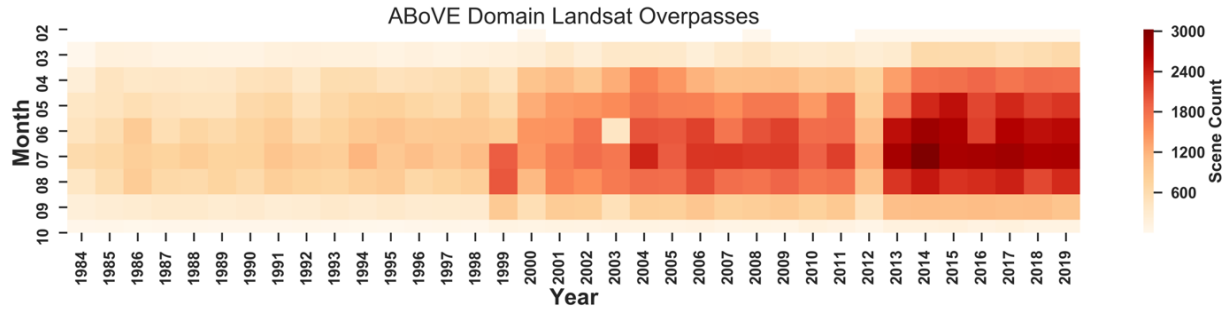

Figure 4.6. Landsat scenes available over the ABoVE domain (n = 278,284). Only June and July scenes (n = 162,720) were used to calculate seasonal composites. Scenes from winter months were excluded because of their high solar zenith angle (> 60 degrees). Scene counts varied between Landsat-5 (n = 66,825), Landsat-7 (n = 65,902), and Landsat-8 (n = 29,993). Note if

this analysis had been conducted at a charge of $600 per scene the data used to create the seasonal composites for this study would have cost over $97 million USD.

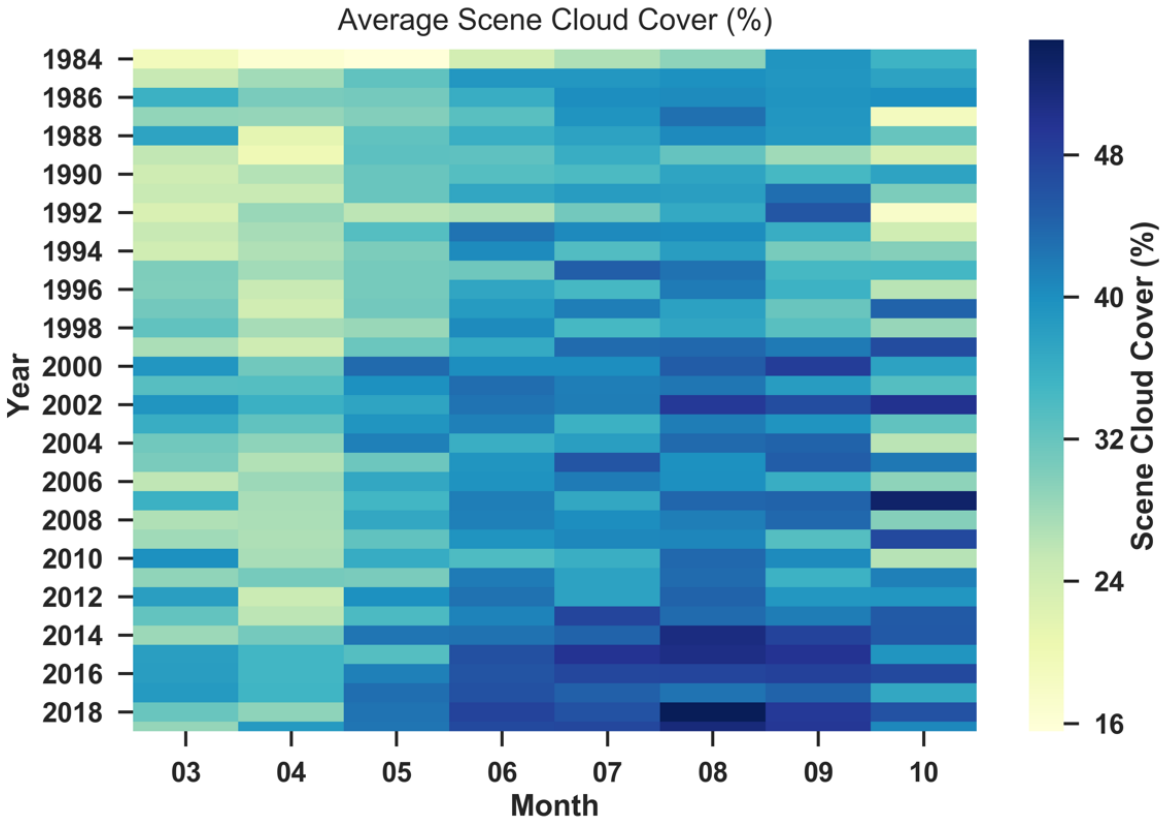

Figure 4.7. Average scene cloud cover (%) by month and year for Landsat scenes available over the ABoVE domain from 1984 – 2019. Cloud cover is higher in the summer, peaking at an average of 42% and 43% in August and September.

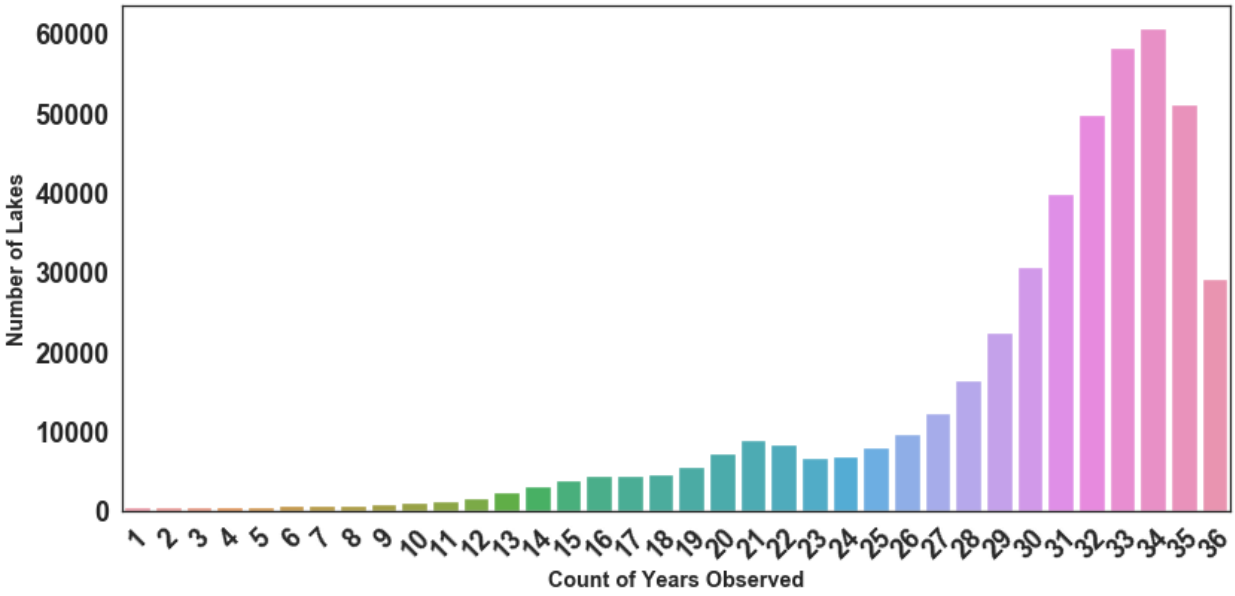

Figure 4.8. Lakes binned by the number of years that cloud-free summer composites (June-July) are available. The majority of lakes (93%) have > 20 years of data.

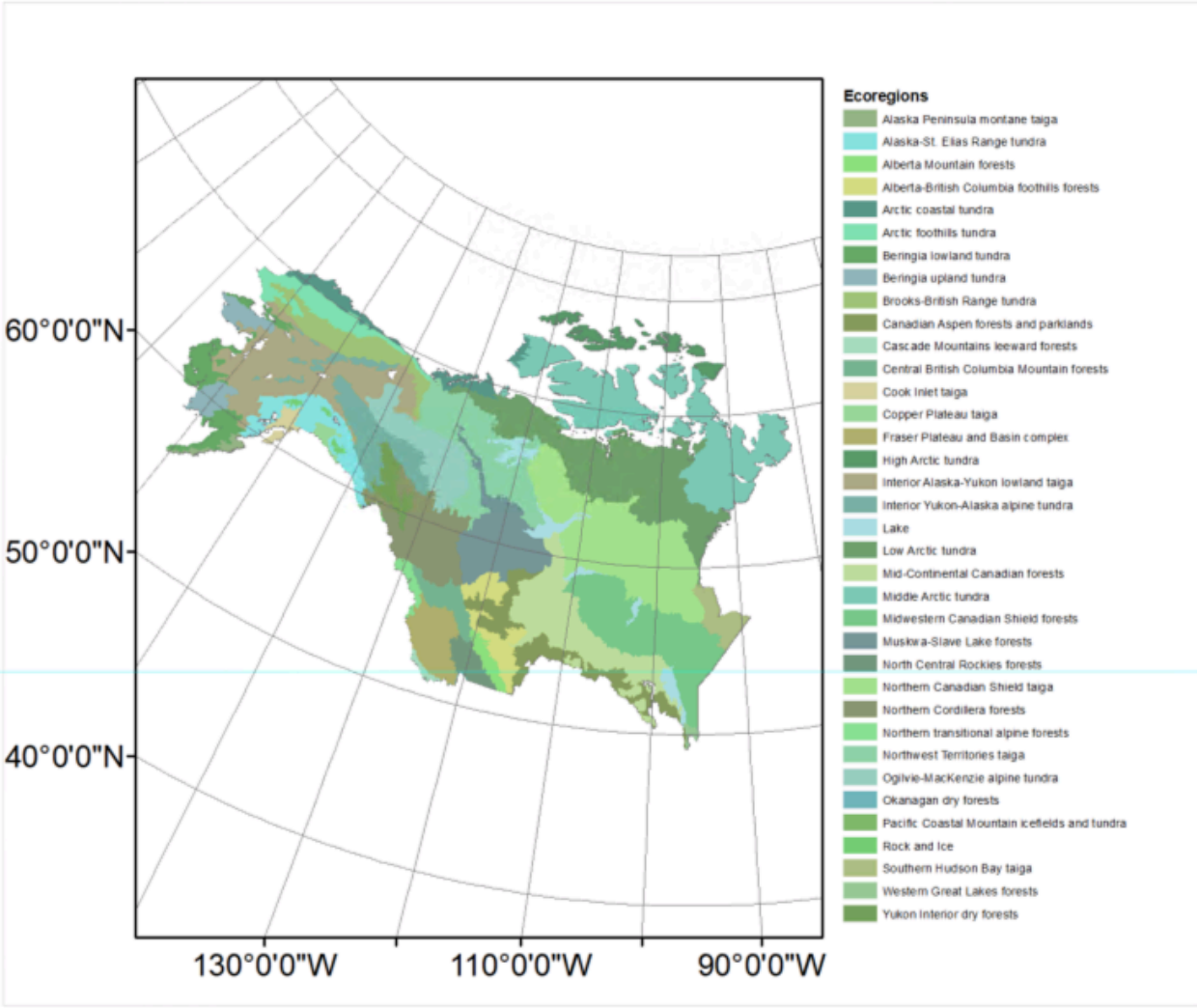

Figure 4.9. Ecoregions of the ABoVE Domain

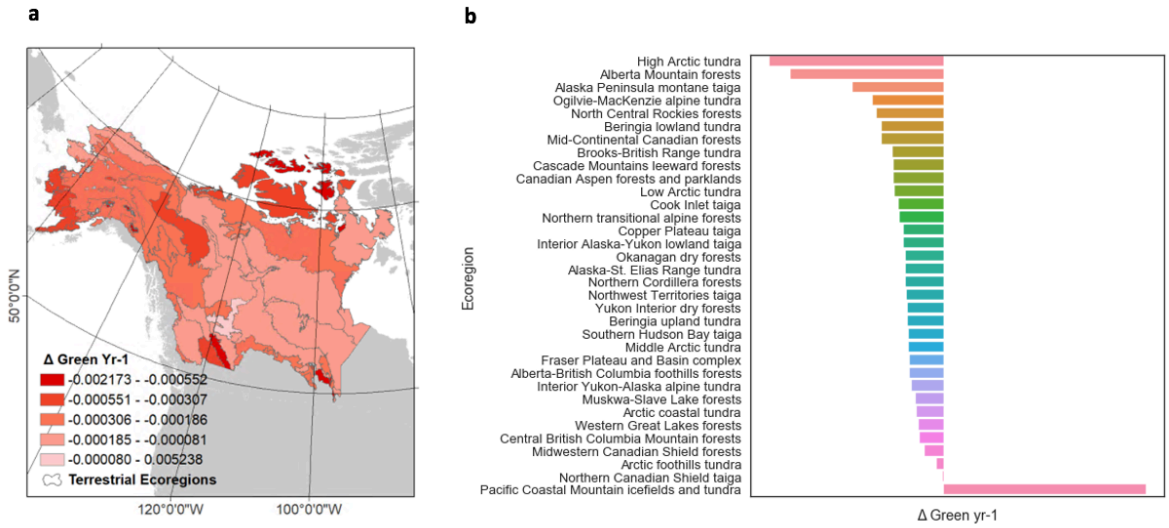

Figure 4.10. Change in greenness per year summarized by the 34 terrestrial ecoregions (Olson 2001) found in the North American arctic and boreal zone. Comparative spatial patterns by ecoregion (a) and shown ranked by magnitude and order of sign (b).

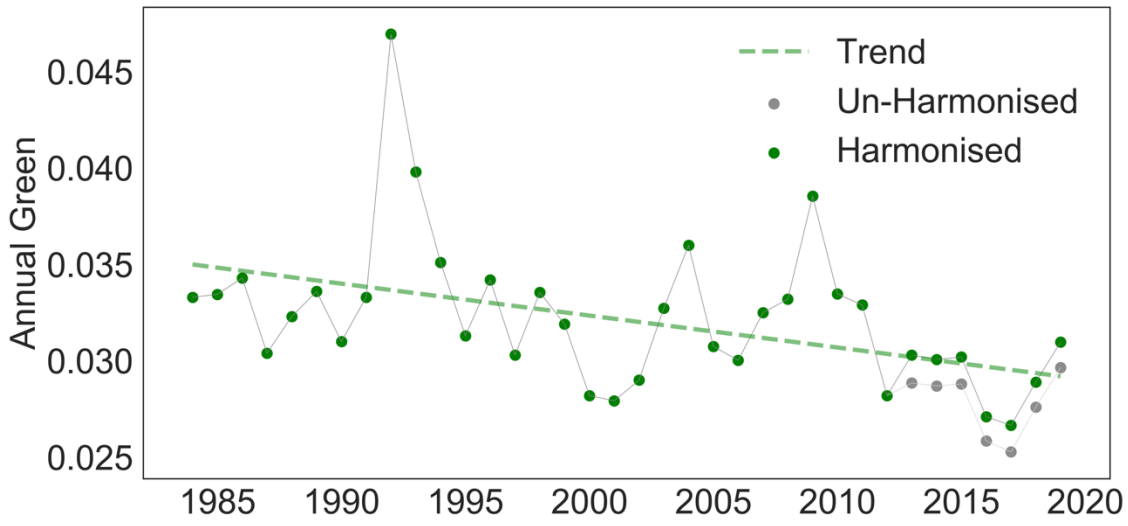

Figure 4.11. Impact of harmonization on green trend (1984 – 2019). The overall negative trend is statistically significant for both the un-harmonized (Mann Whitney trend test, Z=-3.22, *P*=1X 10^{-3}, n = 472,889) and harmonized (Mann Whitney trend test, Z=-2.88, *P*=3.8 X 10^{-3}, n = 472,889) time series.

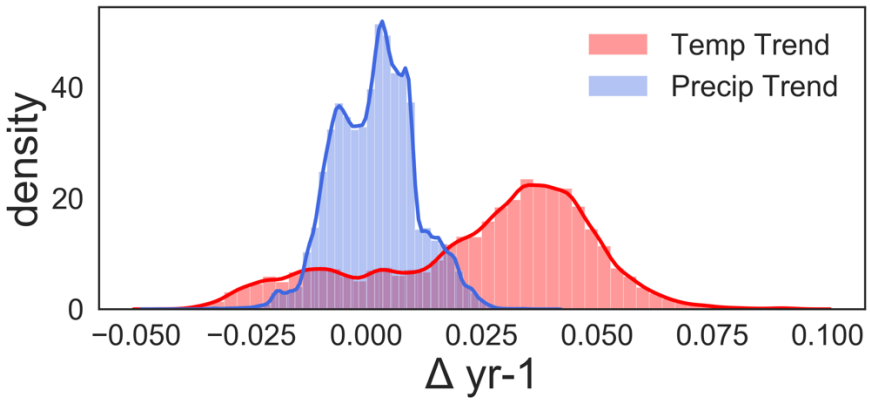

Figure 4.12. Density plot of distribution of temperature and precipitation change (g) calculated by basin for each lake assigned a basin using the GLCP dataset (see materials and methods).

Table 4.1 Number of lakes and trend in greenness by biome. Lakes in the rock and ice biome (n = 14) were not included in this analysis.

Biome	Δ Green yr-1	No. of Lakes
Tundra	-0.000265	247167
Boreal Forests/Taiga	-0.000193	217263
Temperate Conifer Forests	-0.000194	5793
Temperate Grasslands, Savannas & Shrublands	-0.000255	2463
Temperate Broadleaf & Mixed Forests	-0.000131	189

Table 4.2. Tukey HSD comparison of groups results.

Multiple Comparison of Means - Tukey HSD, FWER=0.05

Group 1	Group 2	Mean Diff	Lower	Upper	Reject
Boreal Forests/Taiga	Temperate Broadleaf & Mixed Forests	0	-0.0001	0.0001	False
Boreal Forests/Taiga	Temperate Conifer Forests	-0.0001	-0.0001	0	True
Boreal Forests/Taiga	Temperate Grasslands, Savannas & Shrublands	-0.0001	-0.0001	-0.0001	True
Boreal Forests/Taiga	Tundra	-0.0001	-0.0001	-0.0001	True
Temperate Broadleaf & Mixed Forests	Temperate Conifer Forests	-0.0001	-0.0001	0	True
Temperate Broadleaf & Mixed Forests	Temperate Grasslands, Savannas & Shrublands	-0.0001	-0.0002	0	True
Temperate Broadleaf & Mixed Forests	Tundra	-0.0001	-0.0002	-0.0001	True
Temperate Conifer Forests	Temperate Grasslands, Savannas & Shrublands	0	0	0	True
Temperate Conifer Forests	Tundra	0	-0.0001	0	True
Temperate Grasslands, Savannas & Shrublands	Tundra	0	0	0	False

Table 4.3. Number of unique HydroLAKES per basin level for the GLCP dataset. Note 21 lakes are not found in the GLCP likely due to GLCP data processing choices.

Basin Level	Count of Lakes	Percent of Total Lakes
lev02	970	0.2%
lev03	2,715	0.6%
lev04	3,530	0.7%
lev05	6,446	1.4%
lev06	8,412	1.8%
lev07	15,269	3.2%
lev08	19,564	4.1%
lev09	18,827	4.0%
lev10	3,353	0.7%
lev11	30	0.0%
lev12	393,652	83.3%
Total	472,768	

Table 4.4. Landsat growing season greenness (GSG) satellite observations and GPP calculations. Landsat lake surface reflectance in the green band (560 nm) during June, or growing season greenness (GSG), for the first (1984 – 1994) and last (2009 – 2019) decade of the study period averaged across all lakes. GPP was calculated using the previously published relationship between Landsat GSG and GPP for arctic-boreal lakes (Kuhn et al. 2020) (type 2 major axis regression: y = 385.81x – 0.45; $r2 = 0.69$; $p = 2.6 \times 10$

Total ABoVE Domain Lake Area (km2):	1984 GSG	1984 GPP (g O2 m-2)	2019 GSG	2019 GPP (g O2 m-2)	Change in GPP (g O2 m-2)	Total ABoVE Domain Change in GPP* (Tg O2)	Total ABoVE Domain Change in Carbon Uptake* (Tg C)
417,152.40	0.0349	779.83	0.0298	662.57	117.27	48.92	58.70

Chapter 5. FINAL SUMMARY

5.1 KEY FINDINGS

The studies presented here build from each other and are united by the themes of satellite remote sensing, freshwater ecology and cloud-computing. Altogether, this work analyzes trends in color and chemistry in freshwater ecosystems, leverages *in situ* measurements to constrain uncertainties in remote sensing model results, and explores major drivers of lake color change in arctic-boreal ecosystems.

Chapter 2 demonstrates the retrieval of common water quality properties in three diverse river systems. Utilizing thousands of *in situ* measurements collected during river cruises in Brazil and the United States, we map spatial patterns in chlorophyll-*a* and turbidity across the Amazon, Columbia and Mississippi Rivers. We quantify error introduced during atmospheric correction, a core element of satellite imagery processing. We found higher uncertainties in chlorophyll-*a* versus turbidity estimates and were able to achieve levels of uncertainty (3 – 30% MAPD) comparable to global ocean primary productivity models. Ultimately, choice of atmospheric correction could bias results by as much as 59%. Despite this, we discovered that the standard Landsat land surface reflectance product had adequate performance over turbid waters. This finding is significant because it lowers the barrier to entry for aquatic remote sensing by utilizing a readily-available surface reflectance product.

Using the framework developed in Chapter 2, we extracted lake color from global satellite sensors for a subset of lakes within the ABoVE Domain. We conducted intensive field surveys of diverse lakes in interior Alaska to fully characterize their color and chemistry. Combining these datasets, we found that lake reflectance in both the green (560 nm) and the red-edge (703 nm) could be used to infer gross primary productivity as estimated by stable oxygen

isotopes collected in the field. We also did a detailed comparison of surface reflectance from satellite, airborne and *in situ* measurements, discovering that sensors disagreed the most in the near-infrared wavelengths (MAPD median 54%, interquartile range of 8 - 60%) and agreed the most in the green wavelengths (MAPD median = 29%, interquartile range 8 - 53%).

The utility of green reflectance in identifying patterns in GPP observed here is consistent with decades of ocean color remote sensing, which utilizes green and blue reflectance as a primary driver of satellite productivity models. Given the ecological significance of greenness and its stability across remote sensing platforms, we chose to focus Chapter 3 on decadal trends in green reflectance in the myriad lakes of Alaska and northwestern Canada. Using the moderate resolution (30m) Landsat archive and quality control techniques honed in Chapters 1 and 2, we create annual growing season greenness composites spanning the past 35 years across the ABoVE domain. We discover that 26% of lakes are experiencing significant changes in color, and that 97% of those lakes show declining greenness. Lakes with declining greenness were more likely to be found in watersheds also experiencing warmer air temperatures and increased precipitation. This result provides evidence in support of the hypothesis that environmental change is reconfiguring hydrologic connectivity, altering the timing, magnitude and delivery of organic carbon to lake ecosystems with significant implications for carbon cycling and ecosystem productivity. More field studies are needed to verify these patterns and confirm the mechanistic driver of this uneven color change across diverse arctic-boreal lake ecosystems.

5.2 Conclusion and Future Directions

"The outcome of any serious research can only be to make two questions grow where only one grew before." -Thorstein Veblen

Multiple lines of research converge in this dissertation, resulting in a set of studies characterizing ecological properties and processes in large temperate and tropical rivers of the US and Brazil and shallow arctic-boreal lakes of northwestern Canada and Alaska. These diverse ecosystems share the common feature of being remote, spatially complex and under-studied in terms of high-quality *in situ* measurements for validating remote sensing models. This dissertation provides evidence that satellite remote sensing is a feasible tool for freshwater monitoring at large scales (Glasgow et al. 2004) when appropriately constrained by field data.

Decades of early research in ocean optics (Jerlov 1976; Mobley 1994; Kirk 1994) have laid the foundation for the use of ocean color in monitoring seasonal and spatial variations in ocean primary productivity, global marine biogeochemical cycles and fisheries research (O'Reilly et al. 1998). Advances in cloud computing and *in situ* sensors have further accelerated monitoring efforts. This work harnesses these parallel advances to identify spatial patterns in ecological properties and processes, including turbidity, chlorophyll-*a* and gross primary productivity, of diverse waterbodies from the individual lake to the continental scale.

This work bridges scales, moving from intensive field studies of individual waterbodies to continental and decadal scale time series analysis. We also combine diverse data streams, weaving together global satellite remote sensing with climate, terrain, hydrography and detailed *in situ* data. We examine lake reflectance from a range of sensors, including handheld, above-water devices to moderate (30m) and high (5m) spatial resolution satellite and airborne sensors. These tools capture the color of water's surface, a fundamental variable that has been designated an Essential Climate Variable (ECV) by the Global Climate Observing System (GCOS) (Global Climate Observing System 2011). By tethering observation of color to coincident optical and biogeochemical measurements, we are able to generate new insights into freshwater ecosystem

processes at larger scales. This dissertation advances our understanding of the performance of contemporary satellites in mapping freshwater ecosystem biogeochemistry from lake color, including by capturing novel datasets of freshwater optical properties, testing methodologies for inland water remote sensing, and analyzing drivers of color change in arctic-boreal lakes.

The research presented in this dissertation advances our understanding of how satellite remote sensing can be used to characterize ecological properties and processes in lakes and rivers. However, many questions remain. The remote sensing of inland waters, or optical hydrology, draws its primary inspiration from decades of research in optical oceanography.

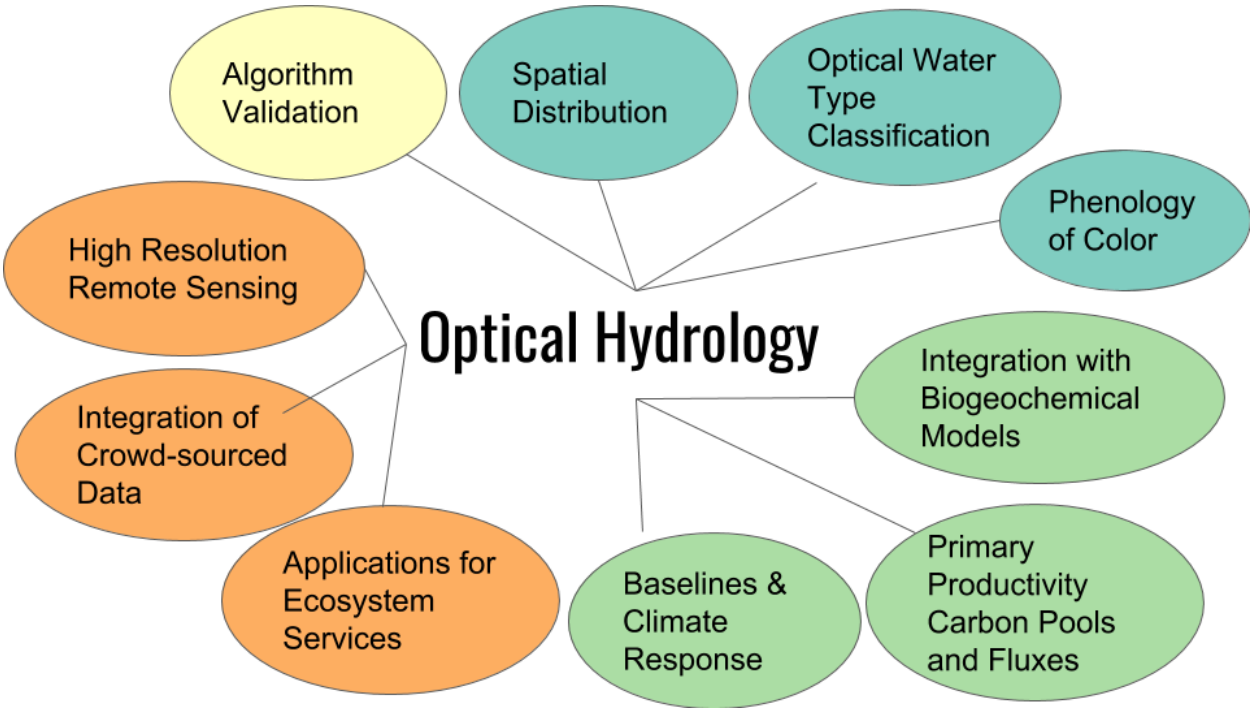

Figure 5.1 Major themes and future directions for optical hydrology, as modeled off the research threads emergent in the ocean color literature.

Optical hydrology is inherently interdisciplinary (Figure 5.1), drawing from many fields, including aquatic biogeochemistry, landscape ecology, data science, physical oceanography, computer science and surface water hydrology. Many questions arise from this research along

these themes. For example, how well can we detect seasonal signatures of productivity in freshwater ecosystems? To what degree will bottom reflectance be separable from water column reflectance across ecosystem types? How widespread are color shifts in freshwater ecosystems in other regions of the planet? To what extent will lake and river productivity shift as the climate continues to warm? These questions among many others remain from this research.

The studies presented here are analogous to the steps taken by the Ocean Color community in the late 1970s. This dissertation contributes to the revolution of our understanding of biogeochemical processes in inland waters at regional and global scales and establishes baselines for monitoring the anthropogenic impacts to rivers and lakes worldwide.

CURRICULUM VITAE

Catherine Kuhn

Doctoral Candidate, University of Washington
School of Environmental & Forest Sciences
Phone: 773-343-7887, Email: ckuhn@uw.edu

EDUCATION

Ph.D.	Environmental Science, University of Washington, School of Environmental and Forest Sciences Seattle, WA Dissertation: Bio-optical and biogeochemical properties of freshwater ecosystems using field, airborne and satellite data	(Expected 2021)
MESc.	Environmental Science, Yale University, School of Forestry & Environmental Studies New Haven, CT Thesis: Patterns in stream greenhouse gas dynamics from mountains to plains in northcentral Wyoming	2015
B.A.	English Literature, Loyola University Chicago, IL *magna cum laude*	2006

IN PREPARATIONS PUBLICATIONS

Kuhn, C., John, A., Butman, D. (in prep 2020) "Declining color in arctic-boreal lakes." Submitted *PNAS.*

Liu, S., Butman, D., Kuhn, C., Raymond, P. (in review 2020) "A new synthesis of direct pCO_2 measurement from global streams and rivers argues for the importance of increasing regional representativeness". Intended Journal: *Nature Geoscience*.

B. Tellman, B., Sullivan, J., Kettner, A., Kuhn, C., Doyle, C., Brakenridge, B., Ericksen, T., Slayback, D. (in review 2020) "A Global Inventory of Flood Events and Exposure Trends." *Nature.*

PUBLICATIONS & WRITING

Kuhn, C., Johnston, S., John, A., S.E., Bogard, M., Striegl, R., Dornblaser, M., Spencer, R., Wickland, K., and Butman, D. (accepted 2020) "Gross primary productivity in boreal lakes estimated from satellite and *in situ* measurements." *Environmental Research Letters*.

Pretty, T., Chanyi, C., Kuhn, C., Gray, D. (accepted 2020) “Factors influencing the structure of macroinvertebrate communities in subarctic lakes affected by forest fires.” *Canadian Journal of Fisheries and Aquatic Sciences*.

John, A., Hellander, A., Ausmees, K., Kuhn, C., Tan, A. “SWEEP: Accelerating Scientific Research Through Scalable Serverless Workflows”. 12th IEEE/ACM International Conference on Utility and Cloud Computing. Conference Paper. December 02–05, 2019, Auckland, New Zealand.

O’Dwyer, M., Butman, D., Striegl, R., Dornblaser, M., Wickland, K., Kuhn, C., Bogard, M.J. (accepted 2020) “Patterns of Greenhouse Gases Under-Ice in Lakes of Interior Alaska.” *Environmental Research Letters*.

Kuhn, C., Ward, N., Loken, L., Sawakuchi, H., Crawford, J., Stadler, P., Richey, J., Striegl, R., Butman, D. (2019). Performance of Landsat-8 and Sentinel-2 surface reflectance products for river remote sensing retrievals of chlorophyll-*a* and turbidity. *Remote Sensing of Environment*, *224*, 104-118.

Ross, M., Topp, S., Appling, A., Yang, X., Kuhn, C., Butman, D., Pavelsky. T. (accepted 2019). “AquaSat: a dataset to enable remote sensing of water quality for inland waters.” *Water Resources Research.*

Bogard, M., Kuhn, C., Johnston, S.E., Striegl, R., Holtgrieve, G., Dornblaser, M., Spencer, R., Wickland, K., and Butman, D. (2019) “Negligible terrestrial carbon cycling in many lakes of the arid circumpolar landscape.” *Nature Geosciences*, 12.3: 180.

Stadler, P., Loken, L.C., Crawford, J.T., Schramm, P.J., Sorsa, K., Kuhn, C., Savio, D., Striegl, R.G., Butman, D., Stanley, E.H. and Farnleitner, A.H., (2019). Spatial patterns of enzymatic activity in large water bodies: Ship-borne measurements of beta-D-glucuronidase activity as a rapid indicator of microbial water quality. *Science of The Total Environment*, 651, 1742-1752.

Routh, D., Seegmiller, L., Bettigole, C., Kuhn, C., Oliver, C., & Glick, H. (2018). Improving the Reliability of Mixture Tuned Matched Filtering Remote Sensing Classification Results Using Supervised Learning Algorithms and Cross-Validation. *Remote Sensing*, 10(11), 1675.

James, J.N., Kates, N., Kuhn, C., Littlefield, C.., Miller, C., Bakker, J., Butman, D.. and Haugo, R. (2018). The effects of forest restoration on ecosystem carbon in western North America: A systematic review. *Forest Ecology and Management*, *429*, 625-641.

Schwarz B., Pestre, G., Tellman, B., Sullivan, J., Kuhn, C., Mahtta, R., Pandey, B., Hammett, L. (2018) “Mapping Floods and Assessing Flood Vulnerability for Disaster Decision-Making: A Case Study Remote Sensing Application in Senegal.” In: Mathieu PP., Aubrecht C. (eds) *Earth Observation Open Science and Innovation.* ISSI Scientific Report Series, vol 15.

Kuhn, C., Bettigole, C., Glick, H., Seegmiller, L., Raymond, PA., Oliver, C. (2017) "Patterns in stream greenhouse gas dynamics from mountains to plains in northcentral Wyoming." *J. Geophys. Res. Biogeosci.,* 122, 2173–2190, doi:10.1002/2017JG003906.

Crawford, J. T., Butman, D.E., Loken, L., Stadler, P., Kuhn, C. and Striegl, R. (2017) Spatial Variability of CO_2 Concentrations in the Lower Columbia River. *Inland Waters* 7.4 (2017): 417-427.

Glick, H. B., Routh, D., Bettigole, C. Seegmiller, L., Kuhn, C., and Oliver, C. D. "Modeling The Effects of Locational Error on Map Accuracy Statistics." *Photogrammetric Engineering and Remote Sensing.* 82.10 (2016): 789-802.

Glick, H. B., Bettigole, C., Routh, D., Seegmiller, L., Khadka, A., Kuhn, C., and Oliver, C. D. (2014) Wyoming's Changing Agricultural Landscape: Demographic Trends among Farm and Ranch Operators, 1920-2007. *Rangelands,* 36(6)

GRANTS & FUNDING

- Graduate & Professional Senate Award ($500) June 2019
- College of the Environment Travel Award ($1,000), Dec 2018
- Director's Graduate Student Travel Fund ($500), Oct 2018
- Graduate School Fund for Excellence and Innovation ($500), Oct 2018
- NASA Earth and Space Science Fellowship ($135,000), 2018
- CUAHSI Instrument Discover Travel Award ($973), 2017
- Integral Environmental Big Data Award ($6,000), 2017
- Northwest Scientific Association Student Grant ($1,000), 2017
- Achievement Rewards for College Students ($17,500), 2015-2017
- AGU Student Travel Funding, Private Donor, University of Washington ($400), December 2015
- Ucross Ranch Conservation Science Research Support Award ($18,000), September 2014
- Carpenter Sperry Research Award (matching fund, $500), Yale University F&ES, April 2014
- F&ES Jubitz Research Fund ($3,800) Yale University F&ES, April 2014
- Master's Student Travel Fund ($300) Yale University F&ES, April 2014
- Master's Research Grants ($1,000) Yale Institute for Biospheric Studies Small Grants Program, April 2014
- Stopwaste.org Waste Audit and Field Trip Grant, 2008 – 2013
- Eco-Stewards Classroom Collaboration Grant, 2008 - 2013
- Parent Teacher Association Community Garden Grant, 2012
- Donor's Choose Classroom Funds, 2009-2011
- John A. Maclean Tuition Scholarship ($15,000), Yale University F&ES, April 2013
- McNeill/Donahue Scholarship for Outstanding Scholarship, September 2004
- The Damen Scholarship for Academic Merit, August 2002

HONORS & AWARDS

- University of Washington Husky 100, 2019
- Graduate Student of the Year, UW School of Forestry & Env. Science, 2018
- Outstanding Student Presentation Award, American Geophysical Union Conference, Dec 2017
- Outstanding Speaker Award, Yale Masters Student Research Colloquium ($200), April 2015
- Best Student Oral Presentation, Society for Ecological Restoration Conference, May 2014
- Teacher of the Month Earth Team Eco-Stewards, 2012
- Biology & Environmental Science Teaching Fellow, Oakland Teaching Fellows Program, 2008
- ETS Praxis Recognition of Excellence on Teaching Content Exam, 2007
- Dean Charles W. Hart Award for Excellence in Literary Study, 2006
- McNeill/Donahue Scholarship for Outstanding Scholarship, 2006
- The Damen Scholarship for Academic Merit, 2006

SCIENTIFIC LEADERSHIP & SERVICE

Reviewer	*JGR:Biogeosciences*, *Remote Sensing of the Environment, Limnology & Oceanography Letters, Global Biogeochemical Cycles, Environmental Science and Technology*	current
Data Science Lead	Global Database for Freshwater pCO2 measurements, UW Geohackweek	2018
Panel Organizer & Chair	Women in Science Panel Discussion	2017
Student Chair	University of Washington School of Forestry & Environmental Science Hydrology Faculty Hire Search Committee	2016
Student Notetaker	NSF Award No: 1557186. RCN: Coastal Rainforest Margins Research Network - understanding materials flux in linked terrestrial and marine ecosystems in the face of climate change	2016
Student Chair	University of Washington Civil and Environmental Engineering Geospatial Faculty Hire Search Committee	2016
Student Notetaker	University of Washington Freshwater Initiative Mixer	2016

TEACHING

Graduate Teaching Assistant	CEE 498, 599, SEFS 521 Special Topics – Advanced Remote Sensing of the Environment, University of Washington, Seattle, WA	Winter 2020

	• Led redesign of lab modules for teaching fundamentals of environmental remote sensing in Google Earth Engine • Delivered lectures on fundamental physics of optical and thermal remote sensing	
Course Content Creator	INFO 180 - Introduction To Data Science, University of Washington, Seattle, WA • Designed python, statistics and data science content modules for new, scalable introductory data science course • Developed content using an XML software framework	2018
Guest Lecturer	CEE 498, 599, SEFS 521 Special Topics – Advanced Remote Sensing of the Environment, University of Washington, Seattle, WA • Introduction to multispectral remote sensing • Presented hands-on workshop for Google Earth Engine	2016 - 2018
Guest Lecturer	CEE 578 - Water Resources • Research presentation - The Color of Water: Monitoring Freshwater Vulnerability to Fragmentation & Global Change	Spring 2018
Graduate Teaching Assistant	Evaluating the Impact of Forest Management on Ecosystem Services in the Pacific Northwest • Joint course between the Nature Conservancy, University of Washington and the Forest Service • Co-directed a student-driven systematic literature review process	Spring 2017
Instructor	Introduction to GitHub, GeoHack Week, University of Washington eScience Institute, Seattle WA • Guided lecture and project-based curriculum development for GeoHack week instructors, co-taught Github session	2016 - 2018
Secondary Guest Lecturer	Chief Sealth, Duwamish River Field Day, Seattle WA Delivered interactive lecture to 100+ high school freshman about watershed ecology and conservation	2016
Middle School Guest Lecturer	NASA Space Grant Consortium Bilingual Summer Camp, Seattle WA	Winter 2015

- Taught middle school English language learners about the carbon cycle including an interactive fieldtrip to local creek

Graduate Teaching Fellow	Yale F&ES 734b Biological Oceanography, Yale University, New Haven CT	2013
Graduate Teaching Fellow	Yale F&ES 551 Mixed Methods for Social Research, Yale University, New Haven, CT	2013
Secondary School Instructor	Biological Connections to Energy and the Environment, Skyline High School, Oakland CA • Designed and delivered project-based, hands on lessons for diverse students to increase scientific literacy • Trained extensively in human-centered, equitable instruction focused on empowering students from a variety of backgrounds and skill levels	2008-2013
Secondary School Instructor	Advanced Placement Environmental Science, Skyline High School, Oakland, CA • Taught college-level environmental science course with a special focus on support for first-generation college students	2011-2013
Secondary School Instructor	Anatomy & Physiology, Paul Robeson High School, Oakland CA • Designed and delivered human health and biology curriculum targeting youth in high risk situations • Collaborated with Opera Piccolo Theater Therapy Coach to design integrated Sex Ed Curriculum resulting in a community performance piece attended by 300 parents, students, and community members.	2008-2009
Secondary School Instructor	English Language Arts, Salina Central High School, Salina, KS • Student progress monitoring, daily lesson planning, departmental collaboration • Developed Language Arts curriculum for gifted and talented students	2007-2008

MENTORING

Participant	UW Civil & Environmental Engineering Career Dinners & Discussion Program	2018
Mentor	SEFS Graduate Student Peer Mentoring Program	2018 -

	• Mentored 2 incoming doctoral students	2020
Mentor	Butman Lab Undergraduate Student (Rachel Yonemura, Madeline Rubenstein) • Advised on scientific research design • Standardized and taught lab procedures for carbon analysis	2015-2020
Mentor	Women in Science At Yale • Mentored two female undergraduate students on scientific career navigation	2014-2015
Mentor/ Mentee	Environmental Leadership and Mentoring at Yale • Mentored an undergraduate student and was mentored by a post-doctoral student in environmental science	2015
Mentor	Beginning Teacher Support and Assessment Program, Oakland, CA • Mentored new teachers on curriculum development and classroom management techniques	2009-2012
Mentor and Coach	Bay Area Institute for Urban Debate • Founded debate program at Paul Robeson High School • Researched and developed debate course content around current environmental and community resource issues • Managed logistics for students to attend local and national debate tournaments • Improved literacy scores for students participating in debate • Helped secure debate scholarships for low-income urban youth at four-year universities	2009-2013

SCIENTIFIC OUTREACH

Invited Speaker, Northwest Data Science Summit, "No evidence of arctic-boreal lake greening", University of British Columbia	2020
Invited Scientist, Climate Change Table Host, YMCA Earth Service Corp Youth Environmental Leadership Summit, Seattle WA	2018-2019
Panelist, CUAHSI Annual Membership Meeting	2018
EOS Buzz Newsletter. Duncombe, Janessa. "Hack Weeks Gaining Ground in the Earth and Space Sciences" https://eos.org/articles/hack-weeks-gaining-ground-in-the-earth-and-space-sciences?utm_source=eos&utm_medium=email&utm_campaign=EosBuzz092118	2018
Invited Blogger, Freshwater Initiative 'Travel Notes' Summer Newsletter & Online Blog http://freshwater.uw.edu/2018/08/09/ground-truthing-greenness-in-arctic-lakes/	2018
Invited Lecturer, Google Booth, 2018, 2019 American Geophysical Union Conference	2018
	2017

Invited Lecturer, Community Evening Lecture Series, Olympic Natural Resource Center

University of Washington: Achievement Rewards for College Scientists, selected for public outreach booklet to promote women in science at UW — 2016

The Spectroscope, contributor, public access blog on scientific issues — 2015

Yale Environmental Review, Staff Writer and Peer Editor — 2013-2015

- Monitored peer-reviewed databases to identify innovative environmental research efforts
- Wrote web-based features translating journal articles for a non-expert, public audience
- Revised peer article submissions for style and factual content

Oakland Teaching Fellows, New Teacher Institute, selected for "Fellows Diary" to promote teaching in urban classrooms — 2009

AFFILIATIONS & PROFESSIONAL TRAININGS

- Earth Science Women's Network (ESWN), member
- American Geophysical Union (AGU), member
- Association for the Science of Limnology and Oceanography (ASLO), member
- KQED Public Radio Advanced STEM, Workshop Participant
- Exploratorium Museum of Science & Inquiry, Teacher Institute Graduate
- Chabot Space & Science Center Climate Change, Teacher Institute Member
- National Marine Sanctuary LIMPETS, Teacher Partner
- Skyline Green Academy Linked Learning California Partnership Academy, Board Member

SKILLS

Fieldwork: Wilderness First Aid Training (UW), Boater Safety License (WA), Front Country Leadership Training (Bay Area Wilderness Exchange)
Programming: Basic: Matlab; Int: JavaScript, XML, Markdown; Advanced: R, Python
Geospatial: Google Earth Engine, PostgreSQL, QGIS, Geopandas, ENVI, ArcGIS
Cloud: Google Cloud Platform, Amazon Web Services (EC2, S3)
Lab: gas chromatography, geochemistry, integrated cavity ring spectroscopy, fluorometry, compressed gas handling, laboratory safety and protocol development,
Optics: benchtop and underway fluorometry, spectrophotometry, LISST particle sizer, ac-s spectrometry, hyperspectral radiometry
Teaching: Biogeochemical Cycles, Remote Sensing, Introduction to Big Data, Diversity and Inclusion, Curriculum Development, Project-Based Learning
Numerical & Hydrologic Modelling: Soil and Water Assessment Tool (SWAT), Weka Machine Learning Supervised Classifiers

FIELDWORK

Peace Athabasca Delta, Canada • Carbon flux and optical measurements • Trained 3 graduate students in water chemistry measurements	*Joint effort between NASA, USGS, UNC Chapel Hill, UCLA and UMass Boston*	Summer 2019
Yukon Flats Wildlife Refuge, interior Alaska • Designed and implemented field campaign for sensor-based biogeochemical and optical characterization of arctic lakes in coordination with an airborne campaign • Flux chamber deployment	*Joint effort between NASA, USGS, Department of Fish and Wildlife and University of Washington*	Summer 2018, Fall 2019
San Francisco Bay Estuary • Short term field assistant for discrete and underway biogeochemical sampling for residence time mapping	*USGS California Water Science Center*	Fall 2017
Atlantic Ocean, Coastal Maine • Field deployment of optical sensors • Research cruise for satellite optical validation	*NASA, University of Maine*	Summer 2017
Columbia River Basin • Columbia River Gorge CO2 sensors • Small Stream CO2 sensors	*USGS – NRP, USGS Portland Water Science Center, WA Department of Ecology*	Ongoing
Boreal Alaska • Small stream carbon sampling	*USGS & NASA AirSWOT, ABoVE*	Summer 2016
Bighorn Mountains & Plains, Ucross, Wyoming • Aquatic greenhouse gas field surveys • Remote sensing validation	*Ucross High Plains Stewardship Initiative, Yale School of Forestry & Environmental Studies*	2015-2016
Yale Environmental Watershed, New Haven CT • *In situ* sensors for monitoring watershed hydrology and biogeochemistry	*Hixon Center for Urban Ecology, Yale School of Forestry and Environmental Studies 2007-2009*	2013-2015
Sandy beach monitoring, Northern California • Coordinated sandy beach monitoring with 120 high school freshman students	*National Marine Sanctuary Long Term Monitoring and Experiential Training*	2012-2013
Urban Watershed Restoration, Oakland, CA • Organized restoration field trips for over 500 Oakland students with a focus on nutrient cycling, invasive species and conservation strategies	*Earth Team Eco-Stewards*	2009 - 2012